UNIVERSITÉ DE MONTRÉAL

ÉTUDE DE CIRCUITS INTÉGRÉS MICRO-ONDES PLANAIRES ET NON PLANAIRES

TONGQING WANG
DÉPARTEMENT DE GÉNIE ÉLECTRIQUE
ET GÉNIE INFORMATIQUE
ÉCOLE POLYTECHNIQUE DE MONTRÉAL

THÈSE PRÉSENTÉE EN VUE DE L'OBTENTION DU DIPLÔME
DE PHILOSOPHIAE DOCTOR (Ph.D.)
(GÉNIE ÉLECTRIQUE)
AOÛT 1998

UNIVERSITÉ DE MONTRÉAL

ÉCOLE POLYTECHNIQUE DE MONTRÉAL

Cette thèse intitulée:

ÉTUDE DE CIRCUITS INTÉGRÉS MICRO-ONDES PLANAIRES ET NON PLANAIRES

présentée par: WANG Tongqing
en vue de l'obtention du diplôme de: Philosophiae Doctor
a été dûment acceptée par le jury d'examen constitué de:

M. BOSISIO Renato G., M. Sc. A., président
M. WU Ke, Ph.D., membre et directeur de recherche
M. LAURIN Jean-Jacques, Ph.D., membre
M. KUBINA Stanley J., Ph.D., membre externe

A la mémoire de mon père regretté.

A ma famille.

Remerciements

Je voudrais exprimer ma plus sincère estime au Professeur Ke Wu, pour ses encouragements constants, son soutien et ses conseils qui m'ont guidé tout au long de mon travail de recherche à l'École Polytechnique. L'enthousiasme, la finesse, et la perspicacité de ses jugements techniques et sa très grande expérience m'ont beaucoup apporté et ont énormément contribué au succès de ces recherches. J'exprime aussi des remerciements spéciaux aux membres du jury Ms les Professeurs Rénato G. Bosisio, Jean-Jacques Laurin et Stanley J. Kubina, pour leurs inestimables suggestions et pour le temps précieux qu'ils ont passé pour l'examen de ma thèse et leur participation à la soutenance orale de ma thèse.

Je voudrais aussi affirmer ma sincère gratitude à Ms. les Professeurs Rénato Bosisio, Jean-Jacques Laurin et Cevdet Akyel pour leurs aides et leurs discussions très utiles durant la durée de mes études. Mes remerciements vont aussi vers Jules Gauthier pour la fabrication et l'assemblage des circuits, ainsi que vers René Archambault pour la gestion du systéme informatique et des bancs de mesures. Je remercie grandement les membres des équipes de recherche du Centre de Recherche Poly-Grames, particulièrement M. François Boone, Docteurs Hongming An, Jifu Huang et Liang Han pour l'aide apportée par leur discussion, leur coopération et leur amitié.

Je suis aussi redevable à mon superviseur de maîtrise, le Professeur Quanrang Yang de Southeast University, China, qui m'a introduit au merveilleux monde des circuits intégrés micro-ondes, et qui, sans cesse m'a encouragé dans la poursuite de mes études.

Je voudrais aussi remercier toutes les personnes qui ont contribué, sans souci d'intérêt, à mon développement personnel et professionnel.

Je désire exprimer ma profonde gratitude à ma famille pour leur amour et le soutien qu'ils n'ont jamais cessé de me fournir. Je suis tout particulièrement reconnaissant envers ma femme, Yanyan Zhang, et ma fille Jean Wang, pour leurs encouragements, leur compréhension et leur patience durant toute la durée de mon doctorat.

Enfin, Je voudrais remercier M. le Professeur Ke Wu pour l'aide financière qu'il m'a accordée tout au long de ce cycle d'étude.

Résumé

La technologie des circuits intégrés micro-ondes, monolithiques et hybrides, constitue la clef de voûte pour une multitude d'applications dans l'ingénierie moderne des micro-ondes. Avec la reprise considérable des techniques de communications sans fil, le domaine des circuits intégrés micro-ondes (MIC) est actuellement le sujet d'une activité intense de recherche et d'expérimentation, dans le but de développer des sous-systèmes et des composants compacts caractérisés par de faibles coûts et de hautes performances. Contrairement aux circuits intégrés conventionnels micro-ondes en technologie hybride, il est très difficile et même impossible d'ajuster les performances électriques des circuits intégrés, monolithiques ou en technologie hybride miniaturisée, une fois la fabrication terminée. Ainsi donc, la recherche directement dirigée vers la caractérisation précise des diverses structures courantes de guides d'onde impliquées dans les circuits est pleinement justifiée.

Le travail décrit dans cette thèse est orienté vers l'étude des circuits intégrés micro-ondes planaires et non-planaires. Un travail de recherche et de compréhension des performances électriques d'une classe de configurations de circuits planaires et non-planaires a été réalisé. Voici une rapide description des différentes parties du travail présenté dans cette thèse.

Une version perfectionnée de la méthode spectrale de résolution d'équation différentielle (Enhanced Spectral Domain Approach) a été développée pour la caractérisation de structures guides d'ondes complexes, planaires et non-planaires.

Cette méthode est basée sur une analyse en domaine spectral et du théorème de la conservation de la puissance. La relation entre les champs électriques tangentiels et les champs magnétiques tangentiels, aux frontières ouvertes d'un milieu constitué de couches homogènes superposées, est établie conformément aux procédures classiques de la méthode spectrale, alors que l'équation caractéristique est dérivée à partir du théorème de conservation de la puissance. Une formulation généralisée basée sur la puissance, est proposée pour le calcul de l'impédance caractéristique.

Les performances électriques d'une structure guide d'onde uniplanaire placée dans un environnement composite ont été étudiées. Les effets de trois schémas différents de montage de ruban suspendu (sur socle, dans une rainure, et sur socle inversé), sur la constante de propagation des modes fondamentaux, la fréquence de coupure et les modes d'ordres supérieurs, pour des lignes couplées à fentes sont présentés et discutés en détail. Une classe de configurations uniplanaires blindées dans des réceptacles à sections circulaires, elliptiques, rectangulaires et trapézoïdales pour des applications de circuits intégrés micro-ondes monolithiques ou hybrides, a été analysée. Leurs performances électriques sont caractérisées par les constantes de propagation et les valeurs d'impédance caractéristique. Il a été montré que la largeur de bande monomode de rubans blindés avec des micro-membranes peut être significativement augmentée par l'utilisation d'un certain profile de cavité de blindage.

L'étude et la compréhension d'un coupleur en technologie hybride, uniplanaire, en anneau, utilisant un inverseur de phase ont été réalisées. Une nouvelle théorie de design et de réalisation de coupleur, utilisant un inverseur de phase en vue d'une réduction de taille et d'un élargissement de largeur de bande de fréquence, a été développée. Les

critères de conception pour un coupleur en anneau en technologie hybride avec inverseur de phase, sont discutés. La largeur de bande effective du nouveau coupleur proposé peut être améliorée de 28% dans le cas d'un design exigeant au minimum 20dB de perte par réflexion. Une classe d'inverseurs de phase uniplanaires est présentée avec leurs aspects techniques. Des résultats expérimentaux montrent que le coupleur proposé possède une largeur de bande de plus d'une octave de 1.43 GHz à 2.95 GHz avec un couplage de 3.5±0.5 dB indépendamment du port d'entrée. L'isolation est supérieure a 20 dB sur une largeur de bande de plus de 1.8 octave.

Une nouvelle approche par partition de domaine est proposée pour modéliser des circuits micro-ondes de formes arbitraires et résoudre aussi bien des problèmes aux valeurs propres que pour étudier des discontinuités. L'algorithme de base repose sur une stratégie empruntée à la méthode des différences finies, avec un réseau d'interconnexions. La matrice caractéristique qui relie la valeur des champs aux frontières de chaque petit sous domaine, est directement dérivée à partir des équations de Maxwell et par l'utilisation des différences centrées et de calcul de moyenne. Cette formulation présente l'avantage d'une convergence rapide tout en conservant une facilité d'adaptation à une grande gamme de géométries, propre aux techniques d'étude de domaines discrétisés. Deux problèmes typiques d'étude de circuit planaire et en guide d'onde ont été analysés afin de valider la formulation.

Abstract

Hybrid and monolithic microwave integrated circuit technology is a corner stone for diverse modern microwave engineering applications. With the revival of wireless techniques, the field of microwave integrated circuits (MIC's) is currently experiencing intense research activity aimed at developing compact components and subsystem with the features of low-cost and high-performance. Unlike conventional hybrid MIC's, it is extremely difficult and even impossible to adjust the electrical performance of miniaturized hybrid and monolithic MIC's once they are fabricated. Therefore, research directed towards the accurate characterization of various practical guided-wave structures involved in the circuits is fully justified.

The work reported in this thesis is oriented towards the study of planar and non-planar MICs. A comprehensive investigation of the electrical performance of a class of planar and non-planar circuit configurations has been achieved. Following is a summary of the work described in this document.

An enhanced spectral domain approach (SDA) has been developed for characterization of complex planar and non-planar guided-wave structures. The method is based on the combination of spectral domain analysis and power conservation theorem. The relationship between tangential electric and magnetic fields at boundary apertures of multi-layered uniform medium is established in terms of the conventional SDA while a characteristic equation is derived through the power conservation theorem. A

generalized power-based formulation is proposed for calculation of characteristic impedance.

The electrical performance of uniplanar guided-wave structures with composite housings has been studied. The effects of three suspended mounting schemes (pedestal, groove, inverse pedestal) on the propagation characteristics of fundamental modes and the cutoff frequency of higher-order modes in coupled slotline are discussed in detail. A class of self-shielded uniplanar configurations with circular, elliptic, diamond and trapezoidal cross-section housings for hybrid and monolithic MIC application are analyzed. Their electrical performance is characterized in terms of propagation constant and characteristic impedance. It is found that the monomode bandwidth of membrane-based microshield lines can be significally increased by using certain shielding cavity profiles.

A comprehensive study of a uniplanar hybrid ring coupler using phase inverter has been achieved. A new design theory and practice using a phase inverter for size-reduction and band-broadening of the coupler are developed. Design criteria of reverse-phase hybrid ring couplers are discussed. Effective bandwidth of our new proposed coupler can be increased by 28% for a design requirement of 20-dB return loss. A class of uniplanar phase inverters and their technical aspects are also presented. Experimental results show that the proposed coupler has a bandwidth of more than one octave from 1.43 to 2.95 GHz with 3.5±0.5 dB coupling for any port. The isolation is better than 20 dB for more than 1.8 octave bandwidth.

A novel domain-partitioning approach has been proposed to model arbitrarily shaped microwave circuit problems (eignvalue and discontinuities). The basic algorithm is set up from a finite-difference strategy with networking interconnection. The characteristic matrix which relates boundary field quantities of a small subdomain is derived directly from Maxwell's equations by using central differencing and averaging. This formulation has the advantage of rapid convergence while preserving the feature of versatility of the discrete domain techniques. Two typical waveguide and planar circuit problems are analyzed in order to validate the formulation.

Table des matières

Liste des tableaux

Liste des figures

Liste des acronymes

CAO	:	Conception Assistée par Ordinateur
CBCPW	:	Conductor-Backed CoPlanar Waveguide
CPS	:	CoPlanar Strip
CPU	:	Central Processing Unit
CPW	:	CoPlanar Waveguide
DPA	:	Domain-Partitioning Approach
ESDA	:	Enhanced Spectral Domain Approach
H(M)MIC	:	Hybrid/Monolithic Microwave Integrated Circuit
MAB	:	Minimum Autonomous Block
MCS	:	Micro-Coplanar Strip
MIC	:	Microwave Integrated Circuit
MMIC	:	Monolithic Microwave Integrated Circuit
PCS	:	Personal Communication Services
SDA	:	Spectral Domain Approach
TE	:	Transverse Electric
TEM	:	Transverse ElectroMagnetic
TLM	:	Transmission Line Matrix
TM	:	Transverse Magnetic
TRL	:	Thru-Reflect-Line
WLAN	:	Wireless Local Area Network

Chapitre I

Introduction

Les années récentes ont été témoins du changement vital de la place des applications micro-ondes dans l'ingénierie, du secteur militaire vers les marchés économiques grands publiques. La renaissance du secteur des communications sans fil a donné une nouvelle signification et de nouveaux objectifs aux technologies micro-ondes qui étaient traditionnellement orientées vers les domaines de la défense militaire. Diverses applications commerciales émergeantes en micro-ondes et en bande millimétrique sont brièvement présentées dans la figure Fig. 1.1. Leur statut présent, leurs tendances futures et les spécifications techniques ont été largement commentée dans [1,2]. Parmi ces applications, les circuits intégrés micro-ondes monolithiques et hybrides miniaturisés pouvant être réalisés à grande échelle, tout en présentant une grande fiabilité, sont fortement désirés afin de réduire les coûts de production. Le domaine des circuits intégrés micro-ondes est actuellement sujet à des activités de recherches intenses dans le but de développer des composants compacts, ou des sous-systèmes parfaitement adaptés aux exigences des nouvelles applications actuelles.

1.1 Rapide survol de la technologie des circuits intégrés micro-ondes (MIC)

Il est bien connu que les MIC reposent sur l'utilisation de la technologie des circuits planaires formés partiellement ou en totalité, sur une surface plane de diélectrique, par une ou plusieurs dépositions et une opération de gravure. Le circuit en entier, peut être produit en grand nombre à faible coût par photolithographie. Les caractéristiques

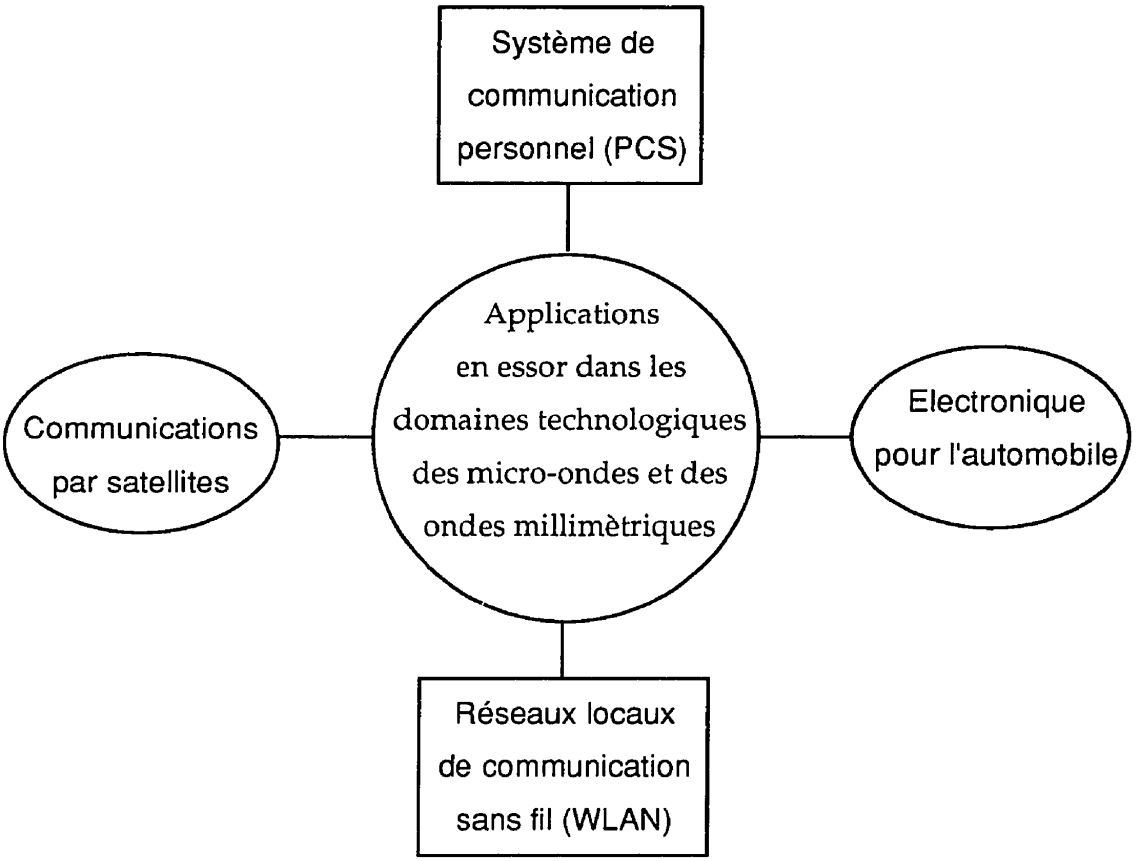

Figure 1.1 Applications en essor dans les domaines technologiques des micro-ondes et des ondes millimétriques.

techniques des MIC sont leur petite taille, leur faible poids, et leur haute fiabilité. Les premiers travaux concernant la technologie des MIC remontent aux années 1950. Les premiers circuits étaient gravés sur des substrats recouverts d'une couche de cuivre, et l'implantation des composants se faisait par l'intermédiaire de fils soudés. Cette technique a été perfectionnée durant les années 1960 et 1970 par le développement des technologies de déposition de couches minces mais aussi de couches épaisses et par la

grande diversité des méthodes d'assemblage de composants. A la fin des années 1970, l'avancement de la technologie des circuits planaires couplé avec le rapide développement des composants semi-conducteurs micro-ondes, particulièrement des MESFET sur arséniure de gallium et les progrès des technologies des matériaux et de fabrication, a aboutit à l'émergence de la technologie des circuits intégrés micro-ondes monolithiques (MMIC). En technologie MMIC, les circuits passifs et actifs et leurs interconnexions sont réalisés en grands nombres sur le même substrat semi-conducteur. Ces développements et les applications des technologies M(M)IC sont présentés en détail dans [3,4]. La comparaison entre les principales caractéristiques liées aux approches des circuits MIC hybrides et monolithiques est présentée dans le tableau 1.1. La lecture de ce tableau permet d'affirmer que les circuits MMIC coexisteront avec les circuits MIC hybrides à faible coût, car leurs caractéristiques respectives sont complémentaires. En particulier, du fait du faible coût des premières réalisations de circuit MIC hybride, de nouvelles configurations de design peuvent être d'abord validées en technologie hybride, puis transposées vers des circuits monolithiques plus coûteux à tailles plus réduites.

Tableau 1.1 Comparaison entre les principales caractéristiques des circuits hybrides MIC et des circuits monolithiques MIC.

Propriétés	Hybride	Monolithique
Fabrication en grand nombre.	Non	Oui
Miniaturisation.	Non	Oui
Large bande/ faible sensibilité aux parasites	Non	Oui
Facilité d'implantation de composants actifs.	Oui	Non
Faible coût de dèmarrage du processus de fabrication.	Oui	Non
Isolation	Oui	Non

En technologie MIC, la structure des guides d'onde planaires est constituée d'éléments blocs selon le développement des divers composants fonctionnels ou sous-systèmes. L'étude des structures de guide d'onde planaires fut un sujet de recherche important dans le domaine des circuits MIC. Ces dernières années, le développement explosif des applications commerciales micro-ondes et en ondes millimétriques pour le grand publique, a considérablement accru les activités de recherche dans ce domaine d'une part pour explorer les diverses nouvelles configurations de circuits planaires et d'autre part pour caractériser précisément leur performances électriques.

1.2 Lignes de transmissions planaires et techniques de modélisation

Les lignes de transmissions planaires constituent le point le plus essentiel dans les circuits MICs. Les premiers travaux concernant les lignes de transmission planaires en micro-onde ont été effectués en 1952, lorsque Grieg et Englemann [5] ont les premiers, proposé la ligne micro-ruban qui fut utilisée comme un substitut des guides d'onde non-planaires et des câbles coaxiaux. Leur structure était hautement compacte mais à très grande rugosité. Elle ne fut pas acceptée facilement pour les utilisations micro-ondes à cause des ses pertes importantes. A la fin des années soixantes, avec la disponibilité de diélectriques dotés de hautes constantes diélectriques, de matériaux diélectriques à faibles pertes et avec la demande croissante de circuits micro-ondes miniaturisés pour les besoins de l'aérospatiale et des applications satellites, l'intensité de l'intérêt pour les circuit micro-rubans fut renouvelée. Il résulta le rapide développement de l'utilisation des lignes micro-rubans. A cette époque, deux autres types de lignes de transmission planaires furent aussi inventés : il s'agit des lignes à fentes, et des lignes coplanaires (CPW), respectivement proposées par S. B. Cohn [6] et par C. P. Wen [7]. Ces deux configurations utilisent seulement une seule face du

substrat, et permettent une réalisation aisée de terminaison de ligne en circuits fermés et une intégration facile de un ou plusieurs composants montés en parallèle. Cependant elles furent utilisées moins fréquemment que les lignes micro-rubans lors de la premières phase du développement des MIC. Leurs avantages furent quelque peu effacés par la complexité de leur mécanisme de propagation, due à l'absence de mode quasi-TEM pour la ligne à fentes, et à la présence du mode de ligne à fentes, pour la ligne coplanaire.

Avec la croissance des fréquences d'opération, particulièrement dans la bande des fréquences millimétriques, l'utilisation de la ligne micro-ruban traditionnelle devint problématique à cause de l'augmentation des pertes, de la présence des modes supérieures et des couplages parasites. Dans les années 1970, de nombreux efforts ont été faits pour surmonter les inconvénients de la ligne micro-ruban. Une classe de structures guide d'onde combinant une géométrie planaire et une autre non-planaire, telle celle des lignes suspendues blindées ou celle des lignes à ailettes furent proposées. La caractéristique commune de ces configurations de guide d'onde, est que l'utilisation d'un boîtier métallique enveloppant la structure guide d'onde, élimine ou adoucit les défauts propres à la ligne micro-ruban. La structure à ailette en particulier, et les lignes blindées suspendues ont été très largement utilisées pour les premiers développements de composants divers en bandes millimétriques, en technologie hybride [8, 9].

Durant les dix dernières années, comme plus d'efforts étaient dépensés pour l'étude des circuits intégrés monolithiques en micro-onde et en ondes millimétriques, l'intérêt pour les structures guide d'onde uniplanaires, utilisant seulement une seule face de substrat, fut renouvelé. Les structures de transmission uniplanaires comprennent les lignes

coplanaires, les lignes à fentes, et les lignes à deux rubans coplanaires. Ces structures possèdent des avantages distincts par rapport aux lignes micro-rubans, tels qu'une faible dispersion, une réalisation aisée de connexions parallèles successives de composants passifs ou actifs sans la nécessité de recourir à des trous métallisés vers un plan de masse. Ces caractéristiques ont rendu importantes l'utilisation des structures guide d'onde uniplanaires, lors du design des circuits intégré en micro-ondes ou en ondes millimétriques. Du fait du manque d'information concernant les modes de transmission uniplanaires, l'étude des guides d'onde uniplanaires reçoit aujourd'hui beaucoup plus d'attention de la part de chercheurs travaillant en théorie des champs électromagnétiques ou en conception de circuit. Beaucoup de travaux de recherche ont été répertoriés [10]. Il a été déterminé que les modes de transmission uniplanaires, particulièrement les lignes CPW avec un plan de métallisation sur la face non gravée, souffrent de couplages parasites, de pertes, et de dispersion modale. Connaissant les avantages des structures fermées non planaires, la recherche sur les lignes de transmission uniplanaires blindées grâce à un boîtier de type cavité de résonance, est donc pleinement justifiée.

Les progrès des techniques de réalisation de matériaux semi-conducteurs, auxquels on ajoute les avantages des structures guide d'onde fermées, nous conduisent à considérer une nouvelle sorte de ligne de transmission combinant une partie planaire avec une autre partie non planaire, appelée ligne avec micro-blindage, et proposées en 1991 par N. I. Dib, et d'autres auteurs [11]. La section transversale de cette nouvelle sorte de ligne est présentée à la figure Fig. 1.2. Dans la ligne avec micro-blindage, le ruban conducteur planaire est porté par une membrane diélectrique. Une membrane typique est constituée par une gaufrette de silicium sur laquelle est déposée un film composé de

trois couches $SiO_2/Si_3N_4/SiO_2$, dont les épaisseurs respectives sont de 0.45 μm, 0.35 μm et 0.75 μm. Puisque la membrane est très fine, la ligne avec micro-blindage offre de meilleures performances que les lignes de transmission planaires conventionnelles, en ce qui concerne les phénomènes de dispersion et les pertes diélectriques. De plus, la cavité de blindage métallique minimise les phénomènes de couplage entre lignes adjacentes, et élimine les pertes par rayonnement sous forme de modes parasites. La ligne avec micro-blindage peut être fabriquée de façon monolithique par utilisation des techniques de gravure de diélectrique et de dépositions métalliques. Ces caractéristiques montrent que la ligne micro-blindée est bien adaptée aux applications en ondes millimétriques. De plus, les techniques de micro-usinage du silicium contribuent à un potentiel de développement de composants miniatures intrinsèquement blindés dans les domaines des circuits intégrés micro-ondes et en ondes millimétriques.

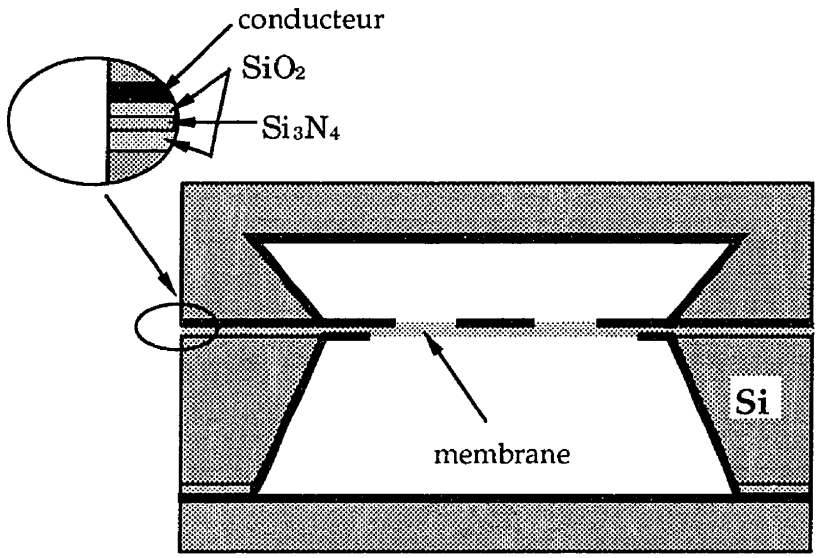

Figure 1.2 Ligne avec micro-blindage

Il doit être souligné que l'amélioration des performances électriques concernant les lignes combinant une partie planaire à une autre partie non-planaire, présente en contrepartie, une perte de simplicité et de flexibilité pour le design de circuit. Du fait de l'enveloppement dans une structure de type cavité métallique, il est difficile d'ajuster les caractéristiques du circuit une fois la fabrication achevée. Ainsi donc, une conception assistée par ordinateur (CAO) précise est essentielle pour le design de tels circuits. Généralement, la CAO de MIC se décompose en trois phases: la modélisation, l'analyse, et l'optimisation. Bien que distinctes, les trois phases s'entremêlent de façon très étroite. Naturellement, l'exécution de l'analyse et de l'optimisation reposent sur la modélisation. Afin d'atteindre les spécifications fixées pour la réalisation du design, dès la première fabrication du circuit, une modélisation précise des phénomènes physiques est nécessaire.

La caractérisation numérique et la modélisation de ligne de transmission planaire ont été un sujet important de recherche lors des vingt dernières années. Plusieurs techniques numériques ont été développées pour la caractérisation des structures guides d'onde planaires. En général, les techniques numériques pour l'étude des MIC peuvent être divisées en trois groupes: le premier repose sur une approche analytique basée sur la résolution de l'équation intégrale du problème, le second comprend les méthode semi-analytiques et semi-discrètes telles la méthode des lignes et enfin les méthodes complètement discrètes comme la méthode des éléments finis ou la matrice des lignes de transmission (TLM). Chaque groupe présente ses avantages et ses désavantages. Par exemple, bien qu'une approche complètement discrète exige un temps de calcul numérique considérable, elle permet en revanche l'étude de structures au géométrie très variées. D'autre part, si une approche analytique est numériquement

plus efficace, son domaine d'application quant à la géométrie de la structure est réduit. Les différents aspects des méthodes numériques sont présentés dans [12]. En pratique, les méthodes numériques sont choisies en fonction d'un compromis entre principalement la précision, la rapidité de calcul, la mémoire requise, et la complexité de la structure. La décision dépends souvent de la géométrie. Quant une structure spécifique est analysée, il est donc nécessaire de redéfinir ou de modifier la méthode utilisée de façon à ce qu'elle soit la mieux adaptée à la géométrie de la structure.

1.3 Organisation de la thèse

Compte tenu des caractéristiques des circuits MIC soulignées ci-dessus, ce travail est centré sur l'étude de circuits MIC combinant des structures planaires et non-planaires. Une attention particulière est portée sur le développement de techniques de modélisation et sur les propriétés électriques de diverses structures composites guides d'onde planaires et non-planaires. Comme la majeure partie du travail rapporté dans ce document a été publié ou soumis pour publication dans des journaux internationaux de références, cette thèse est présentée sous la forme d'une série d'articles. Chaque article présente un sujet spécifique.

La thèse comprend sept chapitres. Dans le chapitre II, une méthode d'analyse spectrale perfectionnée (Enhanced Spectral Domain Approach) est développée pour la caractérisation des propriétés de propagation de structures guides d'onde combinant une partie planaire et non-planaire. Une formulation généralisée basée sur la puissance pour le calcul de l'impédance caractéristique en est déduite. Plusieurs exemples numériques sont traités pour démontrer la validité et le domaine d'étude de la technique proposée pour l'analyse de structures guide d'onde combinant des parties

planaires et non-planaires. Le chapitre est constitué par l'article intitulé "An efficient Approach to modeling of quasi-planar structures using the formulation of power conservation in spectral domain", publié dans IEEE Transaction on Microwave Theory and Techniques, vol. 43, no. 5, May 1995.

Le chapitre III fournit une discussion permettant de comprendre les effets physiques dans les montages suspendus (sur socle, sur socle inversé ou dans des rainures), concernant les caractéristiques de propagation des modes fondamentaux, les fréquences de coupure, et les modes d'ordres supérieurs dans les lignes à fentes couplées. Les profils des champs des modes fondamentaux des lignes à fentes couplées avec et sans socle sont présentés. Le chapitre est illustré par un article publié en mai 1995 dans IEEE Transaction on Microwave Theory and Techniques.

Le chapitre IV traite des caractéristiques de propagation des structure guide d'onde uniplanaires micro-blindées incluant des blindages de formes circulaires, elliptiques, en losange et trapézoïdale. L'influence de divers paramètres sur la fréquence de coupure du mode lignes à fentes dans les lignes à micro-blindage y est déterminée en détails. Ce chapitre présente un article accepté pour publication par International Journal of RF and Microwave Computer-Aided Engineering.

Le chapitre V présente le design d'un coupleur en anneau uniplanaire. Une nouvelle démarche de conception de design, utilisant un inverseur de phase pour obtenir une réduction de taille et un élargissement de bande passante du coupleur en anneau, est proposée. Une discussion explique les critères de design du coupleur en anneau inverseur de phase et les configurations d'une classe d'inverseurs de phase

uniplanaires. Un coupleur en anneau avec 3.5±0.5 dB de couplage sur plus d'une octave de largeur de bande a été réalisé et est présenté. Le chapitre est illustré par un article soumis pour publication dans la revue IEEE Transaction on Microwave Theory and Techniques et qui est actuellement en cours d'examen par le comité de lecture.

Le Chapitre VI décrit le développement d'une nouvelle approche basée sur une partition de domaines, afin de caractériser des circuits micro-ondes de forme arbitraire. Une matrice caractéristique reliant les valeurs des champs aux frontières entre différents petits sous-domaines, est directement déduite des équations aux frontières par utilisation des techniques de différence centrale et de calcul de moyenne. Deux exemples numériques sont inclus pour valider la formulation. Le chapitre repose sur un article publié en avril 1996 dans Microwave and Optical Technology Letters.

Le chapitre VII conclut par une synthèse des différents travaux publiés, et avec des suggestions pour des travaux futurs. En extention à ce travail, la caractérisation de résonnateurs diélectriques cylindriques utilisant la méthode numérique présentée dans le chapitre II (ESDA) est annexée (annexe A).

Références

[1] ALI, F. et HORTON, J. B. (1995). Special Issue of Emerging Commercial and Consumer Circuits, Systems, and Their Applications. IEEE Transactions on Microwave Theory and Techniques, 43, no. 7, part II.

[2] MEINEL, H. (1995). Recent advances on millimeter wave PCN system development in Europe. 1995 IEEE Microwave Systems Conference Proceedings, 3-6.

[3] HOFFMAN, R. (1987). Handbook of Microwave Integrated Circuits. Artech House, Norwood, MA.

[4] PUCEL, R. A., ed. (1985). Monolithic Microwave Integrated Circuits. IEEE Press, NY.

[5] GRIEG, D. D. et ENGELMANN, H. F. (1952). Proc. IRE 40, 1644-1650.

[6] COHN, S. B. (1969). Slot line on a dielectric substrate, IEEE Transactions on Microwave Theory and Techniques, 17, 768-778.

[7] WEN, C. P. (1969). Coplanar Waveguide: A surface strip transmission line suitable for non-reciprocal gyromagnetic device application. IEEE Transactions on Microwave Theory and Techniques, 17, 1087-1090.

[8] CHANG, K. (1985). Millimeter-wave planar integrated circuits and subsystems. Infrared and Millimeter Waves, 14, 79-187.

[9] MENZEL, W. (1985). Integrated fin-line components for communication, radar, and radiometerapplications. Infrared and Millimeter Waves, 13, 77-121.

[10] SHARMA, A. K. et ITOH, T. (1993). Special Issue on Modeling and Design of Coplanar Monolithic Microwave and Millimeter-Wave Integrated Circuits. IEEE Transactions on Microwave Theory and Techniques, 41, no. 9.

[11] DIB, N. I., et al. (1991). Study of a novel planar transmission line. IEEE MTT-S Digest, 2, 623-626.

[12] ITOH, T., ed. (1989). Numerical Techniques for Microwave and Millimeter-Wave Passive Structures. John Wiley & Sons, NY.

Chapitre II

Méthode spectrale améliorée (Enhanced Spectral Domain Approach)

Comme mentionné dans le précèdent chapitre, les techniques complètes de modélisation tenant compte des changements en hautes fréquences pour la simulation précise des performances d'un circuit planaire ou non-planaire, sont exigées pour atteindre l'objectif de réussite en un seul design. Durant les dix dernières années beaucoup d'efforts ont été effectués dans le développement de méthodes numériques capables de caractériser des structures guide d'onde composites. Un grand nombre de méthodes telles la méthode d'adaptation modale (Mode-Matching Method), la technique de la résonance transverse, la méthode des lignes, et la méthode spectrale, ont été proposées et raffinées selon les applications. En générale le choix de la méthode numérique est basé sur un compromis entre la précision, l'efficacité, l'adaptation à la structure étudiée, etc.... et ce choix n'est pas forcément unique. Pour des lignes de transmission planaires, simple couches ou multicouche de diélectrique, la méthode approuvée et utilisée est la méthode spectrale. Ce choix découle principalement de deux observations. La première est que la fonction de Green peut être obtenue analytiquement sous d'une paire de deux formules algébriques. Ensuite, l'utilisation de la méthode des moments et plus particulièrement de la méthode de Galerkin, permet d'obtenir un résultat précis bien que le déterminant associé à l'équation caractéristique, soit de dimension faible. La méthode est habituellement employée en choisissant un jeu de fonctions de base qui satisfait les

conditions de singularité sur le bord des conducteurs, pour l'approche du courant sur les rubans ou des champs dans les fentes.

D'un point de vue mathématique, la méthode spectrale transforme un problème d'équation intégrale dans le domaine spatial en une équation algébrique dans le domaine spectral associé à la théorie des transformations de Fourier. Son principal avantage est la simplification du traitement analytique et numérique. La méthode spectrale conventionnelle impose les conditions frontières au jeu de fonction de base dans le domaine spectral. Ceci impose un certain nombre de restrictions concernant les domaines d'application de la méthode. Notamment, les métallisations sont considérées sans épaisseur, infiniment fines, et aucune discontinuité latérale à la structure ne peut être prise en compte. Or les effets dus à l'épaisseur des métallisations et des autres paramètres négligés peuvent apparaître significatifs aux fréquences millimétriques.

Dans ce chapitre, une méthode spectrale perfectionnée pour l'analyse de structure guide d'onde à parties planaires et non-planaires, est décrite. Cette technique permet de prendre en compte les effets de divers paramètres structurels tels que l'épaisseur non nulle des conducteurs, et des blindages de forme arbitraire tout en préservant les avantages inhérents à la méthode spectrale. La stratégie de la formulation repose sur la combinaison de la méthode spectrale conventionnelle, appliquée à des sous-régions homogènes et sur l'application du théorème de conservation de la puissance à l'interface des différentes sous-régions. Dans le domaine spectral, les champs magnétiques tangentiels aux frontières ouvertes de chaque sous-régions (couche de diélectrique homogène) peuvent être exprimés en fonction des champs électriques correspondants par l'intermédiaire d'une matrice caractéristique. Dans le domaine spatial, les

conditions frontières sont satisfaites aux interfaces en imposant le théorème de conservation de la puissance. En comparaison avec la méthode spectrale conventionnelle, cette technique apparaît plus efficace en terme d'effort de formulation analytique et de précision numérique. Une formulation généralisée reposant sur la conservation de la puissance est développée pour le calcul d'impédance. Le chapitre est constitué par un article publié en mai 1995 dans un numéro de la revue IEEE Transaction on Microwave Theory and Techniques.

Le concept présenté ici ne limite pas l'étude à des structures uniquement planaires. Il peut être utilisé pour l'analyse de résonateurs diélectriques cylindriques rayonnants, comme décrit dans l'annexe A.

An Efficient Approach to Modeling of Quasi-Planar Structures Using the Formulation of Power Conservation in Spectral Domain

Tongqing WANG, and Ke WU, Senior Member, IEEE

Groupe de Recherches Avancées en Microondes et en Électronique Spatiale

(POLY-GRAMES)

Dept. de génie électrique et de génie informatique

École Polytechnique

C. P. 6079, Succ. "A", Montréal, Canada H3C 3A7

Abstract

An enhanced spectral domain approach (SDA) is developed for analysis of complex quasi-planar transmission lines. The method is based on a combination of spectral domain formulation and power conservation theorem. The relationship between electric and magnetic fields is established inside dielectric layers by using the conventional SDA while characteristic equation related to interface conditions is derived through the power conservation theorem. Maintaining the inherent advantages of the SDA, this technique is able to easily handle more complex quasi-planar structures. Generalized power formulation is also presented to calculate characteristic impedance. Convergence behavior is discussed considering the nature of power conservation. Various finlines with finite thickness of conductors are analyzed to demonstrate its applications.

2.1 Introduction

With ever increasing device density and operating frequency in monolithic and hybrid integrated circuits, electromagnetic modeling of various quasi-planar transmission lines is mandatory in accurately predicting circuit performance and efficiently compressing the design cycle. Many analysis methods usually present a compromise between accuracy and efficiency of numerical calculations, which are no longer suitable for the growing demand of accurate analysis over wide frequency spectrum up to the millimeter-wave range. The development of generalized and rigorous field-theoretical approaches, which are able to consider the effect of finite thickness of metal as well as grooves/pedestals, is therefore pertinent for successful applications. So far, a number of hybrid-mode techniques have been presented for analysis of a class of complex quasi-planar structures, mode-matching method [1], complex power conservation technique [2], transverse resonance technique [3, 4], method of lines [5], modified SDA [6, 7], to name a few examples. It has been recognized that the SDA is the most popular technique today. This is mainly driven by two facts. One is that the Green's function and field quantities are handled in the spectral domain through an efficient and simple algebraic algorithm. The other is that Galerkin's technique makes it possible to obtain accurate results with very low determinant order of the characteristic equation. This is usually done through an appropriate choice of basis functions which satisfy the edge singularity of currents on strips or of fields in slots. Its early applications and theoretical framework were reviewed in [8]. Recently, much effort has been made to extend the SDA to modeling of a class of novel and complicated quasi-planar structures. The mixed spectral domain approach was presented in [9, 10] for characterization of suspended planar transmission lines with pedestals and various

dielectric-loaded ridge waveguides. The CPW electrodes including conductor thickness have been analyzed in [11] for the Ti: $LiNbO_3$ electrooptic modulator through an extended spectral-domain approach based on integral equations. This approach has been also used to determine the characteristics of planar transmission lines with finite metallization thickness and lossy substrates containing magnetized ferrites in [12, 13]. However, these modified versions of the SDA may suffer from somehow tedious formulations as the complexity of structures increases. The spectral domain and equivalent boundary method [14] was proposed to model generalized coplanar transmission lines embedded in a bianisotropic multilayered medium. Nevertheless, this approach with a simple analytical process ignored the effect of finite thickness of conductors.

In this work, a novel enhanced spectral domain approach is proposed to analyze propagation characteristics of a class of complex quasi-planar transmission lines. This technique takes into account the effect of various structural parameters such as finite thickness of conductors and grooves/pedestals while maintaining the advantageous nature of the SDA. It is essentially achieved by an appropriate combination of the conventional SDA formulation with the power conservation theorem. In the spectral domain, the tangential magnetic field at boundary apertures of each subregion (homogeneous dielectric layer) can be expressed in terms of its electric counterpart through a characteristic matrix. In the space domain, the boundary conditions at the interfaces are satisfied by imposing the power conservation theorem. Compared to the conventional and other modified SDA, the proposed technique is more efficient in view of analytical effort and numerical accuracy. This is done by avoiding usually lengthy derivation of the Green's function matrix for complex structures. In addition, this

technique features an independent choice of the truncated spectral term in each subregion. The numerical efficiency is, therefore, highly enhanced in terms of the CPU time and memory space. This is in particular important in the analysis of structures containing a large ratio of the lateral width among adjacent subregions. A generalized power formulation is derived for the impedance calculation. Results for finlines with split-housing and finite thickness of metal strips are presented to demonstrate performance and usefulness of the proposed technique.

2.2 Theory

2.2.1 Characteristic Equation

As shown in Fig. 2.1(a), a generalized planar structure is composed of an arbitrary number of strips/fins deposited on different interfaces of a multilayer dielectric substrate. The consideration of finite metal thickness as well as housing grooves or box frames is important for millimeter-wave applications [2, 15]. Exact electromagnetic characteristics of such a structure can be symbolically described by the following space-domain integral equation in the frequency domain:

$$\vec{E}_t = \iint_s \vec{\vec{G}}(\vec{r} \mid \vec{r}') \cdot \vec{J}_t(\vec{r}')ds \tag{2.1}$$

where $\vec{\vec{G}}$ stands for the dyadic Green's function, and $\vec{E}_t, \vec{J}_t$ are the tangential components of electric fields and current density at interfaces involving strips/fins. In the spectral domain, the convolutional equation (2.1) is transformed into a simple algebraic equation, such that,

$$\tilde{\vec{E}}_t = \tilde{\tilde{\vec{G}}} \cdot \tilde{\vec{J}}_t \tag{2.2}$$

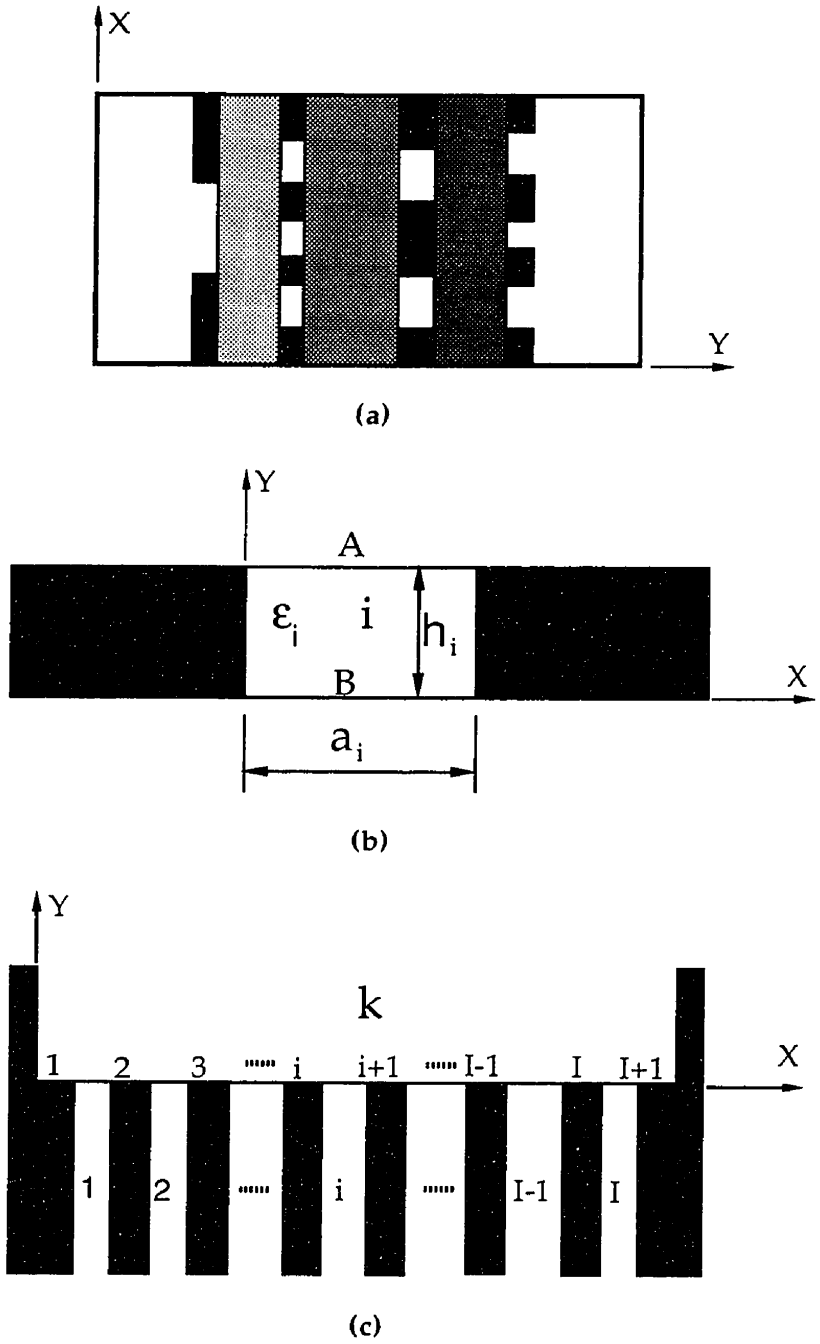

Fig. 2.1 (a) Cross section of a generalized planar transmission line, (b) any subregion of (a), and (c) any interface of (a).

The tilde over these quantities indicates the spectral-domain transform. Obviously, the key to apply this approach is to obtain the spectral domain Green's function $\tilde{\tilde{G}}$ for a specific structure. So far, a variety of modifications and improvements related to the SDA for analysis of planar structures are mainly on derivation of the Green's function. With regard to complex multilayer structures considering finite thickness of metal, grooves and pedestals, the analytical process gets much more involved and may become very difficult as the number of subregions including dielectrics, conductors and grooves/pedestals increases. To solve this bottleneck problem, a novel enhanced SDA is introduced for generalized planar structures. For a concise demonstration of its principle, perfect conductors and isotropic/lossless dielectrics are assumed.

The whole structure is divided into a number of rectangular homogeneous subregions which are interconnected to each other and bounded by lateral conducting walls. The electromagnetic fields in the i^{th} subregion in Fig. 2.1(b) can be expanded in the spectral domain,

$$\begin{pmatrix} \vec{E} \\ \vec{H} \end{pmatrix}^i = \sum_{n=-\infty}^{+\infty} \begin{pmatrix} \tilde{\tilde{E}}(y) \\ \tilde{\tilde{H}}(y) \end{pmatrix}_n^i \cdot e^{-j(\alpha_n^i \cdot x + \beta \cdot z)} \tag{2.3}$$

where

$$\begin{pmatrix} \tilde{\tilde{E}}(y) \\ \tilde{\tilde{H}}(y) \end{pmatrix}_n^i = \frac{1}{a_i} \int_{a_i} \begin{pmatrix} \vec{E} \\ \vec{H} \end{pmatrix}^i \cdot e^{j(\alpha_n^i \cdot x + \beta \cdot z)} \cdot dx \qquad with \ \alpha_n^i = \frac{2n\pi}{a_i} \tag{2.4}$$

Substituting (2.3) into Maxwell's curl equations yields,

$$\underbrace{\begin{bmatrix} 0 & \nabla\times \\ \nabla\times & 0 \end{bmatrix}}_{\overline{\overline{D}}} \cdot \underbrace{e^{-j(\alpha_n^i \cdot x + \beta \cdot z)} \cdot \begin{pmatrix} \tilde{\tilde{E}}(y) \\ \tilde{\tilde{H}}(y) \end{pmatrix}_n^i}_{\overline{A}} = j\omega \cdot \underbrace{\begin{bmatrix} \varepsilon & 0 \\ 0 & -\mu_0 \end{bmatrix}^i}_{\overline{\overline{M}}} \cdot \overline{A} \tag{2.5}$$

In this matrix equation, $\overline{A}$ is a column vector consisting of electric and magnetic fields for the n^{th} spectral component. Using a coordinate transform (rotation) similar to [6], a decoupled equation of the y-directed transverse TE and TM fields is obtained,

$$\frac{d}{dy}\begin{pmatrix} E_u \\ H_v \\ E_v \\ H_u \end{pmatrix}_n^i = \begin{bmatrix} 0 & j\omega\mu_0 & 0 & 0 \\ \gamma^2/j\omega\mu_0 & 0 & 0 & 0 \\ 0 & 0 & 0 & -\gamma^2/j\omega\varepsilon \\ 0 & 0 & -j\omega\varepsilon & 0 \end{bmatrix}_n^i \cdot \begin{pmatrix} E_u \\ H_v \\ E_v \\ H_u \end{pmatrix}_n^i \tag{2.6}$$

with $\gamma^2 = \alpha^2 + \beta^2 - \omega^2 \cdot \varepsilon \cdot \mu_0$. Note that the relationship between the original and transformed field components is characterized by the coordinate transform. Transmission line solution of (2.6) leads to two matrix equations which relate aperture fields to each other at lower and upper boundaries, such that,

$$\begin{pmatrix} \tilde{H}_x^- \\ -\tilde{H}_z^- \end{pmatrix}_n^i = \frac{1}{j\omega\mu_0\gamma}\begin{bmatrix} \gamma^2-\beta^2 & -\alpha\cdot\beta \\ -\alpha\cdot\beta & \gamma^2-\alpha^2 \end{bmatrix}_n^i \left\{ \frac{1}{th(\gamma\cdot h)}\begin{pmatrix} \tilde{E}_z^- \\ \tilde{E}_x^- \end{pmatrix} - \frac{1}{sh(\gamma\cdot h)}\begin{pmatrix} \tilde{E}_z^+ \\ \tilde{E}_x^+ \end{pmatrix} \right\}_n^i \tag{2.7}$$

and

$$\begin{pmatrix} \tilde{H}_x^+ \\ -\tilde{H}_z^+ \end{pmatrix}_n^i = \frac{1}{j\omega\mu_0\gamma}\begin{bmatrix} \gamma^2-\beta^2 & -\alpha\cdot\beta \\ -\alpha\cdot\beta & \gamma^2-\alpha^2 \end{bmatrix}_n^i \left\{ \frac{1}{sh(\gamma\cdot h)}\begin{pmatrix} \tilde{E}_z^- \\ \tilde{E}_x^- \end{pmatrix} - \frac{1}{th(\gamma\cdot h)}\begin{pmatrix} \tilde{E}_z^+ \\ \tilde{E}_x^+ \end{pmatrix} \right\}_n^i \tag{2.8}$$

The superscripts (-) and (+) denote the interfaces at $y=+0$ and $y=h_i-0$, respectively. Naturally, the tangential components of electric field at the top and bottom metallic ground planes of the shielding box are zero.

In the space domain, the tangential electric and magnetic fields should satisfy the remaining boundary and continuity conditions at the interfaces as illustrated in Fig. 2.1(c). In view of the interface geometry, these conditions can separately be stated in two different parts:

$$\begin{pmatrix} \vec{E}_t^- \\ \vec{H}_t^- \end{pmatrix}^k = \sum_{i=1}^{I} \begin{pmatrix} \vec{E}_t^+ \\ \vec{H}_t^+ \end{pmatrix}^i \quad \textit{on} \text{ apertures}$$

$$\begin{pmatrix} \vec{E}_t^- \\ \vec{H}_t^- \end{pmatrix}^k = \sum_{i=1}^{I+1} \begin{pmatrix} 0 \\ \vec{J}_t^+ \end{pmatrix}^i \quad \textit{on} \text{ conductors} \tag{2.9}$$

in which the subscript "t" refers to the x-z plane, and "k" is the notation of the region connected to an I-furcated waveguide junction. On the basis of the complementary property between $\vec{E}_t$ and $\vec{J}_t$, the power conservation in the transverse direction should hold, which is determined by the following equation,

$$\int_{a_k} (\vec{E}_t^- \times \vec{H}_t^{-*})^k \, dx = \sum_{i=1}^{I} \int_{a_i} (\vec{E}_t^+ \times \vec{H}_t^{+*})^i \, dx \tag{2.10}$$

Invoking Parseval theorem, (2.10) is transformed into the spectral domain such that

$$\frac{1}{a_k} \sum_{n=-\infty}^{+\infty} \begin{pmatrix} \tilde{E}_x^- \cdot \tilde{H}_z^{-*} \\ \tilde{E}_z^- \cdot \tilde{H}_x^{-*} \end{pmatrix}_n^k = \sum_{i=1}^{I} \frac{1}{a_i} \sum_{n=-\infty}^{+\infty} \begin{pmatrix} \tilde{E}_x^+ \cdot \tilde{H}_z^{+*} \\ \tilde{E}_z^+ \cdot \tilde{H}_x^{+*} \end{pmatrix}_n^i \tag{2.11}$$

Substituting (2.7) and (2.8) into (2.11), a set of linear homogeneous equations is derived. The propagation constant β can be obtained simply through the application of Galerkin's technique. In numerical calculations, the infinite sum of (2.11) in the spectral domain is truncated to a finite number. The spectral terms of both sides in (2.11) may be chosen independently as long as the power conservation is guaranteed. As will be shown in the next section, smaller number of spectral terms in a subregion with small lateral widths is required to achieve accurate results. This process greatly enhances the numerical efficiency in terms of the CPU time and memory space.

2.2.2 Characteristic Impedance

The characteristic impedance is a crucial parameter in computer-aided design of passive and active circuits. In the following, various finlines are considered as examples of analysis. Note that there is no unique definition of impedance in the non-TEM structures in which path integrals of modal fields are arbitrary. On the basis of practical consideration, the voltage-power definition seems to be more appropriate for slot-like structures. Considering the finite thickness of conductors, the two different slot voltages (V_A and V_B) may be obtained which depend on the upper and lower boundary apertures (A and B integral paths in Fig. 2.1(b), for example). As expected at higher frequencies, the difference between two voltages will be more visible as the thickness increases. Therefore, the average voltage may be defined such that $V_0 = \frac{1}{h_1} \cdot \int_0^{h_1} \left(\int_y E_z \cdot dx \right) \cdot dy$.

This can, in practice, be simplified by assuming a linear variation of V along the y-direction. As a result, V_0 is equal to $(V_A + V_B)/2$.

The total power P is determined by adding up contributions P_i from all partitioned subregions. In the spectral domain, an explicit formulation of P_i can be derived in terms of the field components in the u-v coordinate system:

$$P_i = \frac{1}{2a_i}\sum_{n=-\infty}^{+\infty}\underbrace{\begin{pmatrix} \frac{\beta}{\omega\mu_0} & \frac{\omega\varepsilon\beta}{\gamma^2} & \frac{\alpha}{\omega\mu_0} \end{pmatrix}_n^i}_{\bar{\bar{c}}} \cdot \underbrace{\begin{pmatrix} P_a \\ P_b \\ P_c \end{pmatrix}_n^i}_{\bar{p}} \tag{2.12}$$

where

$$\begin{aligned} P_a &= (|E_u^-|^2 + |E_u^+|^2)\cdot\frac{sh(2\gamma h)-2\gamma h}{4\gamma\cdot sh^2(\gamma h)} + E_u^-\cdot E_u^+\cdot\frac{\gamma h\cdot[1-sh(\gamma h)]}{sh(\gamma h)\cdot th(\gamma h)} \\ P_b &= (|E_v^-|^2 + |E_v^+|^2)\cdot\frac{sh(2\gamma h)+2\gamma h}{4\gamma\cdot sh^2(\gamma h)} - E_v^-\cdot E_v^+\cdot\frac{\gamma h\cdot[1+sh(\gamma h)]}{sh(\gamma h)\cdot th(\gamma h)} \\ P_c &= \frac{1}{\gamma\cdot th(\gamma h)}\left(E_u^-\cdot E_v^- + E_u^+\cdot E_v^+ - (E_u^-\cdot E_v^+ + E_u^+\cdot E_v^-)\cdot\frac{1}{ch(\gamma h)}\right) \end{aligned} \tag{2.13}$$

In these equations, $E_{u,v}^{+,-}$ are known field quantities defined in the i^{th} subregion, which are directly related to the original fields in the x-z coordinate system through a simple rotation [6]. Obviously, a simple and easy-to-handle formulation is proposed for power calculation that is usually lengthy. This is in particular meaningful in the case of complex multilayer structures considering finite thickness of metals, supporting grooves and pedestals.

2.2.3 Numerical Convergence

Prior to showing examples of this new algorithm, it is useful to examine inherent behavior of numerical convergence. The Galerkin's technique requires that unknown

tangential electric fields at boundary apertures of the i^{th} subregion be expanded in terms of a complete set of basis functions such that

$$\begin{pmatrix} E_x \\ E_z \end{pmatrix}^i = \begin{pmatrix} \sum_{q=1}^{+\infty} \eta_q \cdot f_q(x) \\ \sum_{s=1}^{+\infty} \zeta_s \cdot g_s(x) \end{pmatrix}^i \tag{2.14}$$

where η_q and ζ_s are the weighted coefficients to be determined. It is known that a good convergence towards exact results can only be achieved by choosing appropriate basis functions which correctly describe the field singularity at relevant conductor edges. Due to the difference of convergence rate between the expanded basis functions and their Fourier series , the basis functions satisfying the edge conditions should be considered to yield efficient calculation with a low order of matrix equation. In this work, a set of sinusoidal basis functions modified by an edge condition term [16] is used in the analysis. The Fourier transform of the basis functions for the symmetrical case, to name an example, is given by

$$\begin{aligned} \tilde{f}_q(\alpha) &= (-1)^{q-1} \frac{\pi w}{4} \left(J_0\left(\alpha \frac{w}{2} + (q-1)\pi \right) + J_0\left(\alpha \frac{w}{2} - (q-1)\pi \right) \right) \\ \tilde{g}_s(\alpha) &= (-1)^{s-1} \frac{j\pi w}{4} \left(J_0\left(\alpha \frac{w}{2} + s\pi \right) - J_0\left(\alpha \frac{w}{2} - s\pi \right) \right) \end{aligned} \tag{2.15}$$

with J_0 being the zero-order Bessel function of the first kind. The index n denoting the spectral terms is ignored in (2.15) for simplicity. The choice of the limiting spectral term for the basis functions mainly depends on the convergence nature of $\tilde{f}_q$. It is easily found that the asymptotic behavior of $\tilde{f}_q$ is in accordance with $\alpha^{-0.5}$ as $n \to \infty$. This suggests

that the relative convergence criterion such that $N_k / N_i = C \cdot a_k / a_i$ as already discussed in [15] should be fulfilled for any adjoining subregions in which N_k and N_i are the limiting spectral terms for the basis functions defined in the subregions a_k and a_i, respectively. The coefficient C is then determined by the relative field intensity regarding the relevant adjoining subregions, thereby depending on the structural parameters as well as the spectral terms. The value of C falls usually into the range of 0.2 to 5. C is larger than 1 as a_k / a_i is smaller than 1, for example. In general, the convergence behavior of the propagation constant and characteristic impedance is different with respect to the spectral terms for a given number of the basis functions. This will be discussed subsequently.

2.3 Numerical Examples

In the following, asymmetrical finlines are analyzed as examples to demonstrate performance and applications of the proposed approach. The basis functions used throughout the paper are truncated at q=3 and s=2, which turn out to be sufficient. To begin with, frequency-dependent characteristics of the finline depicted in Fig. 2.2 are calculated and shown in Table 2.1. Our results are in excellent agreement with [9, 15], thereby validating the proposed approach. Fig. 2.3 shows dispersion curves and characteristic impedance of the dominant mode for a bilateral finline with three different thickness of lines. The results for the zero thickness agree well with [16]. The computer program is implemented in a PC486 with 50 MHz clock speed. The CPU time is about 2 seconds per frequency sample.

The effect of the modal voltages $((V_A, V_B, V_0))$ defined at different positions across the slot on the characteristic impedance is illustrated in Fig. 2.4. The results indicate that

the relative deviation of characteristic impedance increases linearly with the thickness of conductors. As expected, such an effect is more pronounced at higher frequencies. Obviously, the difference of modal voltages is attributed to the integral path over different intensity of electric field across the slot with finite thickness. On the other hand, the difference in convergence behavior between the propagation constant and characteristic impedance is exhibited in Fig. 2.5 for the asymmetrical finline(see Fig. 2.2). The number of spectral terms in subregions other than "t" is set to be 600, while the reference values of β_0 and Z_0 is obtained as $n_2 = 600$. It is observed that the convergence rate of β_0 is more rapid as a function of the spectral term than that of Z_0. This indicates that power spectrum are widely spread over a large range of terms. The slow convergence of power calculation compared to the dispersion analysis may be explained by involving the "double" field singularity such as $E_x \times H_y$. Nevertheless, Fig. 2.5 suggests that sufficiently accurate results are obtained for the given structure as n_2 exceeds 40.

Table 2.1 Comparison of calculated and measured frequency-dependent results for guided wavelength of the asymmetrical finline. Structural parameters: $w = 1.25$ mm, $d = 0.254$ mm, $\varepsilon_r = 9.9$, $a_1 = 4.42$ mm, $a_2 = 6.42$ mm, $t = 0$ mm, $h_1 = 5.41$ mm, $h_2 = 5.16$ mm.

Frequency (GHz)	Measured λ_g (mm)	Calculated λ_g (mm)		
		[15]	[9]	This work
17.6	12.50	12.42	12.37	12.37
18.0	12.09	12.07	12.02	12.02
18.4	11.75	11.73	11.68	11.68
18.8	11.46	11.42	11.37	11.37
19.2	11.18	11.17	11.07	11.07
19.6	10.94	10.83	10.78	10.78
20.0	10.62	10.56	10.51	10.51

Fig. 2.6 presents dispersion characteristics including the first higher-order mode and characteristic impedance by considering the effect of finite metallization thickness. It is shown that the influence of the finite thickness is significant on the characteristic impedance over the frequency band of interest. Increasing the metallization thickness decreases the propagation constant and characteristic impedance of the dominant mode. However, the cutoff frequency of the first higher-order mode in the case of $t = 100\ \mu m$ moves slightly upwards compared to the case of $t = 50\ \mu m$. This may stem from an opposite field perturbation in the y-direction by the separation of housing and concerned metallization thickness. The dispersion curves and characteristic impedance are plotted in Fig. 2.7 for different housing separation (or contrast of the shielding). In this case, the results considering the effect of finite thickness display similar dispersion characteristics as in [15] for the situation of vanishing thickness. The increase in the housing separation pulls downwards the cutoff frequency of the first higher-order mode for the given structure. Shown in Fig. 2.8 are the dispersion and characteristic impedance of the even- and odd-modes against different slot widths for a coupled asymmetrical finline with finite thickness. Of course, In contrast to the odd-mode, nearly dispersionless characteristics are observed for the even-mode (quasi-TEM mode) over the frequency of interest.

2.4 Conclusion

A novel strategy of using the spectral-domain approach called the enhanced SDA is proposed for accurate theoretical characterization of generalized planar multilayer and multiconductor structures. The approach is formulated by combining the conventional SDA in homogeneous zones and the power conservation theorem at interfaces of

different zones. The principal features of the proposed approach are to simplify the derivation of Green's function and extend the inherent advantages of the existing SDA into handling practical complex structures considering finite metallization thickness, housing grooves/separation, and pedestals. The algorithm is easily implemented on a personal computer. A unified yet easy-to-use power formulation is also derived to determine the characteristic impedance for design consideration. The work features a study on convergence characteristics of the propagation constant and impedance. With the power conservation, the limiting number of spectral terms in each subregions can be chosen independently, thereby providing the possibility of reducing drastically calculation expense in terms of memory size and CPU time. Applications of the validated method are demonstrated through calculation and analysis of various asymmetrical finlines. It is believed that the proposed approach can find applications in CAD of a wide range of quasi-planar circuits.

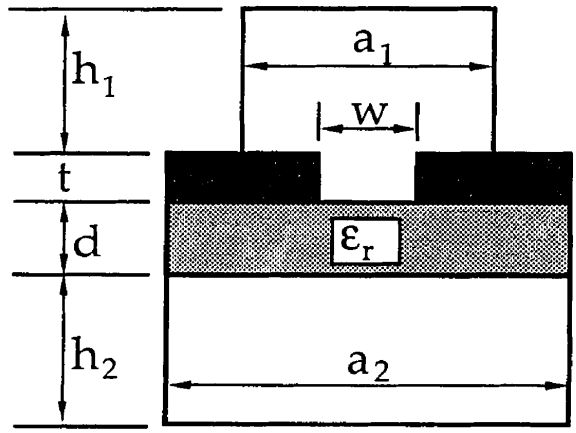

Fig. 2.2 Structure and dimensions of the asymmetrical finline.

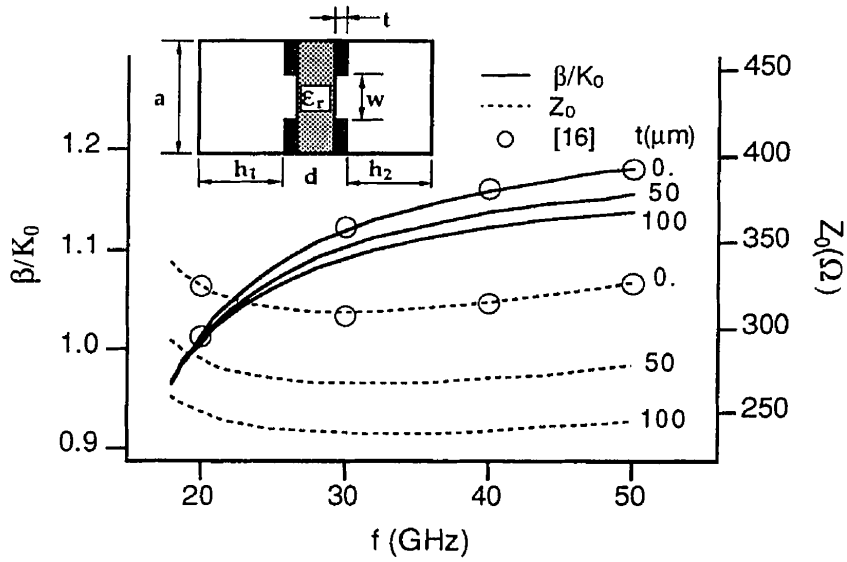

Fig. 2.3 Dispersion characteristics of the normalized propagation constant and characteristic impedance versus different finite thickness of metallization for a bilateral finline with parameters: w=0.3 mm, d=0.125 mm, ε_r=3.75, a=3.556 mm, $h_1+t=h_2+t$=3.431. mm.

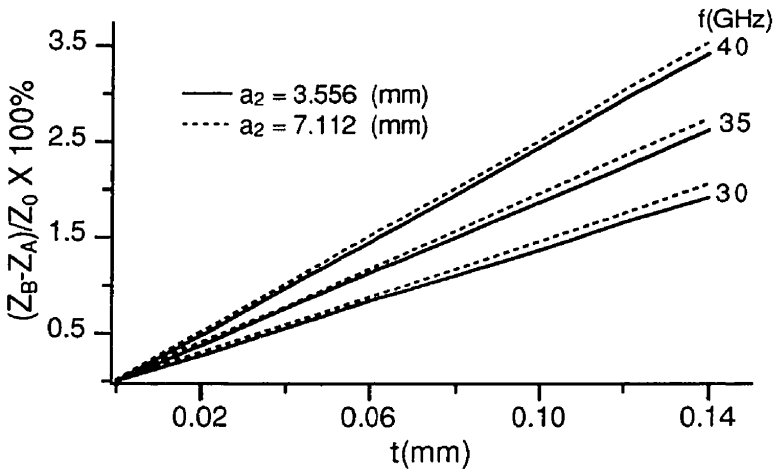

Fig. 2.4 Relative deviation of the characteristic impedance as a function of the metallization thickness for different definition of voltage in terms of field path integral in the finline (see Fig. 2.2). w=0.2 mm, d=0.254 mm, ε_r=3.75, a_1=3.556 mm, $h_1=h_2+t$=3.431 mm.

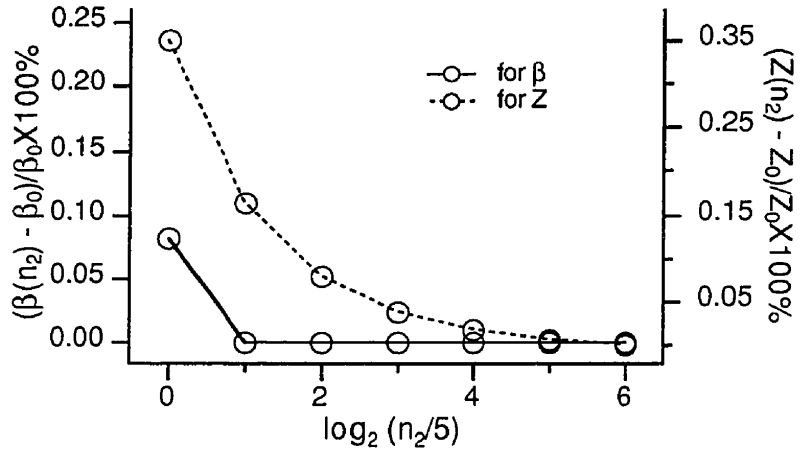

Fig. 2.5 Convergence behavior of the propagation constant and characteristic impedance versus the limiting number of spectral terms n_2 in Fig. 2.2 with w=0.4 mm, d=0.254 mm, ε_r=3.75, a_1=3.556 mm, a_2=7.112 mm, t=0.1 mm, $h_1=h_2+t$=3.431 mm, f=35 GHz.

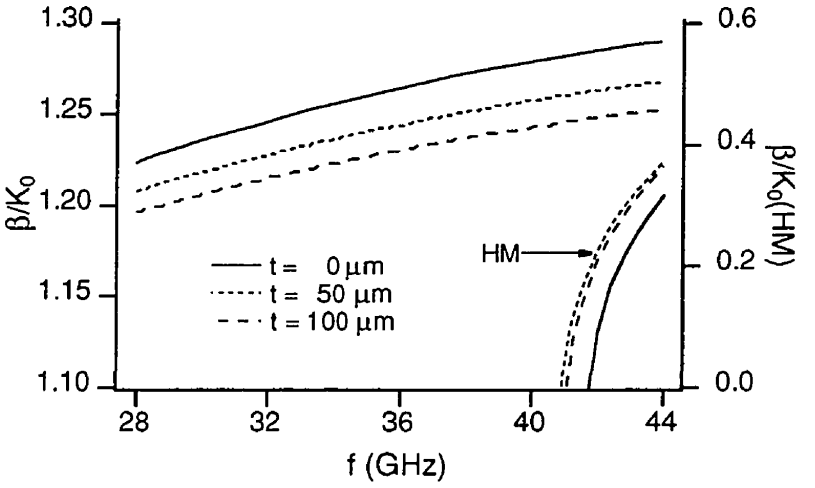

(a)

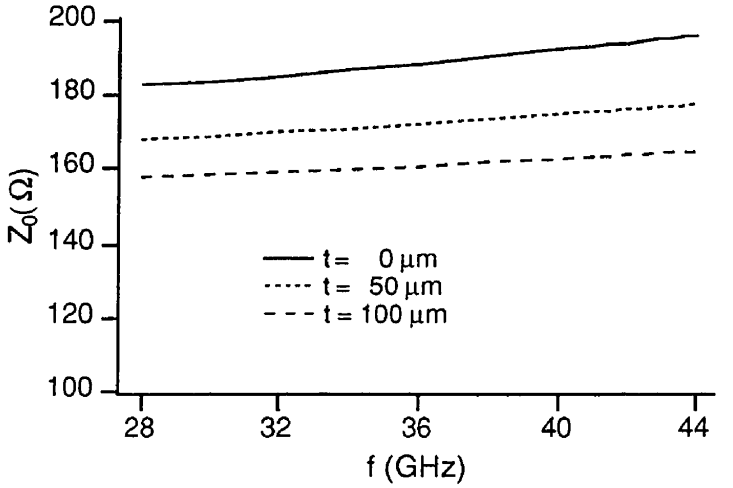

(b)

Fig. 2.6 Dispersion characteristics for different thickness of metallization of the asymmetrical finline (see Fig. 2.2) with w=0.4 mm, d=0.254 mm, ε_r=3.75, a_1=3.556 mm, a_2=7.112 mm, $h_1=h_2+t$=3.431 mm, (HM refers to the first higher-order mode). (a) Normalized propagation constant. (b) Characteristic impedance.

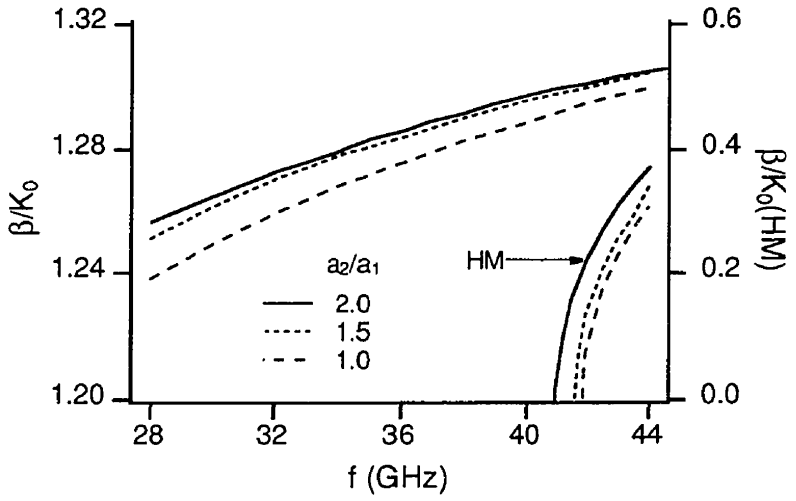

(a)

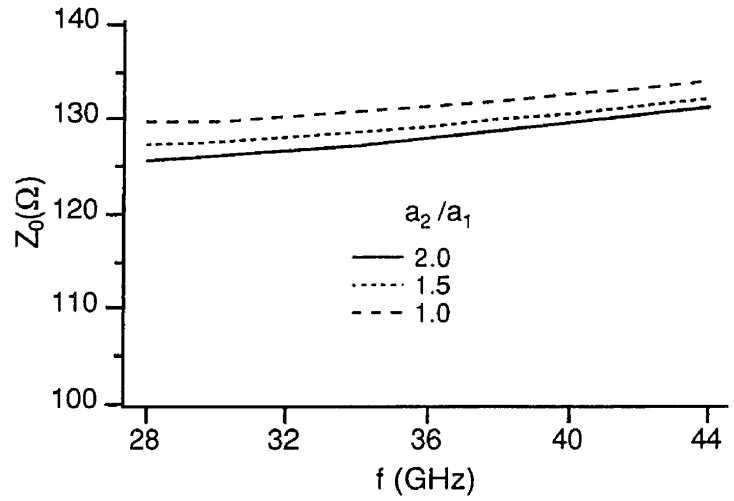

(b)

Fig. 2.7 Frequency-dependent characteristics for different dimension ratio a_2/a_1 described in the asymmetrical finline (see Fig. 2.2) with w=0.2 mm, d=0.254 mm, ε_r=3.75, a_1=3.556 mm, t=0.05 mm, $h_1=h_2+t$=3.431 mm. (HM refers to the first higher-order mode). (a) Normalized propagation constant. (b) Characteristic impedance.

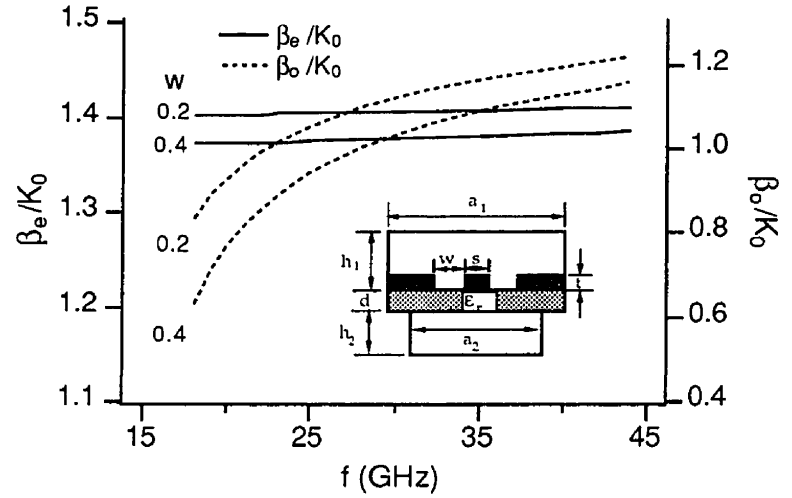

(a)

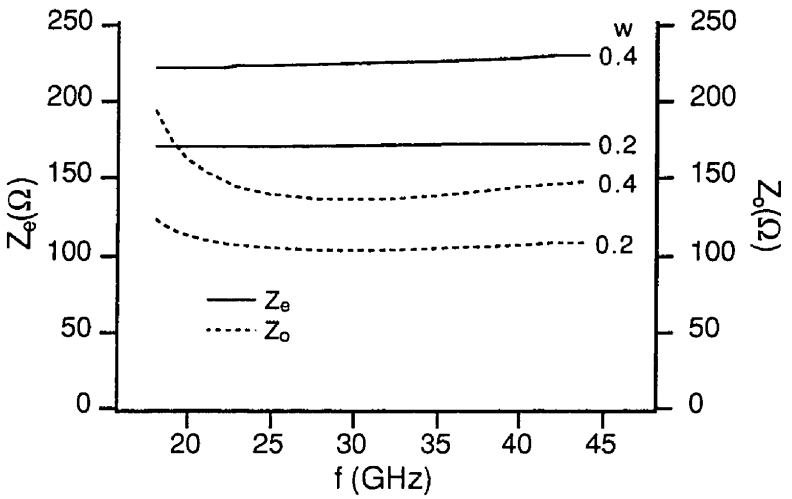

(b)

Fig. 2.8 Dispersion characteristics of an asymmetrical coupled finline for different slotwidth with d=0.254 mm, ε_r=3.75, a_1=3.556 mm, a_2=2 mm, t=0.05 mm, $h_1=h_2+t$=3.431 mm, s=0.2 mm, (the letters "e" and "o" denote the even mode and the odd mode, respectively). (a) Normalized propagation constant. (b) Characteristic impedance.

References

[1] A. Beyer, "Analysis of the characteristics of an earthed fin line," *IEEE Trans. Microwave Theory Tech.*, vol. MTT-29, pp. 676-680, July 1981.

[2] R. R. Mansour and R. H. Macphie "A unified hybrid-mode analysis for planar transmission lines with multilayer isotropic/anisotropic substrates," *IEEE Trans. Microwave Theory Tech.*, vol. MTT-35, pp.1382-1391, December 1987.

[3] J. Bornemann and F. Arndt, "Calculating the characteristic impedance of finlines by transverse resonance method," *IEEE Trans. Microwave Theory Tech.*, vol. MTT-34, pp.85-92, January 1986.

[4] J. Bornemann, "A Scattering-type transverse resonance technique for the calculation of (M)MIC transmission line characteristics," *IEEE Trans. Microwave Theory Tech.*, vol. MTT-39, pp.2083-2088, Dec. 1991.

[5] Uwe Schulz and R. Pregla,"A new technique for the analysis of the dispersion characteristics of planar waveguides," AEU, Band 34, Helt 4, pp.169-173, 1980.

[6] T. Itoh, "Spectral domain immitance approach for dispersion characteristics of generalized printed transmission lines," *IEEE Trans. Microwave Theory Tech.*, vol. MTT-28, pp. 733-736, July 1980.

[7] C. M. Krowne, "Fourier transformed matrix method of finding propagation characteristics of complex anisotropic layered media," *IEEE Trans. Microwave Theory Tech.*, vol. MTT-32, pp.1617-1625, December 1984.

[8] R. H. Jansen, "The spectral-domain approach for microwave integrated circuits," *IEEE Trans. Microwave Theory Tech.*, vol. MTT-33, pp. 1043-1056, Oct. 1985.

[9] C. H. Chan, K. T. Ng, and A. B. Kouki, "A mixed spectral-domain approach for dispersion analysis of suspended planar transmission lines with pedestals,"

IEEE Trans. Microwave Theory Tech., vol. MTT-37, pp. 1716-1723, November 1989.

[10] K. T. Ng and C. H. Chan, "Unified solution of various dielectric-loaded ridge waveguides with a mixed spectral-domain method," *IEEE Trans. Microwave Theory Tech.*, vol. MTT-37, pp. 2080-2085, December 1989.

[11] T. Kitazawa, D. Polifko, and H. Ogawa, "Analysis of CPW for LiNbO3 optical modulator by extended spectral-domain approach," *IEEE Microwave and Guided Wave Letters*, vol. 2, no. 8, pp. 313-315, August 1992.

[12] T. Kitazawa et al., "Planar transmission lines with finitely thick conductors and loss substrates," 1991 *IEEE* MTT-S digest, pp.769-772.

[13] T. Kitazawa, "Analysis of shielded striplines and finlines with finite metallization thickness containing magnetized ferrites," *IEEE Trans. Microwave Theory Tech.*, vol. MTT-39, pp. pp.70-74, Jan. 1991.

[14] F. L. Mesa, R. Marqués, and M. Horno, "A general algorithm for computing the bidimensional spectral Green's dyad in multilayered complex bianisotropic media: the equivalent boundary method," *IEEE Trans. Theory Tech.*, vol. MTT-39, pp. 1640-1649, September 1991.

[15] P. Espes, P. F. Combes, J.-M. Goutoule, and B. Theron, "Asymmetrical finline for space applications using millimeter waves," *IEEE Trans. Microwave Theory Tech.*, vol. MTT-37, pp.289-298, February 1989.

[16] L. P. Schmidt and T. Itoh, "Spectral domain analysis of dominant and higher order modes in fin-lines," *IEEE Trans. Microwave Theory Tech.*, vol. MTT-28, pp. 981-985, September 1980.

Chapitre III

Caractéristiques de lignes à fentes couplées avec différent type de montage

Comme plus d'efforts ont été concentrés sur les circuits intégrés hybrides et monolithiques micro-ondes et en ondes millimétriques, l'intérêt pour les lignes de transmission de type coplanaire a été renouvelé. Parallèlement, diverses lignes à fentes incluant des configurations couplées ont été intensément utilisées dans le développement de composant fonctionnel tel que des filtres, des coupleurs directifs, des dispositifs à ferrite. Comparé aux lignes micro-rubans, le principal avantage des circuits coplanaires résident dans la facilité d'insertion de composants actifs ou passifs connectés aussi bien en série qu'en parallèle.

Les lignes couplées à fentes sont constituées de deux fentes, donc de trois parties conductrices. Un ruban centrale est placé à la surface du diélectrique avec deux demi-plans métalliques de part et d'autre. Il peut véhiculer deux modes orthogonaux dominant. Ils sont typiquement appelés, dans les configurations symétriques, modes pair et impair. Ces deux modes dominant sont des modes hybrides bien que le mode pair soit quasi-TEM. Le guide d'onde coplanaire inventé par C. P. Wen peut être considéré comme une ligne à fentes couplée spéciale dans laquelle le mode impair est supprimé.

La ligne de transmission coplanaire utilise seulement une seule face du substrat. Dans sa forme originale, aucun conducteur n'est présent sur l'autre face. Cependant, en pratique, les circuits coplanaires sont placés sur un support métallique plan pour satisfaire des nécessités d'ordre mécanique formant ainsi une topologie avec plan de masse. Les performances électriques avec plan de masse ont été étudiées par un grand nombre de chercheurs. Il a été trouvé que ce type de structure possède un certain nombre d'inconvénient tels que des phénomènes de pertes, de conversion d'un mode à l'autre, et de résonances multiples, susceptible de dégrader les performances électriques d'une structure opérant à hautes fréquences. Afin de palier et d'éviter ces problèmes, une configuration avec substrat suspendu est préférable. Dans une structure coplanaire suspendue, le montage sur rainure est habituellement utilisé pour supporter mécaniquement le substrat. Malheureusement, la structure avec rainure présente des désavantages intrinsèques. La présence des rainures est responsable d'une diminution significative de largeur de bande. D'autre part, l'isolation électrique et l'efficacité des demi-plans de masse sont affectées par la présence du plan de support métallique. La réalisation mécanique précise du plan de support est requise pour assurer que le diélectrique est correctement suspendu. Ce chapitre traite des caractéristiques des lignes à fentes couplées suspendues. Deux nouvelles stratégies de montages suspendus sont proposées, l'une avec socle et l'autre avec socle inversé. La méthode spectrale perfectionnée décrite dans le chapitre II est utilisée pour déterminer les caractéristiques de propagation des modes fondamentaux et des modes d'ordres supérieurs dans le cas de lignes à fentes couplées suspendues avec socle ou rainure ou socle inversé. Les effets des différents schémas de montage sur la fréquence de coupure des premiers modes d'ordres supérieurs, et des modes pairs et impairs des lignes à fentes couplées sont étudiés. Les profils des champs des modes fondamentaux des lignes à fentes couplées

supportées par des socles de différentes tailles sont illustrés. Le corps de ce chapitre est présenté par un article publié en mai 1995 dans la revue IEEE Transaction of Microwave Theory and Techniques.

Effects of Various Suspended Mounting Schemes on Mode Characteristics of Coupled Slotlines Considering Conductor Thickness for Wideband MIC Applications

Tongqing WANG, and Ke WU, Senior Member, IEEE

Groupe de Recherches Avancées en Microondes et en Électronique Spatiale

(POLY-GRAMES)

Dept. de génie électrique et de génie informatique

École Polytechnique

C. P. 6079, Succ. "A", Montréal, Canada H3C 3A7

Abstract

Propagation characteristics of fundamental and higher-order modes are determined in coupled slotlines with three suspended mounting schemes (pedestal, groove, inverse pedestal) for wideband applications of microwave and millimeter-wave integrated circuits. The analysis is based on a novel enhanced spectral domain approach (ESDA) that combines essentially the conventional spectral domain technique with the power conservation theorem. Numerical results, considering also the influence of finite conductor thickness, are presented for propagation constants and characteristic impedance of the fundamental modes. Effects of different suspended mounting schemes on cutoff frequencies of first higher-order even and odd modes are discussed in detail. Field profiles of the fundamental modes in coupled slotlines with and without pedestals are shown. The inherent mechanism of mode transition is explained with respect to different pedestal sizes, indicating that the monomode bandwidth can be extended by appropriately choosing the dimension of pedestal in coupled slotlines.

3.1 Introduction

Over the last decade, coplanar-type transmission lines have widely been used in microwave and millimeter-wave hybrid and monolithic integrated circuits as an alternative to microstrip lines. Parallelly, various slotlines including coupled geometry become fundamental transmission media in miniature planar MIC's. Compared to the microstrip line, the main advantages of these lines are that they allow easy implementation of active and passive devices both in series and shunt connections, thereby eliminating the need for via holes and thin substrate, and thus simplifying the fabrication process, as well as permitting direct on-wafer measurements. It is also possible to reduce the parasitic inductance due to the grounded three-terminal devices. In addition, it offers low dispersion and additional degree of freedom for a wide range of characteristic impedance [1,2].

Coplanar waveguide is considered as a special coupled slotline in which the odd mode (with respect to the currents on two side planes) is suppressed. Recent theoretical investigation on coplanar structures is essentially focused on propagation characteristics and discontinuities [2-6]. In practice, a coplanar microwave and millimeter-wave integrated circuit is usually placed on a metallic plane for mechanical support, thus forming a conductor-backed topology. This structure suffers from potential problem of leakage and mode conversion due to interaction among various modes [7,8]. Apart from causing an energy loss of the fundamental mode, the leaky power may be coupled with other parts of the circuit, producing some unexpected electrical effects. Electrical performance of the conductor-backed coplanar waveguides (CBCPW's) have been studied by a number of researchers. An integral equation technique was used to determine the possible mode conversion at the open end in

finite-width CBCPW's [9]. High-order mode profiles for the CBCPW's with bilaterally shielded via-holes were shown and the possible monomode bandwidth was assessed theoretically and confirmed experimentally in [10]. Resonant phenomena in CBCPW's have been also analyzed theoretically and experimentally in [11]. These drawbacks, which deteriorate electrical performance of the CPW structures at higher frequency, can be eliminated by suspended mounting in a shielded rectangular box. In suspended coplanar structure, however, the mounting grooves are usually required. As pointed out in [12-14], the structure with mounting grooves has some intrinsic disadvantages. The mounting grooves make the monomode bandwidth significantly decreased. On the other hand, electrical isolation and grounding are affected due to the split housing. The precise machining of the housing is needed to ensure that the dielectric is properly supported. Note that this kind of structure is not well suited for applications in today's fast developed MMIC technology because the GaAs substrate is relatively thin and fragile.

In order to preserve the advantages of the housing and overcome these shortcomings, two novel mounting strategies with pedestal and inverse pedestal are proposed in this paper as shown in Fig. 3.1. From the viewpoint of numerical analysis, a general structure illustrated in Fig. 3.2 is considered. In order to increase a certain degree of freedom in design aspects, the septum located at the other side of the substrate is introduced. Obviously, the structure of Fig. 3.2 includes all three structures of Fig. 3.1 that consider also the finite thickness of planar conductors. The electrical effect of the finite conductor thickness may be significant at millimeter-wave frequencies, which will be incorporated in the following analysis.

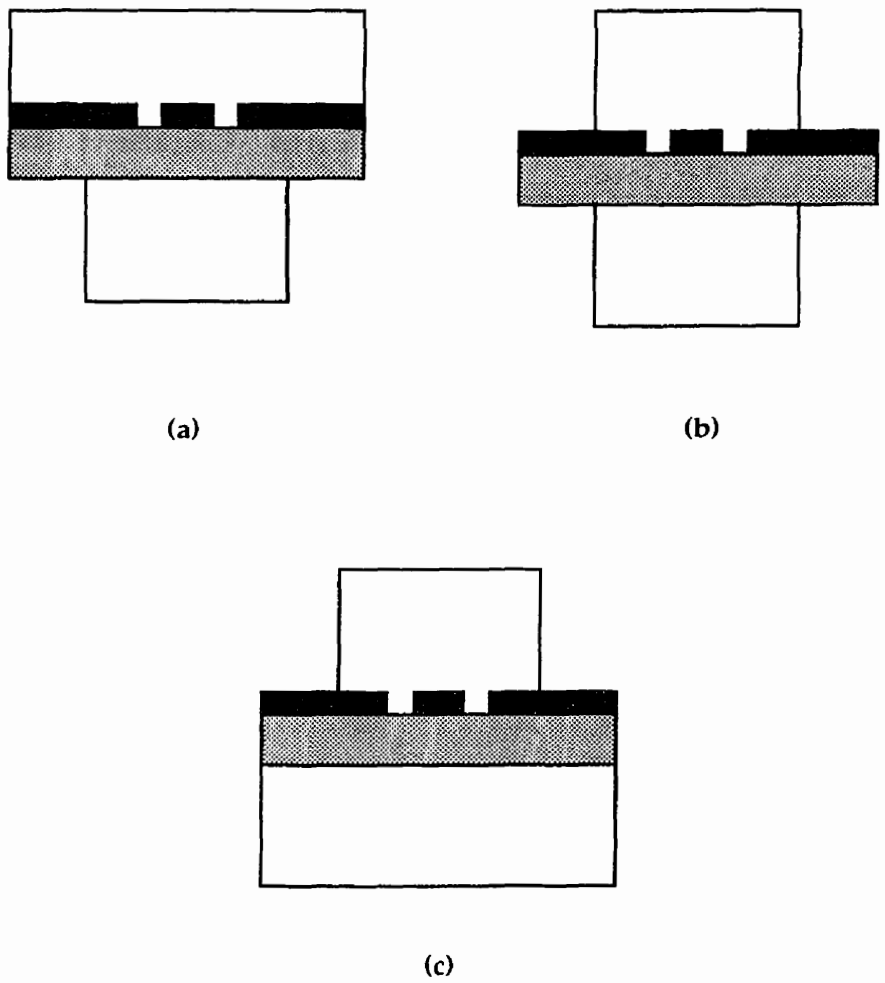

Fig. 3.1 Coupled slotlines with various suspended mountings: (a) pedestal, (b) groove, and (c) inverse pedestal.

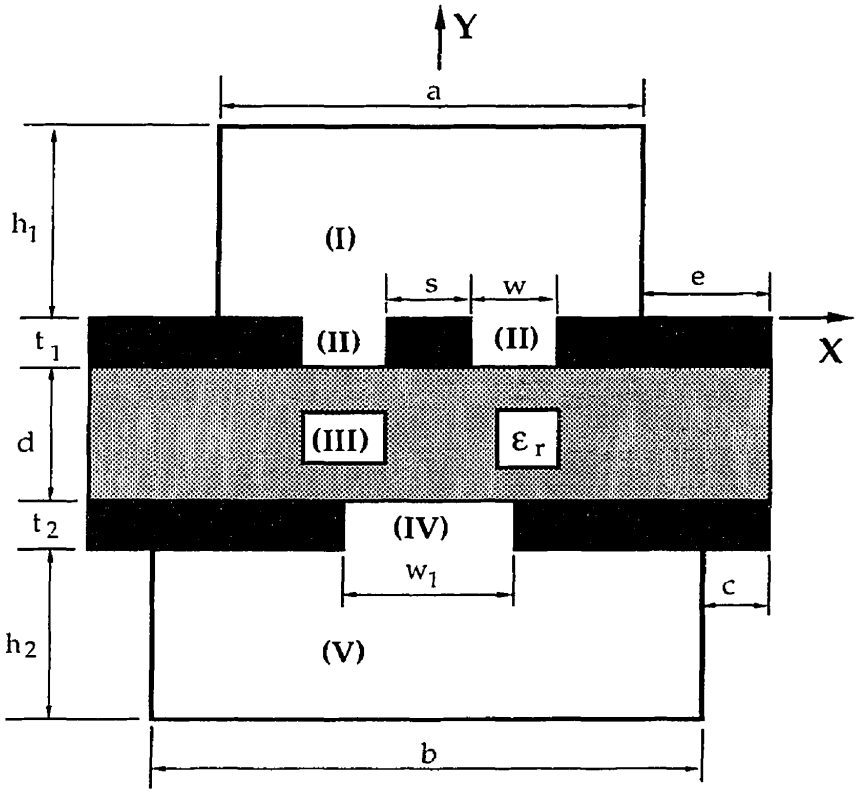

Fig. 3.2 Generalized coupled slotline with septum.

The coupled slotline structure shown in Fig. 3.2 is quite complicated. Therefore, accurate full-wave analysis of its propagation characteristics is the key to its successful practical applications. Although different numerical techniques for solving guided-wave characteristics of these structures have recently been proposed, most of them usually present a compromise between accuracy and efficiency of numerical results as well as application range. In this work, a novel enhanced spectral-domain approach is

developed to determine propagation characteristics of the structure as shown in Fig. 3.2. Compared to the conventional and other modified SDA, the proposed technique is more efficient in terms of analytical effort and numerical accuracy. This is done by avoiding the usually lengthy derivation of the Green's function matrix for complex structures. In addition, this technique features an independent choice of truncated spectral terms in each subregion. Therefore, this method is in particular suitable for the analysis of structures containing a large ratio of lateral widths in adjacent subregions. This is the unmatched advantage over the mode-matching method in solving the same problems. The method is general and easy to handle for programming.

In this paper, numerical results are presented for propagation constants and characteristic impedances of the fundamental modes. Effects of different suspended mounting schemes on cutoff frequencies of first higher-order even- and odd-modes are discussed. Field profiles are shown in an effort to understand better the propagation mechanism of coupled slotlines with pedestal. Mode transition in coupled slotlines against different pedestal sizes is also explained in detail.

3.2 Theory

The enhanced SDA is based on a strategy of combining conventional SDA with the power conservation theorem. More precisely, tangential magnetic field at both boundaries of each stratified subregion (homogeneous dielectric layer) can be expressed in terms of its electric counterpart. On the other hand, the boundary conditions at the interfaces are satisfied by imposing the power conservation theorem in the space domain. A detailed description of the newly developed method for analysis of generalized planar structures will be presented somewhere else [15]. Therefore, only

some highlights are outlined here. At first, as usually done in spectral domain analysis, all conductors are assumed to be electrically perfect. In Fig. 3.2, the whole structure may be divided into five homogeneous rectangular subregions which are interconnected to each other and bounded by lateral conducting walls. Electromagnetic fields in each subregion can be expanded in the spectral domain, such as

$$\begin{pmatrix} \vec{E} \\ \vec{H} \end{pmatrix}^i = \sum_{n=-\infty}^{+\infty} \begin{pmatrix} \tilde{\vec{E}}(y) \\ \tilde{\vec{H}}(y) \end{pmatrix}_n^i \cdot e^{-j(\alpha_n^i \cdot x + \beta \cdot z)} \tag{3.1}$$

where

$$\begin{pmatrix} \tilde{\vec{E}}(y) \\ \tilde{\vec{H}}(y) \end{pmatrix}_n^i = \frac{1}{a_i} \int_{a_i} \begin{pmatrix} \vec{E} \\ \vec{H} \end{pmatrix}^i \cdot e^{j(\alpha_n^i \cdot x + \beta \cdot z)} \cdot dx \tag{3.2}$$

and

$$\alpha_n^i = \begin{cases} \dfrac{(2n-1)\pi}{a_i} & \textit{for} \text{ even - mode} \\ \dfrac{2n\pi}{a_i} & \textit{for} \text{ odd - mode} \end{cases} \tag{3.3}$$

(n) refers to the spectral term; a_i is the width of all possible subregions $(a, w, a+2e, w_1, b)$; and (i) stands for the subregions (I, II, III, IV, V). Note that the even and odd field expansions are only related to the subregions encompassing the symmetric plane excluding the finite conductor thickness gaps (II).

With the help of the conventional spectral-domain analysis, two matrix equations which relate the tangential electric fields to the magnetic counterparts at lower and upper boundary apertures are obtained, such that

$$\begin{pmatrix} \tilde{H}_x^- \\ -\tilde{H}_z^- \end{pmatrix}_n^i = \frac{1}{j\omega\mu_0\gamma}\begin{bmatrix} \gamma^2-\beta^2 & -\alpha\cdot\beta \\ -\alpha\cdot\beta & \gamma^2-\alpha^2 \end{bmatrix}_n^i \left\{ \frac{1}{th(\gamma\cdot h)}\begin{pmatrix} \tilde{E}_z^- \\ \tilde{E}_x^- \end{pmatrix} - \frac{1}{sh(\gamma\cdot h)}\begin{pmatrix} \tilde{E}_z^+ \\ \tilde{E}_x^+ \end{pmatrix} \right\}_n^i \tag{3.4}$$

and

$$\begin{pmatrix} \tilde{H}_x^+ \\ -\tilde{H}_z^+ \end{pmatrix}_n^i = \frac{1}{j\omega\mu_0\gamma}\begin{bmatrix} \gamma^2-\beta^2 & -\alpha\cdot\beta \\ -\alpha\cdot\beta & \gamma^2-\alpha^2 \end{bmatrix}_n^i \left\{ \frac{1}{sh(\gamma\cdot h)}\begin{pmatrix} \tilde{E}_z^- \\ \tilde{E}_x^- \end{pmatrix} - \frac{1}{th(\gamma\cdot h)}\begin{pmatrix} \tilde{E}_z^+ \\ \tilde{E}_x^+ \end{pmatrix} \right\}_n^i \tag{3.5}$$

where the superscripts (-) and (+) denote the lower and upper apertures.

In the space domain, the tangential electric and magnetic fields should satisfy the boundary and continuity conditions at interfaces. On the basis of the complementary property between $\bar{E}_t$ and $\bar{J}_t$ at interfaces, the power conservation in the transverse direction should hold, which is determined by the following equation,

$$\int (\bar{E}_t^- \times \bar{H}_t^{-*}) \cdot dx = \int (\bar{E}_t^+ \times \bar{H}_t^{+*}) \cdot dx \tag{3.6}$$

Invoking Parseval's theorem in (3.6) and substituting (3.4) and (3.5) into (3.6), a set of linear homogeneous equations is derived. The propagation constant β can be obtained simply through the application of Galerkin's technique.

In spectral domain analysis, the selection of basis function is important in order to obtain effective numerical computation. Following the work in [16,17], the tangential electric fields at interfaces in Fig. 3.2 are expanded in terms of the functions

$$\begin{bmatrix} E_x \\ E_z \end{bmatrix} = \sum_{m=1}^{N} \frac{1}{\sqrt{1-\left(\frac{x}{w/2}\right)^2}} \begin{bmatrix} C_{xm}\cdot\cos\left[\frac{m-1}{2}\pi\left(\frac{x}{w/2}-1\right)\right] \\ C_{zm}\cdot\sin\left[\frac{m-1}{2}\pi\left(\frac{x}{w/2}-1\right)\right] \end{bmatrix} \qquad \textit{For} \text{ coupled slot} \qquad (3.7)$$

and

$$\begin{bmatrix} E_x \\ E_z \end{bmatrix} = \sum_{l=1}^{L} \frac{1}{\sqrt{1-\left(\frac{x}{w_1/2}\right)^2}} \begin{bmatrix} D_{xl}\cdot\cos\left[(m-k_0)\pi\left(\frac{x}{w_1/2}-1\right)\right] \\ D_{zl}\cdot\sin\left[(m-k_0)\pi\left(\frac{x}{w_1/2}-1\right)\right] \end{bmatrix} \qquad \textit{For} \text{ pedestal or septum} \qquad (3.8)$$

in which $k_0 = 0.5$ and 1 for the even and odd modes, respectively. It should be noted that the first term of E_z in (3.7) and (3.8) for odd-mode is equal to zero and it is not included in numerical computations. However, it yields a better presentation for the number of basis function considered in the analysis. Characteristic impedances based on the voltage-power definition are calculated for design considerations [18].

3.3 Results

To examine the accuracy of the proposed method, Fig. 3.3 shows frequency-dependent normalized propagation constants and characteristic impedances of both even- and odd- modes for conventional coupled slotlines with different thickness of metallization which denotes $t_1 = 10,\ 50,$ and $100\ \mu m$. Our results promise a good agreement with those

obtained in [12] using the mode-matching method with conservation of complex power technique. The results indicate that the metallization thickness has a significant effect on the propagation characteristics of the fundamental modes.

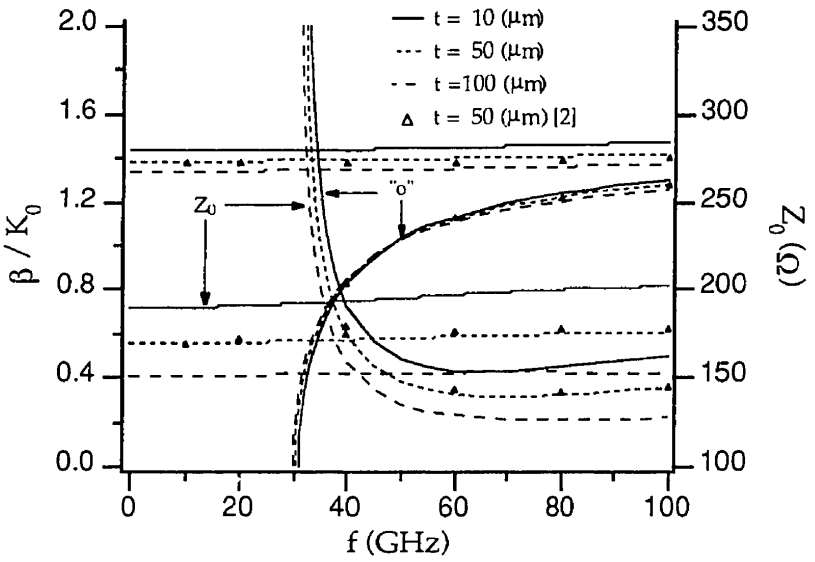

Fig. 3.3 Normalized propagation constants and characteristic impedances of even- and odd-modes versus frequency for different metallization thichness in coupled slotline : $a = b = 1.55$ mm, $h_1 + t_1 = h_2 = 1.44$ mm, $w = s = 0.2$ mm, $d = 0.22$ mm, $t_2 = e = c = 0$ mm, $\varepsilon_r = 3.75$, "o" stands for the odd-mode.

Fig. 3.4 illustrates the effect of the mountings with and without pedestal on the normalized propagation constant and characteristic impedance for the even- and odd-modes as a function of frequency in coupled slotline. It is observed that the effect of choosing different mounting on the even-mode is not significant. This can well be explained by the fact that the field of the even-mode is mainly restricted around the slot region. At low frequencies, the effect of the pedestal mounting on the even-mode is more visible than that of the inverse pedestal. At higher frequencies beyond 22 GHz as

shown in the figure, the characteristic impedance of the pedestal mounting is slightly higher than that of the inverse pedestal mounting. This is because the field is more confined toward the slot region with higher frequencies. As can be expected, the effect of various mounting schemes on the odd-mode is significant. At higher frequencies, the characteristic impedance of the pedestal mounting is lower than that of its counterparts while its normalized propagation constant is higher. This phenomenon can also be attributed to the interaction among various modes. For the pedestal mounting, such an interaction is more pronounced, particularly when the distance between pedestals is small.

Fig. 3.5 shows the effect of the suspended height on the cutoff frequencies of first higher-order even- and odd-modes. As the suspended height varies under the condition of $h_1 + h_2$ = constant, the cutoff frequency of the first higher-order even-mode slightly decreases while that of the odd-mode is significantly affected and a maximum value of $f_c = 96.6$ GHz is attained around $h_1 = 1.5$ mm that corresponds to the middle of the shielded rectangular enclosure. In the coupled slotline, the field of the odd-mode is spread over in the structure.

The influence of three mounting geometries on the first higher-order even- and odd-modes is depicted in detail in Fig. 3.6. The cutoff frequencies of the first higher-order even-mode for the inverse pedestal and the groove mounting decrease as the mounting sizes increase. However, the cutoff frequency for the pedestal mounting increases at first and begins to decrease around $c = 0.12$ mm. This may be explained by the fact that, for a larger pedestal (small c), in addition to the expected strong field concentration in slots, a certain portion of the tangential electric field of the even-mode is also located

between the central conductor and the 90° edge of the pedestal and thus increases overall capacitive effect similar to an H-plane ridge waveguide. However, this effect tends to be negative as long as the distance between pedestals becomes small. This is because the normal (vertical) electric field appears to be dominant over its tangential counterpart. As a result, there is the optimum choice of the pedestal for wideband applications. The effect of mounting geometries on the cutoff frequency of the first higher odd-mode is significantly different from that on its even counterpart. The cutoff frequency of the first higher-order odd-mode for the inverse pedestal mounting is insensitive to the mounting size. This is attributed to the fact that the field of the odd-mode, though its loose distribution, is mainly limited by a certain region that is related to the slots.

Fig. 3.7 shows dispersion characteristics of the normalized propagation constant and characteristic impedances of the fundamental modes for a coupled slotline with both septum and pedestal considering different metallization thickness. The effect of the septum on propagation characteristics is similar to pedestal in this case. It is found that, indeed, the compensation due to the septum introduces an additional degree of freedom for design consideration.

To understand better the propagation mechanism and influence of pedestals on the fundamental modes, the electric field contours are plotted in the whole cross-section. Figs. 3.8--3.10 show the effect of pedestal positions on the electric fields in the case of the even-mode. It is vividly observed that the field under the slots tends to be more compressed with decreasing the distance between the pedestals. Nevertheless, the field above the slots remains nearly unchanged. This clearly indicates that the coplanar

waveguide mode converts gradually into a hybrid microstrip-coplanar waveguide mode. In practical applications, it is therefore important that the field profile at the launching probe or connector should be matched to the desired mode, and the conventional concept on the impedance matching is no longer complete for hybrid mode circuits. It should be noted that the electric flux density D_y is plotted instead of E_y due to the field continuity condition for a better presentation. In Fig. 3.10, it can be seen that E_z is negligible compared to the other fields, confirming the validity of quasi-static analysis at low frequencies. The field profiles for the odd-mode are presented in Figs. 3.11--3.13. This once again confirms the above discussion that the odd-mode fields are spread over the whole structure. Nevertheless, the fields around the slot regions are still dominant. This fact indicates that the effect of the inverse pedestal mounting scheme on the characteristics of the odd-mode is insensitive.

3.4 Conclusion

In this work, the coupled slotlines with various suspended mounting geometries considering finite thickness of planar conductors are analyzed by a recently developed enhanced spectral-domain method. Propagation characteristics and electrical properties of coupled slotline are discussed in detail for wideband applications and design consideration. Influences and features in terms of different mounting schemes are demonstrated for the normalized propagation constant, the characteristic impedances and the cutoff frequency of the first higher-order modes (the even- and odd-modes). The field profiles of the fundamental modes in coupled slotline with pedestals are plotted. The proposed enhanced SDA proves to be a powerful technique to model a class of complex planar structures, thereby offering efficient analysis and accurate design of MIC's for microwave and millimeter-wave applications.

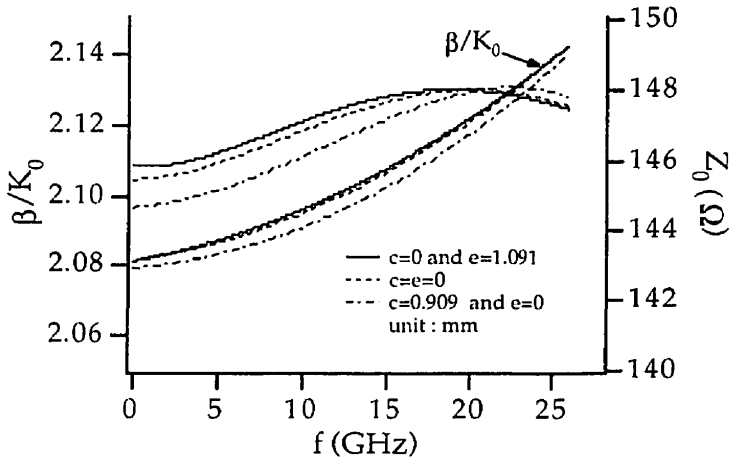

(a)

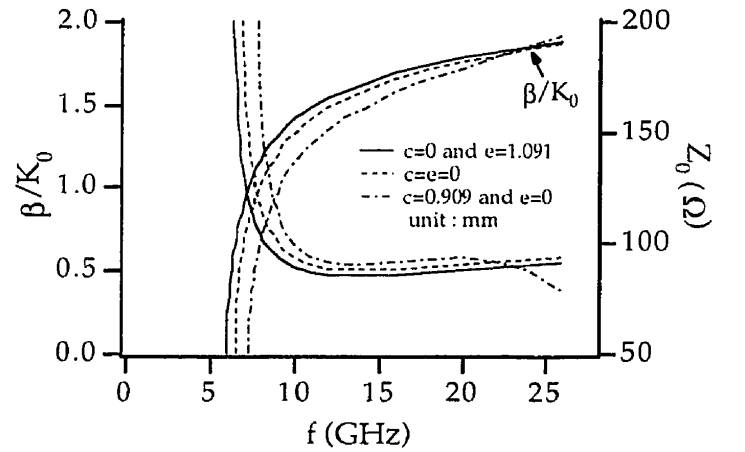

(b)

Fig. 3. 4 Dispersion characteristics and characteristic impedance in coupled slotline with and without pedestals: $a = 4.318$ mm, $h_1 = 5.0$ mm, $h_2 = 5.1$ mm, $w = 0.4$ mm, $s = 0.2$ mm, $d = 0.5$ mm, $t_1 = 50$ μm, $t_2 = 0$ mm, $\varepsilon_r = 9.8$. (a) Even mode. (b) Odd mode.

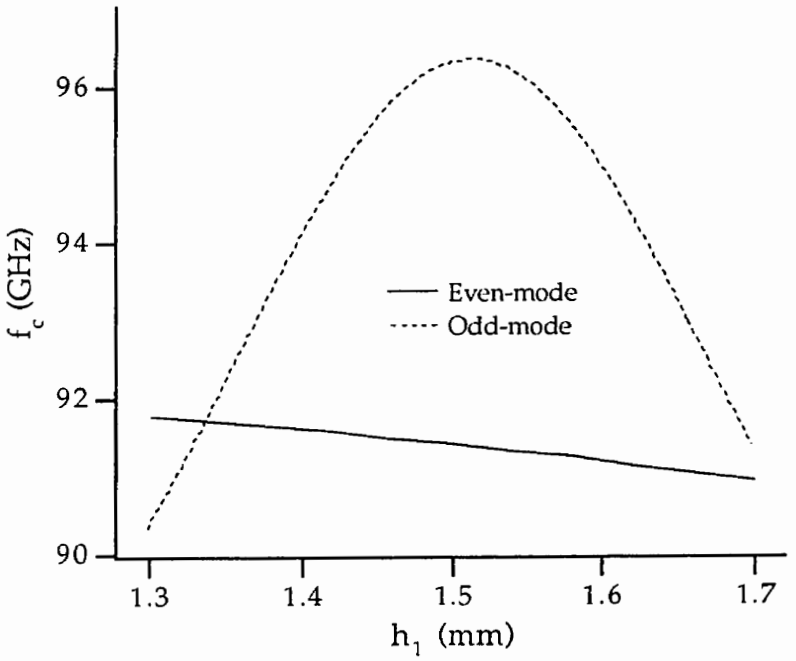

Fig. 3.5 Effect of suspended height (h_1) of substrate on cutoff frequencies of the first higher-order even- and odd-modes in coupled slotline: $a = b = 1.55$ mm, $h_1 + h_2 = 2.845$ mm, $w = s = 0.2$ mm, $d = 0.22$ mm, $t_1 = 35$ μm $t_2 = e = c = 0$ mm, $\varepsilon_r = 3.75$.

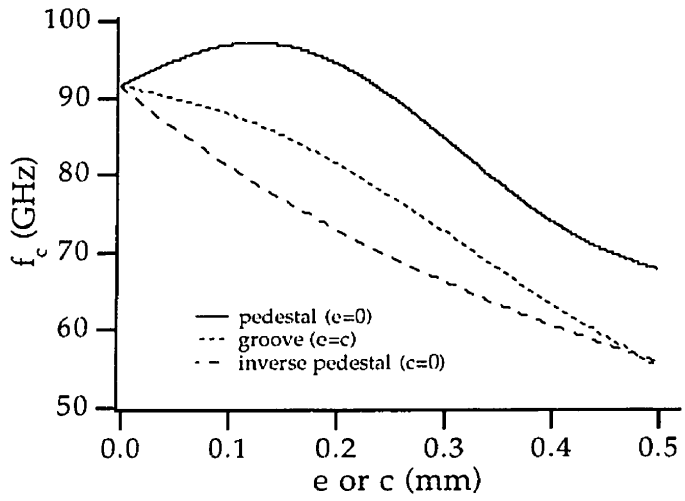

(a) even-mode

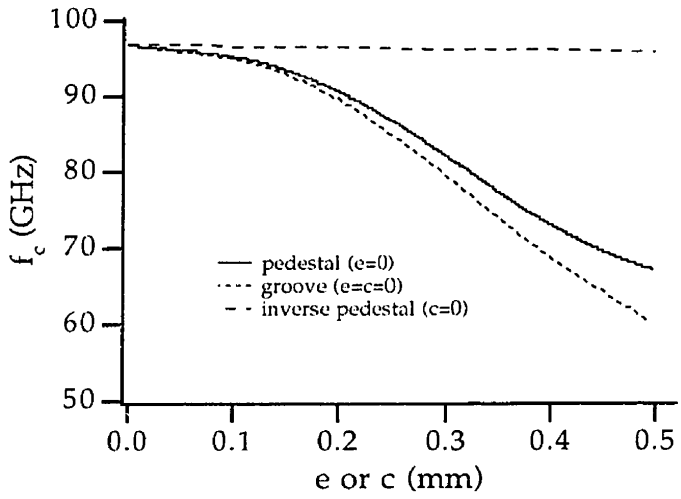

(b) odd-mode

Fig. 3.6 Effect of three suspended mountings on cutoff frequencies of the first higher-order even- and odd-modes in coupled slotline: $a = 1.55$ mm, $h_1 = 1.5$ mm, $h_2 = 1.33$ mm, $w = s = 0.2$ mm, $d = 0.22$ mm, $t_1 = 50$ μm, $t_2 = 0$ mm, $\varepsilon_r = 3.75$.

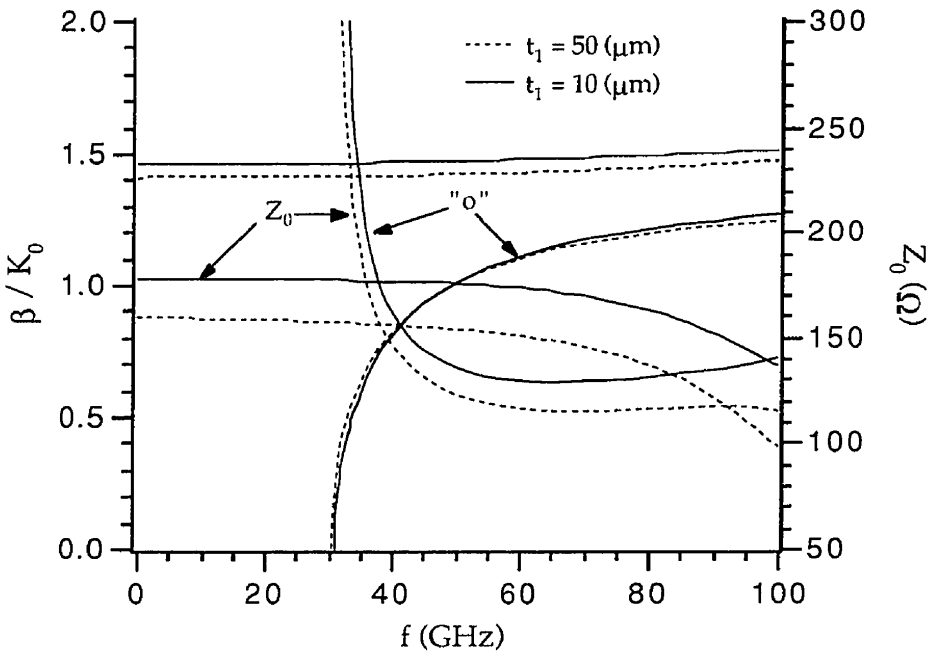

Fig. 3.7 Dispersion characteristics and characteristic impedances in coupled slotline including septum and pedestal: $a = 1.55$ mm, $b = 1.2$ mm, $t_1 = t_2$, $d = 0.22$ mm, $h_1 = h_2 = 1.39$ mm, $w = s = 0.2$ mm, $w_1 = 0.6$ mm, $\varepsilon_r = 3.75$.

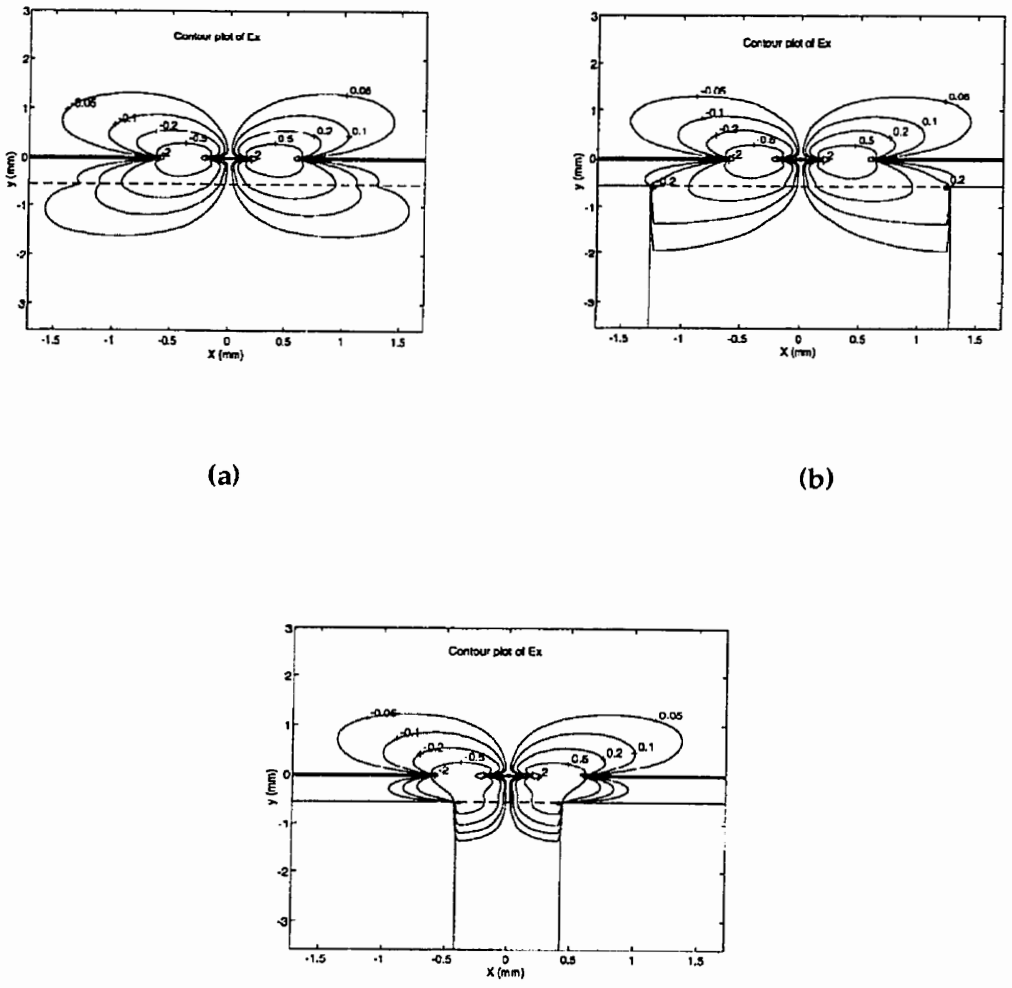

Fig. 3.8 Contour plot of E_x for the even-mode in coupled slotlines with and without pedestals: $a = 4.318$ mm, $h_1 = 5.0$ mm, $h_2 = 5.1$ mm, $w = s = 0.4$ mm, $d = 0.5$ mm, $t_1 = 50$ μm, $t_2 = e = 0$ mm, $\varepsilon_r = 9.8$, $f = 12$ GHz. (a) $c = 0$ mm, (b) $c = 0.909$ mm, and (c) $c = 1.759$ mm.

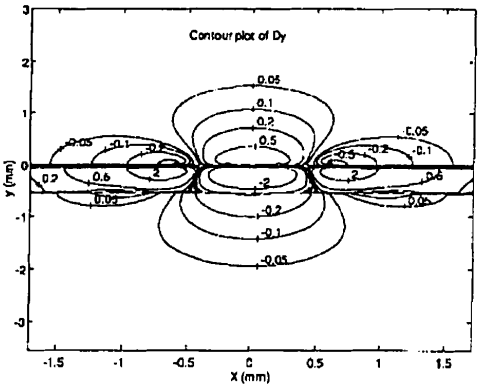

(a)

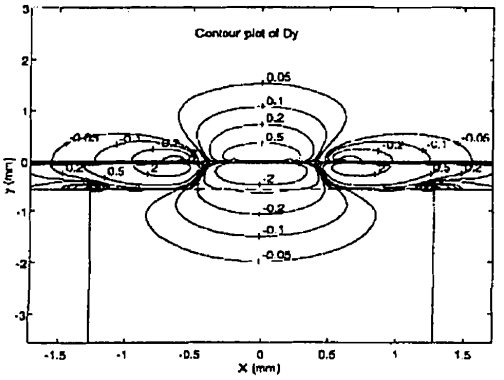

(b)

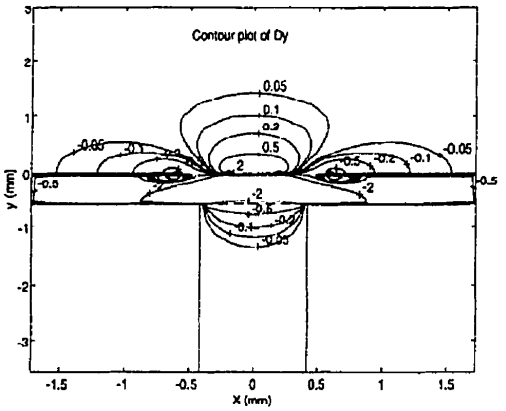

(c)

Fig. 3.9 Contour plot of D_y for the even-mode in a coupled slotline with and without pedestals : the structure parameters and frequency is referred as to Fig. 3.8.

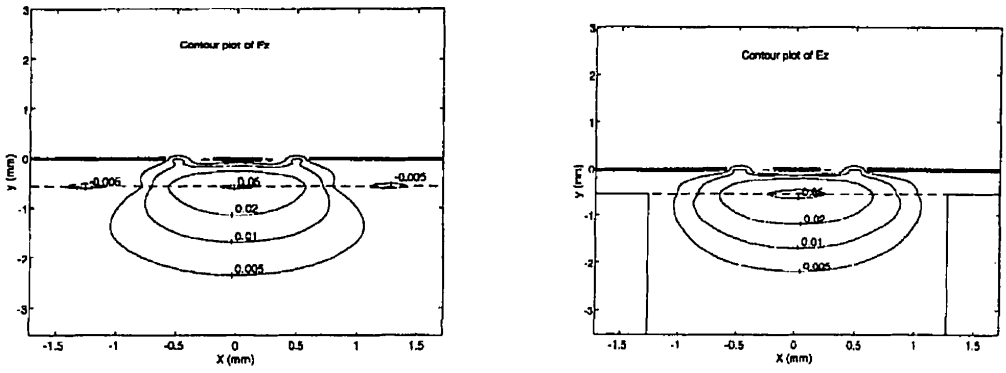

(a) (b)

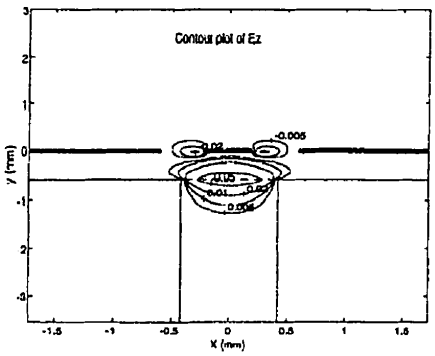

(c)

Fig. 3.10 Contour plot of E_z for the even-mode in a coupled slotline with and without pedestals : the structure parameters and frequency is referred as to Fig. 3.8.

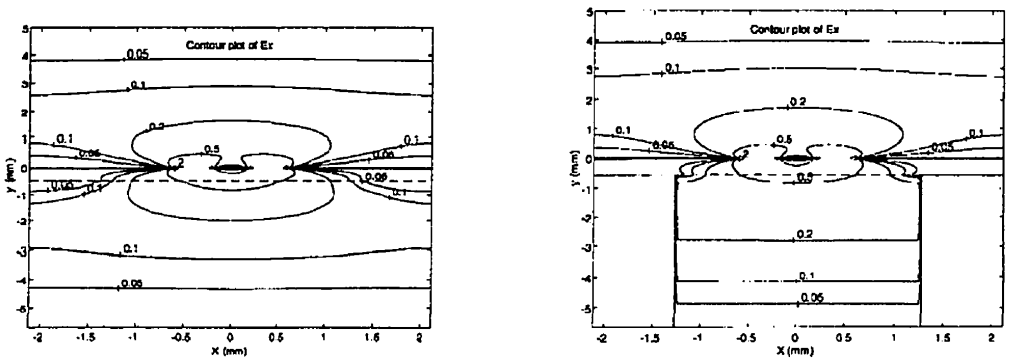

(a) (b)

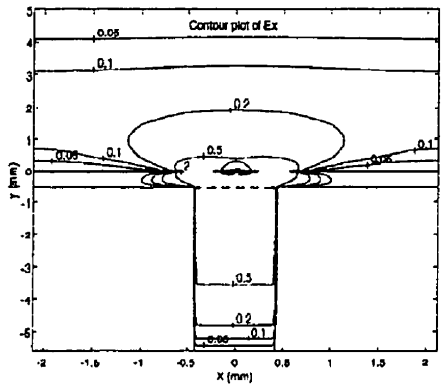

(c)

Fig. 3.11 Contour plot of E_x for the odd-mode in a coupled slotline with and without pedestals : the structure parameters and frequency is referred as to Fig. 3.8.

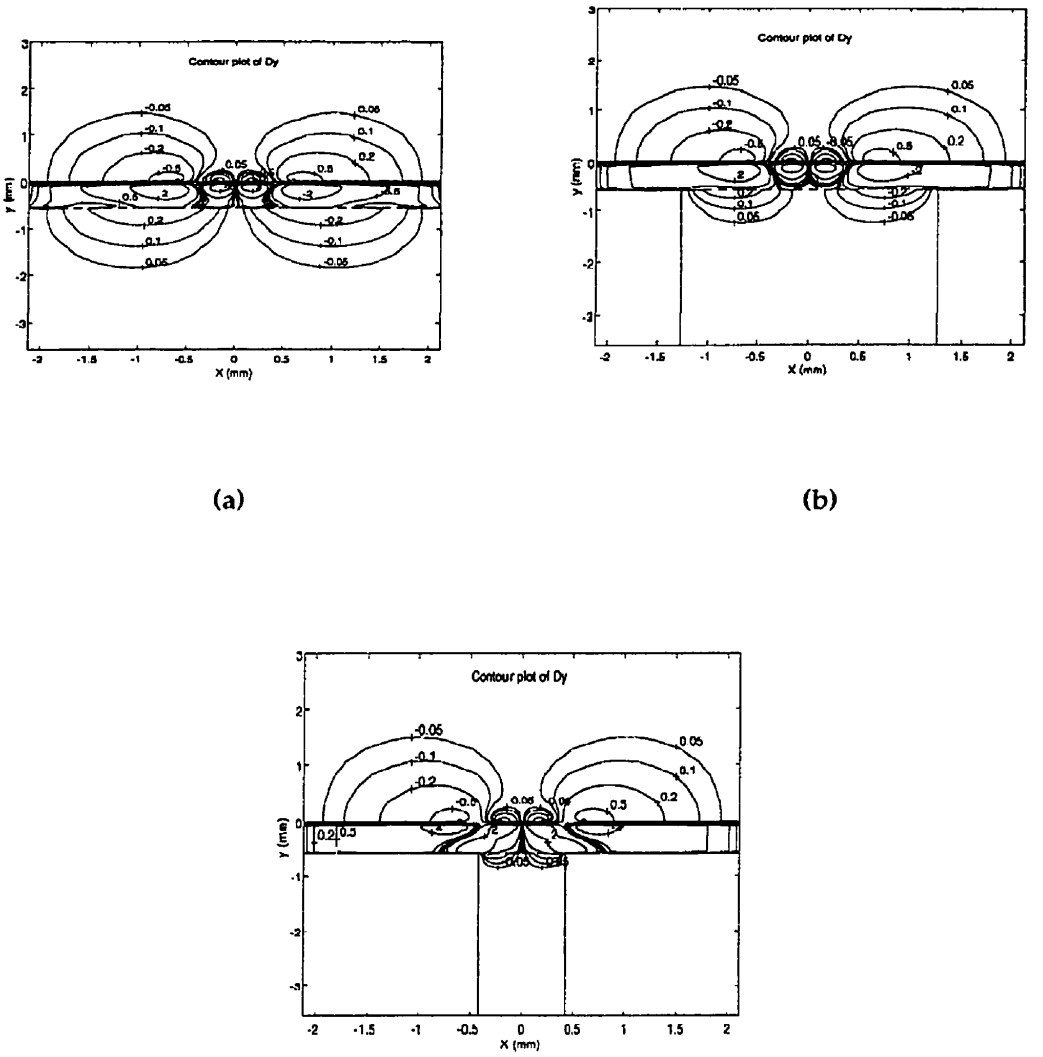

Fig. 3.12 Contour plot of D_y for the odd-mode in a coupled slotline with and without pedestals : the structure parameters and frequency is referred as to Fig. 3.8.

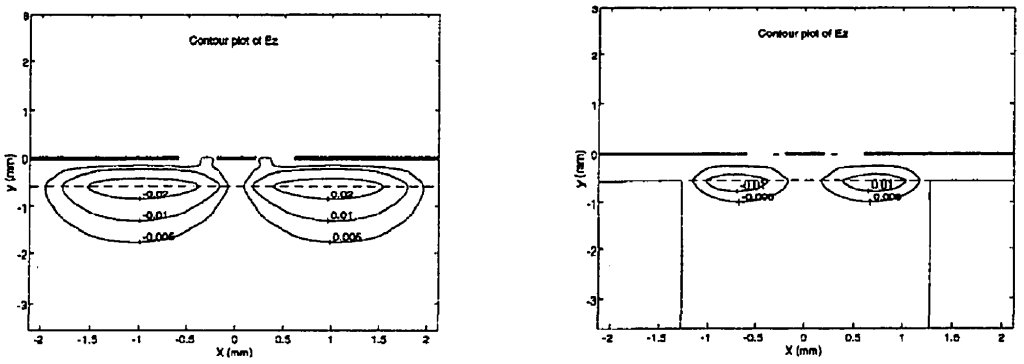

(a) (b)

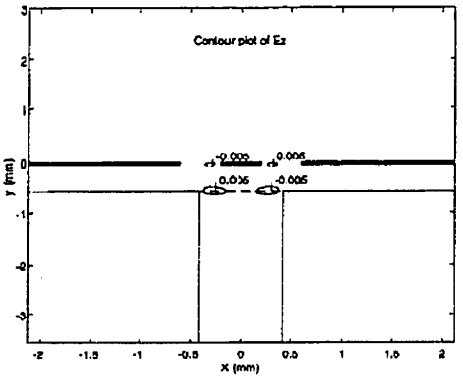

(c)

Fig. 3.13 Contour plot of E_z for the odd-mode in a coupled slotline with and without pedestals : the structure parameters and frequency is referred as to Fig. 3.8.

References

[1] M. Muraguchi, T. Hirota, A. Minakawa, K. Ohwada, and T. Sugeta, "Uniplanar MMIC's and their applications," IEEE Trans. Microwave Theory and Tech., vol. MTT-36, pp.1896-1901, Dec. 1988.

[2] C. Ho, L. Fan, and K. Chang, "Broad-band uniplanar hybrid-ring and branch-line couplers," IEEE Trans. Microwave Theory and Tech., vol. MTT-41, pp.2116-2124, Dec. 1993.

[3] T. Itoh, "Overview of quasi-planar transmission lines," IEEE Trans. Microwave Theory and Tech., vol. MTT-37, pp.275-280, Feb. 1989.

[4] M. Riaziat, R. Majidi-Ahy, and I. J. Feng, "Propagation modes and dispersion characteristics of coplanar waveguides," IEEE Trans. Microwave Theory and Tech., vol. MTT-38, pp.245-251, Mar. 1990.

[5] M. Naghed and I. wolff, "Equivalent capacitances of coplanar wave guide discontinuities and interdigitated capacitors using a 3-deimensional finite difference method," IEEE Trans. Microwave Theory and Tech., vol. MTT-38, pp.1805-1815, Dec. 1990.

[6] F. Alessandri, G. Baini, M. Mongiardo, and R. Sorrentino, "3-D mode matching technique for the efficient analysis of coplanar MMIC discontinuities wit finite metallization thickness," IEEE Trans. Microwave Theory and Tech., vol. MTT-41, pp.1625-1629, Sept. 1993.

[7] H. Shigesawa, M. Tsuji, and A. A. Oliner, "Conductor-backed slot line and coplanar waveguide: dangers and full-wave analysis," in IEEE MTT-s Int. Microwave Symp. Dig., 1988, pp.199-202.

[8] H. Shigesawa, M. Tsuji, and A. A. Oliner, "A new mode-coupling effect on coplanar waveguide s of finite width," in IEEE MTT-s Int. Microwave Symp. Dig., 1990, pp.1063-1066.

[9] R. W. Jackson, "Mode conversion at discontinuities in finite-width conductor-backed coplanar waveguide," IEEE Trans. Microwave Theory and Tech., vol. MTT-37, pp.1582-1589, Oct. 1989.

[10] K. Wu, R. Vahldieck, J. L. Fikart, and H. Minlus, "The influence of finite conductor thickness and conductivity on fundamental and higher-order modes in miniature hybride MIC's (MHMIC's) and MMIC's," IEEE Trans. Microwave Theory and Tech., vol. MTT-41, pp.421-430, Mar. 1993.

[11 W. T. Lo et al, "Resonant Phenomena in conductor-backed coplanar waveguides (CBCPW's)," IEEE Trans. Microwave Theory and Tech., vol. MTT-41, pp.2099-2107, Dec. 1993.

[12] R. R. Mansour and R. H. Macphie, "A unified hybrid-mode analysis for planar transmission lines with multilayer isotropic/anisotropic substrates", IEEE Trans. Microwave Theory and Tech., vol. MTT-35, pp.1382-1391, Dec. 1987.

[13] T. Wang and Z. Sun, "Analysis of novel wideband ridge-loaded finline including finit metallisation thickness and substrate mounting grooves," Electron. Lett., vol.28, no.25, pp.2356-2357, Dec. 1992.

[14] T. Wang and K. Wu, "Enhanced spectral domain analysis of coupled slotlines with septum and pedestal considering finite thickness of conductors for wideband MIC's," in IEEE MTT-s Int. Microwave Symp. Dig., 1994.

[15] Tongqing Wang and Ke Wu "An Efficient Approach to Modeling of Quasi-Planar Structures Using the Formulation of Power Conservation in Spectral Domain," Submitted for IEEE Trans. Microwave Theory and Tech.

[16] R. Jansen, "Unified user-oriented computation of shielded, covered and open planar microwave and millimeter-wave transmission-line characteristics," Microwave Opt. Acoust., vol. 3, pp.14-22, Jan. 1979.

[17] T. Itoh, "Spectral-domain immittance approach for dispersion characteristics of generalized printed transmission lines," IEEE Trans. Microwave Theory and Tech., vol. MTT-28, pp.733-736, July 1980.

[18] J. Bornemann and F. Arndt, "Calculating the characteristic impedance of finlines by transverse resonance method," IEEE Trans. Microwave Theory Tech., vol. MTT-34, pp.85-92, January 1986.

Chapitre IV

Analyse d'une structure guide d'onde uniplanaire auto-blindée

Avec l'augmentation des fréquences d'opération vers les bandes millimétriques, les interconnexions et le blindage des circuits planaires demandent plus d'attention pour éviter les couplages parasites, les radiations responsables des pertes de puissance, et les phénomènes de conversion d'un mode à un autre. En pratique un blindage métallique à section rectangulaire est utilisé pour isoler le circuit, et supprimer tout rayonnement parasite potentiel. Dans le cas des circuits MIC uniplanaires utilisant une seule face de substrat, le signal est véhiculé sur la même interface que celle contenant les plans de masse. Ce type de blindage peut présenter plusieurs inconvénients incluant des couplages de surface à surface, des conversions d'un mode à un autre, et des résonances multiples. En général, un blindage électrique est requis pour chaque circuit individuel, tout en préservant la configuration uniplanaire. Afin de mieux exploiter les avantages des circuits uniplanaires, ce chapitre discute des performances électriques de structures guide d'onde uniplanaire avec auto-blindage à section arbitraire.

Les progrès récents dans le domaine des techniques de réalisation de semi-conducteurs offrent une opportunité fantastique de fabriquer les circuits et leur blindage dans le même temps. Deux principales techniques, soient le micro-usinage et les micro-connexions verticales par fil, ont été décrites dans la presse scientifique. Cette vision d'approche du blindage est rendue possible avec la réalisation de cavités de formes

variables, intégrées au cœur du circuit, suivant n'importe laquelle des trois dimensions spatiales. Ses principaux avantages sont ses performances électriques supérieures et son grand potentiel de faible coût pour les très hautes fréquences d'opération.

Dans ce chapitre, un concept d'auto-blindage, pour des circuits MIC uniplanaire est développé. La structure auto-blindée est différente des techniques de blindages conventionnelles à larges sections métalliques. Le choix de profile de blindage est déterminé à partir de structures guides d'onde et des procédures de réalisation du circuit à protéger. Les techniques de blindage peuvent être classifiées en deux groupes. Le premier est constitué par les blindages à formes adaptées, le second rassemble les blindages réalisés en un seul processus. Le profile des blindages à formes adaptées est compatible avec la structure guide d'onde utilisée pour les connexions. Cette technique est essentiellement utilisée pour les circuits MIC hybrides. Le blindage typique englobe le guide d'onde traditionnel, ce qui apparaît comme une variante des différents systèmes micro-onde. Son principal avantage est naturellement sa facilité de connexion sans transition entre une ligne guide d'onde et le circuit intégré concerné. Les blindages réalisés en un seul processus sont liés aux procédés de fabrication des semi-conducteurs. La mise en boîtier est réalisée en une seule étape, en même temps que le circuit, utilisant les mêmes techniques de fabrication. La section droite de la cavité de blindage peut alors être compliquée et dépend des procédés de fabrication. Les mérites de cette approche réside dans la taille compacte du dispositif final et dans l'élimination des couplages électromagnétique parasites.

La méthode spectrale améliorée (ESDA) décrite au chapitre II est modifiée de façon à pouvoir caractériser une classe de structures guide d'onde uniplanaires avec auto-

blindage à section circulaire, elliptique, en losange ou trapézoïdale. Un modèle numérique approche la forme arbitraire de la section droite par une série de partition disposée en escalier. Les caractéristiques de propagation du mode fondamental des lignes couplées sont mises en lumière. L'influence de divers paramètres structurels sur la fréquence de coupure du mode "ligne à fentes" des lignes micro-blindées est étudiée en détail. Le chapitre est décrit par un article qui a été accepté pour être publié par la revue International Journal of RF and Microwave Computer-Aided Engineering.

Electrical Performance of Self-Shielded Uniplanar Guided-Wave Structures

Tongqing WANG* and Ke WU

POLY-GRAMES Research Center
Dept. de génie électrique et de génie informatique, École Polytechnique
C. P. 6079, Succ. Centre-Ville, Montréal, Canada H3C 3A7

*Nortel (Northern Telecom), Wireless Network
PO Box 3511 Station C, Ottawa, Canada K1Y 4H7

Abstract

This paper presents electrical performance and propagation characteristics of self-shielded uniplanar guided-wave structures including circular, elliptic, diamond, and trapezoidal enclosures. Enhanced spectral domain approach is extended to characterize the guided-wave property of these self-shielded lines. Particular attention is focused on fundamental mode propagation constant and characteristic impedance of coupled uniplanar line having a practical shield profile. Influence of various parameters of the structure on cutoff frequency of the slotline mode is investigated. Interesting features of the self-shielded uniplanar structures are discussed for design consideration. Results are verified with some data available and presented in support of the technical discussion.

4.1 Introduction

A millimeter-wave planar integrated circuit presents the fundamental building block for the future generation of low-cost and low-profile commercial high-speed communication systems and sensors. Usually at low frequency, planar circuits may be easily integrated monolithically or surface-mounted onto multichip modules. However at high frequency (millimeter-wave range), such an integration or surface-mounting becomes much more complicated by the fact that the resulting short wavelength leads to difficult problems for interconnecting and shielding. These interconnecting and shielding issues in design consideration are essentially to prevent parasitic coupling, mode conversion and spurious radiation (power leakage) as well as signal distortion from circuit discontinuities and waveguiding mechanisms. Therefore, an appropriate design of a guided-wave structure is a preliminary consideration in solving these problems. In hybrid/monolithic microwave integrated circuits (H(M)MIC's), the uniplanar technology is known to be a competitive alternative to the conventional microstrip technology from the point of view of performance/cost. Generally speaking, the uniplanar H(M)MIC's consist of CPW, slotline and coplanar strip (CPS) [1]. The principal advantages of the uniplanar technology with respect to its microstrip counterpart have been summarized in [2-5].

In spite of its attractive features, the uniplanar geometry may still have limitations. They are mainly related to surface-to-surface spurious coupling and parasitic radiation of multiple conductors that are located on the same interface. In practice, an electrical shield for each individual circuit is required while the uniplanar benefits can be preserved. To do so, a rectangular metallic enclosure is usually used to achieve necessary electrical isolation between the circuit of concern and its surrounding

environment. Of course, this also attempts to suppress potential parasitic radiation. Such a shielding technique and its electrical performance were studied in the past [6-8]. Nevertheless, this type of shielding may suffer from potential difficulties including mode conversion, multiple resonance and the requirement of a transition between the shielded circuit and conventional guided-wave structure.

With recent advances in the use of semiconductor processing for microfabrication of waveguides, a class of semiconductor-based shielding techniques have received attention. In [9], the development of self-shielded high frequency circuits using a micromachining technique was reported. On the other hand, a vertical microwire technology for shielding application was presented in [10]. This type of shielding technique is able to form a miniaturized cavity having a very flexible shape that is integrated with the core of a circuit. The detailed fabrication procedure and experimental results have been summarized in both papers.

To better exploit the advantages of uniplanar structures, a self-shielding concept for uniplanar H(M)MIC's is developed in this work. The self-shielded structure is different from the conventional counterpart with large metallic enclosures. The circuit configuration using the self-shielding technique should be designed according to the guided-wave structure used in the circuit of concern. The shielding technique may be classified into two groups. One is a conformal shielding while the other can be termed as uniprocessing shielding. In the conformal shielding, the shield profile is compatible with the guided-wave structure used to connect circuits. This technique is essentially used in hybrid MIC's. Some examples are illustrated in Fig. 4.1 (a), (b) and (c). The enclosures are consistent with conventional waveguides that appear in various

microwave systems. The planar circuits are directly inserted into guided-wave structures and compact geometry can be easily made. The main advantage of such shielding is naturally free from a transition between guided-wave line and integrated circuits of concern, which may limit the circuit operating frequency bandwidth. The uniprocessing shielding is referred to as in-situ semiconductor processing technique that is intrinsic. In this case, the shield profile is formed and integrated together with the fabrication of the circuit. Therefore, the cross-sectional shape may be complicated and dependent on the processing technique. A number of micromachined self-shielded topologies have been reported in [11-14]. Fig.4.1(d), (e) and (f) show several geometries that can be fabricated by a micromachining technology. It is noted that CPW configurations with such enclosure can operate in a wideband without the slotline mode as long as the dimension of the enclosure is properly chosen.

Self-shielded circuits exhibit complicated cross-sections. Accurate prediction of their electrical performance relies on field-theoretical modeling techniques which should be able to account for the shield and circuits as a whole. To date, the dispersive propagation constant of planar transmission lines enclosed in circular and elliptic waveguides was calculated by hybrid-mode techniques [15-17]. Microshield lines with V-, elliptic- and circular-shaped enclosures were studied on the basis of a conformal mapping method [18].

In this paper, the enhanced spectral domain approach (SDA) that was developed in [19] is further extended to characterize a class of self-shielded uniplanar guided-wave structures with emphasis on circular, elliptic, diamond and trapezoidal enclosures for H(M)MICs. A step-partition approximate model is used to handle arbitrary cross-

sectional profiles. The analysis is devoted to characteristics of the fundamental mode of coupled lines including the propagation constant and characteristic impedance. The parametric effect of the structure on the cutoff frequency of the slotline mode is examined in detail. Interesting features of self-shielded uniplanar structures are discussed for design consideration.

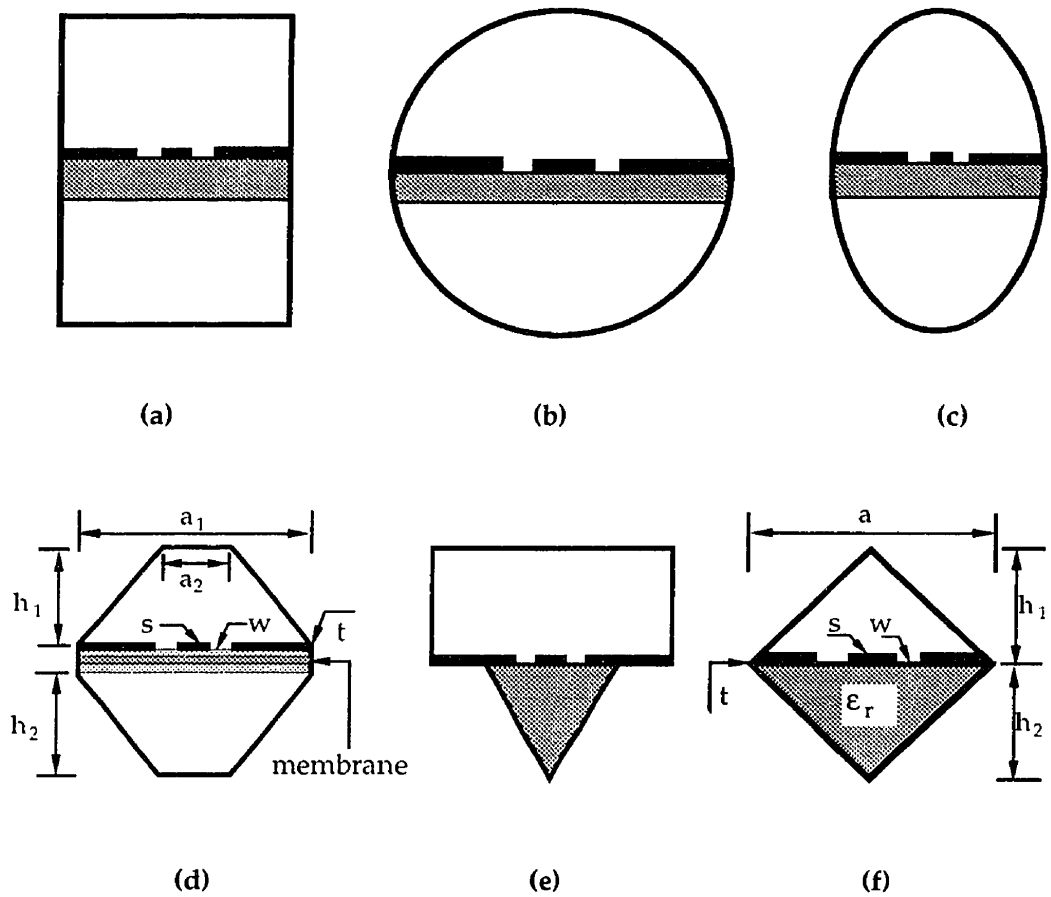

Fig. 4.1 Cross-sectional views of the self-shieled uniplanar guided-wave structures: (a), (b) and (c) are the conformal shielded topologies with rectangular, circular and elliptic enclosures. (d), (e) and (f) are the uniprocessing shielded topologies with trapezoidal, V-shaped and diamond micromachined enclosures.

4.2 Description of Structure and Modeling Technique

The cross-sectional views of the self-shielded uniplanar guided-wave structures are schematically shown in Fig. 4.1. Fig.4.1(a) is a conventional finline that has been widely studied over the last two decades. Fig. 4.1(b) and (c) show uniplanar transmission line inserted in circular and elliptic waveguides. Hybrid-mode analysis of such geometries becomes much more involved since the enclosure is not coordinately conformal with the core planar circuit. In a Cartesian coordinate, the circular and elliptic enclosures are simply described by

$$\left(\frac{x}{b}\right)^2+\left(\frac{x}{b}\right)^2=1 \tag{4.1}$$

with a and b representing the major and minor focal axial distances of the elliptic enclosure, respectively ($a = b$ for the circular case). Fig. 4.1(d), (e) and (f) illustrate the topologies of uniplanar circuit with trapezoidal, V-shaped and diamond enclosures etched by the micromachining technology. Planar conducting strips, to name an example in Fig. 4.1(d), are deposited on a thin substrate by use of the membrane technology and the anisotropic etching of the supporting wafer. A Si membrane is a 3-layered ($SiO_2/Si_3N_4/SiO_2$) structure whose thickness is typically around $0.45\ \mu m$, $0.35\ \mu m$, and $0.75\ \mu m$. respectively. From the point view of numerical modeling, Fig. 4.1(e) and (f) can be viewed as the limiting cases of Fig. 4.1(d). Therefore, a field-theoretical analysis of Fig. 4.1 may be simply unified into that of Fig. 4.1(c) and (d).

The enhanced SDA is basically a combined framework of the conventional SDA with a power conservation theorem. This technique has demonstrated itself to be an efficient tool for the modeling of quasi-planar waveguides with rectangular enclosures. In [20],

this technique has been extended to the analysis of uniplanar guided-wave structure under trapezoidal conductor profile (planar circuit) together with a microshield enclosure. A step-partition model was successfully used in approximating a trapezoidal conductor cross-section. Since the complete analysis technique has been detailed in the relevant papers, only the essential points of the analysis are presented in the following.

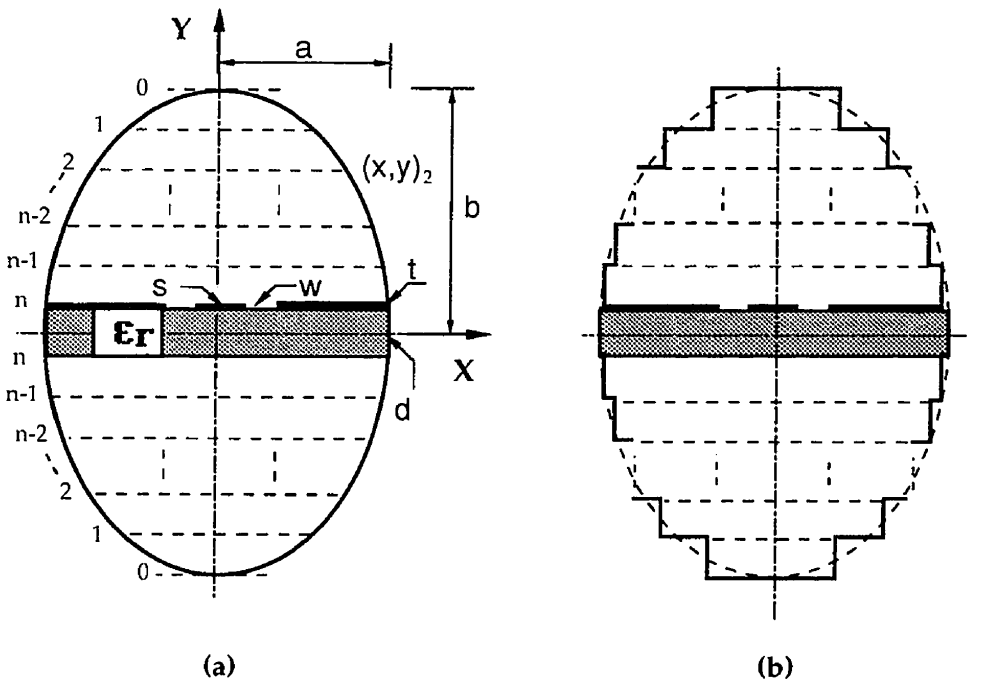

Fig. 4.2 A step-partition model of the elliptic cross-section. (a) Segmentation of the elliptic cross-section. (b) Rectangular approximation of the segments.

Fig. 4.2 shows a step-partition model of elliptic cross-sectional enclosure. To obtain fast numerical convergence, each segment of Fig. 4.2(a) is approximated by a rectangular cross-section having the same height (h) and surface area as depicted in Fig. 4.2(b). In a microshield circuit, the membrane is a multilayered dielectric film. So, the whole

structure can be regarded as a multilayered geometry with the same lateral width. The conventional SDA leads to a spectral domain matrix relationship between the transformed electric and magnetic fields. The use of a coordinate transform yields a set of spectral domain equations that relate the tangential fields defined at the interfaces to each other in the original domain. The application of a power conservation model presented in [19] and the Parseval theorem yields linear homogeneous equations. The propagation constant is then obtained by use of the Galerkin's technique. It is known that the definition of characteristic impedance for non-TEM mode transmission lines is not unique. For slot-type guided-wave structures, the definition of voltage-power is more suited for practical applications. In this work, characteristic impedance of the uniplanar geometry is calculated from the voltage-power definition, considering the average voltage model [19] due to the effect of finite conductor thickness. It should be noted that the impedance is obtained on the basis of a coupled line model. The characteristic impedance of a CPW, for example, is half of the related even-mode counterpart.

4.3 Results and Discussion

The above-described technique allows us to develop a generalized computer program that can determine electrical properties of a class of self-shielded uniplanar guided-wave structures including rectangular, trapezoidal, V-shaped, diamond, circular, and elliptic enclosures. First, the developed algorithm has been carefully verified with other published works. To validate the modeling technique suited for self-shielded guided-wave structures, a circular microslot line is calculated and its propagation constant and characteristic impedance of both even- and odd-modes are shown in Fig. 4.3. Our results are in good agreement with those obtained by a technique of combining the

singular integral equation with Green's function technique presented in [17] except for a minor difference for the odd-mode propagation constant around the cutoff frequency. In addition, Fig. 4.3 indicates that the characteristic impedance of both modes decreases with frequency. No results are available for this in [17]. It is also observed that the characteristic impedance of the fundamental mode (even mode) remains almost dispersionless at low frequency until the appearance of the first higher-order mode (odd mode in this case). This implies that the effect of higher-order modes on the fundamental mode is significant, and characteristics of these higher-order modes are essentially determined by the related shield. This suggests that an appropriate design of shield for a millimeter-wave circuit present a challenging issue. In practice, the design of a shield profile should be in accordance with the underlying circuit specifications.

Note that an appropriate selection of the basis function and spectral term in the enhanced SDA is important for effectively obtaining accurate results. It is known that fast convergence of SDA towards right results can only be achieved by choosing the appropriate basis functions which correctly describe the field singularity at relevant conductor edges. The sinusoidal basis functions with the modification of an edge condition term given in [21] are used in the present analysis. Since the self-shielded uniplanar line presents a more complex shape of the cross-section, more terms of the basis functions are required. In this work, 6 basis functions and 700 spectral terms are used in the following calculations and they are found to be sufficient for less than 1% error. On the other hand, the step-partition model used to approximate the irregular enclosures should be examined. Fig. 4.4 plots numerical convergence of the propagation constant and characteristic impedance for both odd- and even-modes as a function of the number of discrete segments (n) for a microslot line having a circular enclosure. It is

observed that the even-mode converges faster than the odd-mode. This is easily explained by the different field profile of both modes. The electromagnetic field of the even-mode is much more confined to the slot with reference to its odd counterpart. Fig. 4.4 also indicates that a relative convergence can be readily achieved within 0.5% of error as long as the number of segments is selected beyond 6 except for the characteristic impedance of the odd-mode. As the number of segments is greater than 9, the relative error for the odd-mode impedance is less than 0.7%. The error analysis is made with the reference to results of $n=12$

Fig. 4.5 shows frequency-dependent characteristics of the propagation constant and characteristics impedance for the two modes of a coupled slotline inserted in circular waveguide. The finite thickness of metallization is considered in the calculations for two different slots. The dispersion of the fundamental mode is always small, suggesting that this structure has ability to support wideband signal transmission. The effect of slot width on the propagation characteristics is highly pronounced for both modes. In the case, the propagation constants decrease while the characteristic impedances increase with the slot width. This is also understandable from the field distribution of the two modes over the cross-section. Characteristic impedance of both odd- and even-modes of a coupled slotline with an elliptic enclosure is presented in Fig. 4.6, in which the influence of finite thickness of the conducting strip is emphasized with $t=10\ \mu m$, $50\ \mu m$, and $100\ \mu m$. It can be seen that the finite thickness has a significant effect on the characteristic impedance of the even-mode. Normally, the larger conductor thickness lowers characteristic impedance of both modes.

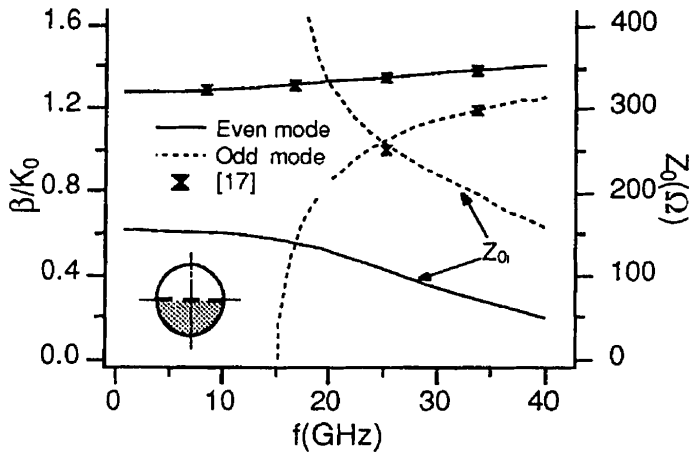

Fig. 4.3 Dispersion characteristics of the normalized propagation constants and characteristic impedances of a coupled microslot line enclosed in a circular waveguide with the geometric parameters: $a = b = 3.5687$ mm, $w = 1.07061$ mm, $s = 2.4981$ mm and $\varepsilon_r = 2.22$.

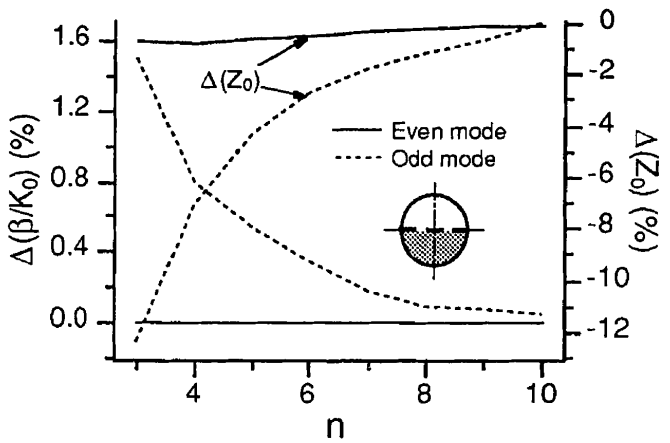

Fig. 4.4 Convergence behavior and error analysis of the normalized propagation constant and characteristic impedance for a coupled microslot line enclosed in a circular waveguide versus the number of segment (n). The same parameters as used in Fig. 4.3 with the reference value of $n = 12$ at $f = 30$ GHz.

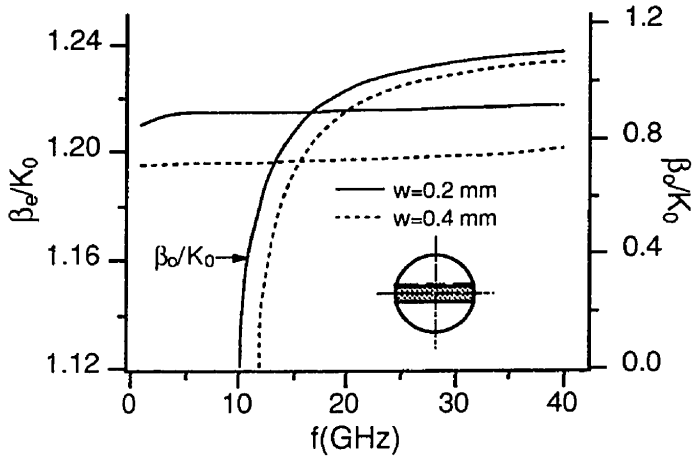

(a)

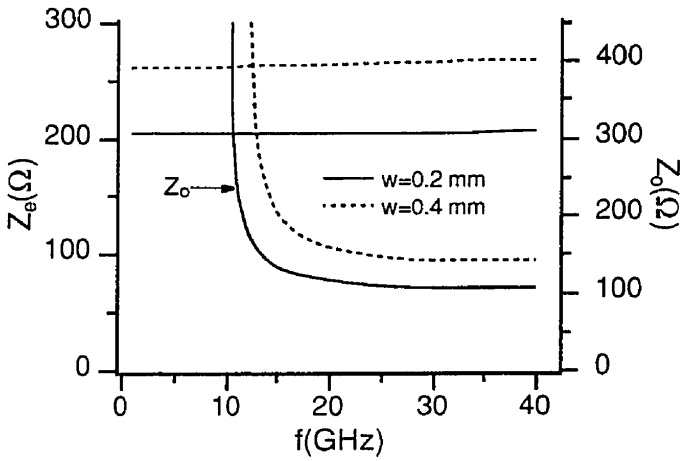

(b)

Fig. 4.5 Frequency-dependent characteristics of both even- and odd-modes of a coupled slotline with a circular waveguide for two different slotwidths with the geometric parameters: $a = b = 3.5687$ mm, $s = 0.2$ mm, $d = 0.254$ mm, $t = 35$ μm and $\varepsilon_r = 2.22$. (a) Normalized propagation constant. (b) Characteristic impedance.

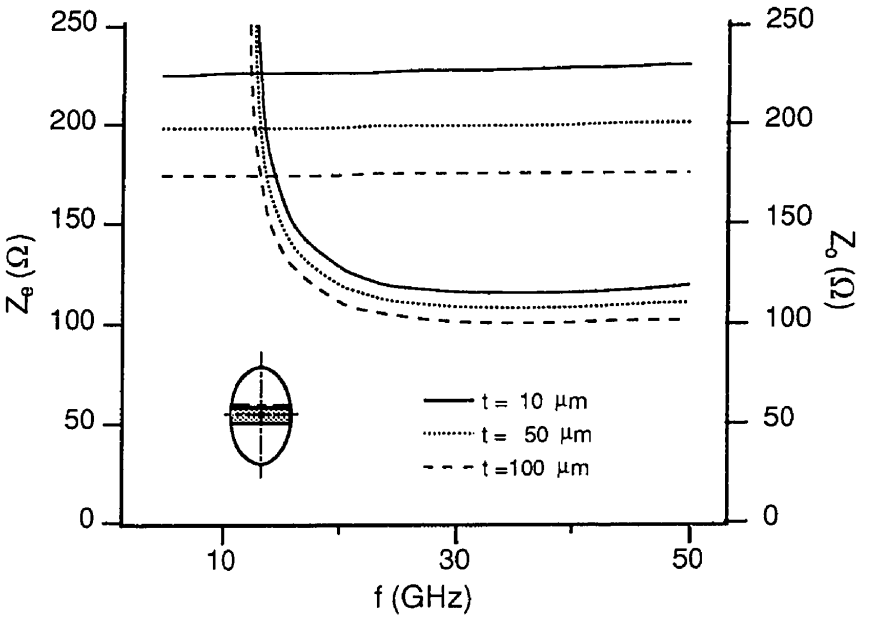

Fig. 4.6 Characteristic impedance of both even- and odd-modes of a coupled slotline enclosed in elliptic waveguide for different metallization thickness with the geometric parameters: $a = 4$ mm, $b = 2.5$ mm, $w = s = 0.2$ mm, $d = 0.254$ mm and $\varepsilon_r = 2.22$

Having presented the conformal shielded uniplanar structures with circular and elliptic enclosures, we discuss now the electrical performance of the uniprocessing shielded structures on the basis of the micromachining technology. In the following analysis, the dimensions of all the tri-layered membrane are set to be 0.45/0.35/0.75 μm for $SiO_2/Si_3N_4/SiO_2$ The relative dielectric permittivity of SiO_2 and Si_3N_4 is 4 and 7, respectively. Fig. 4.7 shows frequency-dependent propagation constant and characteristic impedance of the fundamental mode for a microshield CPW considering the effect of finite thickness of conductor and membrane as well as the enclosure cavity profile. It is indicated that the normalized propagation constant remains almost dispersionless and is slightly greater than 1. The cavity topology presents an effect only on the characteristic impedance of the mode. This effect depends on the corner angle α defined in the figure and is a little bit more pronounced for a small angle. As expected, the fields are much more disturbed by the side walls of the micro-cavity as the corner angle α is smaller than 90^{o}. This means that the fields inside the slots are slightly reduced as is the characteristic impedance.

Fig. 4.8 presents guided-wave characteristics of the fundamental mode for a CPW embedded in a diamond enclosure. Two widths of the central conductor are considered in the calculations. It is found that the propagation constant increases with frequency and the characteristic impedance decreases. In addition, the effect of the central conductor width is significant on propagation characteristics. In a practical uniplanar circuit such as CPW, air-bridges are usually required to suppress potential unwanted slotline modes. Since the enclosure is to some extent equivalent to the role of the air-bridges, it can also be presumed that it should have a non-negligible influence on the monomode bandwidth of a microshield structure.

Fig. 4.9 and Fig. 4.10 give the parametric effects of microshield lines with rectangular and V-shaped enclosures on the cutoff frequency of the slotline mode. Note that the profile of a diamond enclosure can be viewed as a physical composition of two V-shaped housings. First, the V-shaped structure presents a wider monomode bandwidth than its rectangular counterpart, with the planar layered membrane suspended in the air. This is because the effective cross-sectional signal path of the V-shaped is shorter than that of the rectangular. Fig. 4.9 shows a quasi-linear decreasing of the cutoff frequency for the slotline mode against the lateral width of the microshield cavity for which two heights of the suspended membrane are considered. The cutoff frequency is pulled down by 35% as the lateral width increases from 0.8 mm to 1.5 mm. This quantitative study suggests that the monomode bandwidth be enhanced by reducing the lateral width of the cavity. In a membrane based microshield circuit, the effect of an air-bridge on its electrical performance is expected to be much more significant than that of the conventional MMIC's since the thin membrane has no ability to confine the fields within it. Therefore, the use of an adequate microshield cavity topology instead of air-bridge is a good strategy of improving the circuit performance. It should be pointed out that the effect of a microshied cavity on the discontinuity of a circuit is different from that of an air-bridge. Fig. 4.10 indicates a quasi-linear increasing of the cutoff frequency versus the slot width for three different central conductor widths. In this example, the V-shaped presents always a better performance than its rectangular counterpart.

4.4 Conclusion

This paper presents the electrical characteristics of a class of self-shielded uniplanar guided-wave structures having various enclosures. They are classified into two

categories, namely, conformal shielding and uniprocessing shielding topologies on the basis of the fabrication and transmission compatibility. The enhanced spectral domain approach (SDA) has been successfully extended into the efficient modeling of these irregular structures under the framework of a step-partition model. The circuit performance and design aspects of these guided-wave structures are discussed in terms of propagation constant and characteristic impedance for circular, elliptic, diamond, trapezoidal enclosures. It is found that certain microshield cavity profiles such as V-shaped are better than their counterparts and they can be effectively used to suppress the unwanted slotline mode. The monomode bandwidth of membrane-based microshield lines is studied and the parametric effect on the bandwidth is usually significant. In addition, the cavity profile may be also influential on the characteristic impedance of the microshield line.

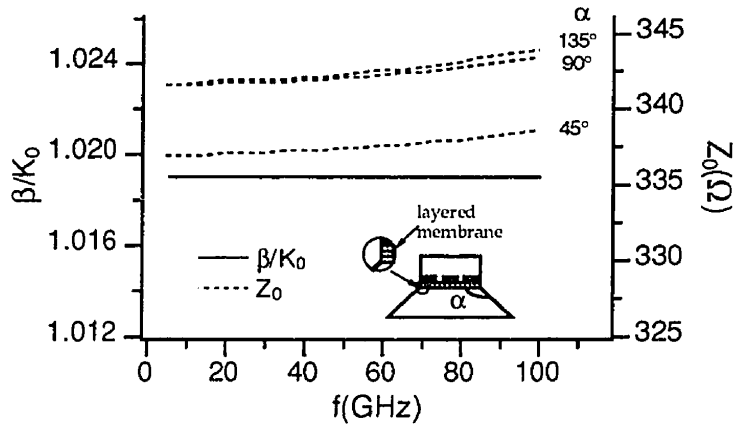

Fig. 4.7 Normalized propagation constant and characteristic impedance of even-mode of a microshield line for micromachined enclosures having different corner angles with the geometric parameters (dimensional description with respect to Fig. 4.1(d) : $a_1 = a_2 = 1200\ \mu m$, $h_1 = 510\ \mu m$, $h_2 = 350\ \mu m$, $w = 400\ \mu m$, $s = 100\ \mu m$, $t = 3\ \mu m$, and parameters of the membrane given in the paper.

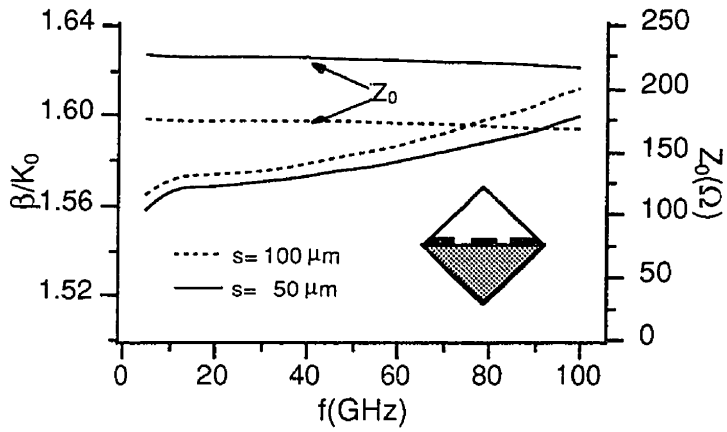

Fig. 4.8 Normalized propagation constant and characteristic impedance of the fundamental mode of a microshield line with a diamond enclosure for two widths of the central conductor and parameters are (dimensional description with respect to Fig. 4.1(f): $a = 700\ \mu m$, $h_1 = h_2 = 350\ \mu m$, $w = 200\ \mu m$, $t = 2\ \mu m$, and $\varepsilon_r = 4$.

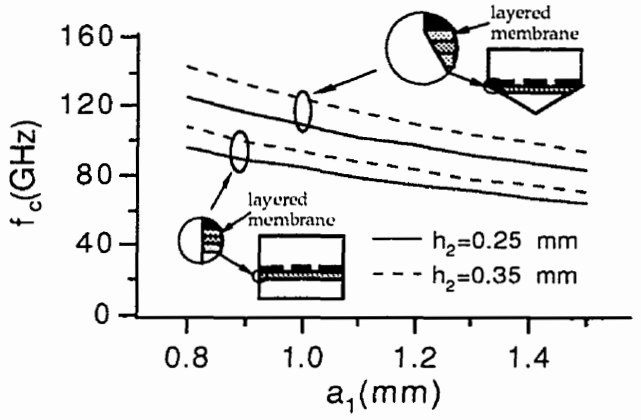

Fig. 4.9 Cutoff frequency characteristics of the slotline mode of a microshield line for two suspended heights housed in rectangular and V-shaped enclosures versus the lateral width of the cavity with the geometric parameters (dimensional description with respect to Fig. 4.1(d) : $h_1 = 510$ μm, $w = s = 40$ μm, $t = 2$ μm, and the membrane parameters given in the paper.

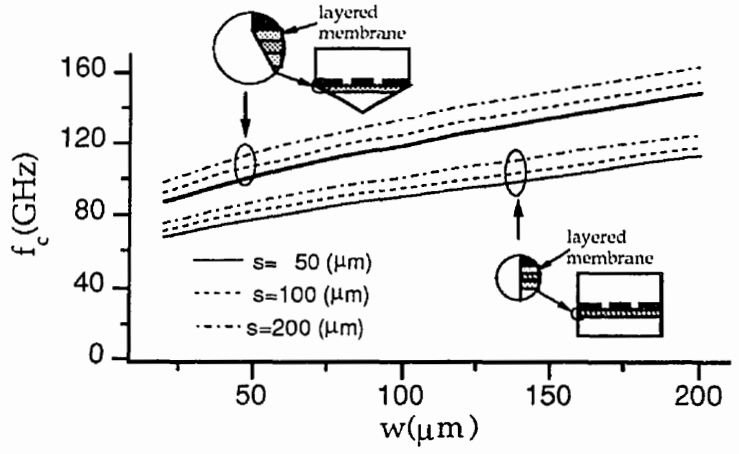

Fig. 4.10 Cutoff frequency characteristics of the slotline mode of a microshield line for three central conductor widths housed in rectangular and V-shaped enclosures versus the slot width with the geometric parameters (dimensional description with respect to Fig. 4.1(d) : $a_2 = 1200$ μm, $h_1 = 510$ μm, $h_2 = 350$ μm, $t = 2$ μm, and the membrane parameters given in the paper.

References

[1] T. Hirota, Y. Tarusawa, and H. Ogawa, "Uniplanar MMIC hybrids - a proposed new MMIC structures," IEEE Trans. Microwave Theory Tech., vol. MTT-35, pp. 576-581, June 1987.

[2] M. Abdo Tuko and I. Wolff, "Novel 36 GHz GaAs frequency doublers using (M)MIC coplanar technology," in IEEE MTT-S Int. Microwave Symp. Dig., June 1992, pp.1167-1170.

[3] C. H. Ho, L. Fan, and K. Chang, "Broad-band uniplanar hybrid-ring and branch-line couplers," IEEE Trans. Microwave Theory Tech., vol. MTT-41, pp. 2116-2124, Dec. 1993.

[4] N. I. Dib, R. N. Simons, and L. P. B. Katehi, "New uniplanar transitions for circuit and antenna applications," IEEE Trans. Microwave Theory Tech., vol. MTT-43, pp. 2868-2873, Dec. 1995.

[5] K. Wu, Y. Xu, and R. G. Bosisio, "Theoretical and experimental analysis of channelized coplanar waveguides (CCPW) for wideband applications of integrated microwave and millimeter-wave circuits," IEEE Trans. Microwave Theory Tech., vol. MTT-42, pp. 1651-1659, Sept., 1994.

[6] M. Tsuji and H. Shigesawa, "Packaging of printed-circuit lines: a dangerous cause for narrow pulse distortion," IEEE Trans. Microwave Theory Tech., vol. MTT-42, pp.1784-1790, Sept. 1994.

[7] J.-W. Huang and C.-K. C. Tzuang, "Mode-coupling-avoidance of shielded conductor-backed coplanar waveguide(CBCPW) using dielectric lines compensation," in IEEE MTT-S Int. Microwave Symp. Dig., May, 1994, pp.149-152.

[8] Y.-D. Lin and P.-M. Chi, "Mode-coupling phenomena of packaged coplanar waveguide with mounting grooves," in IEEE MTT-S Int. Microwave Symp. Dig., May 1994, pp.1145-1148.

[9] R. F. Drayton and L. P. B. Katehi, "Development of self-packaged high frequency circuits using micromachining techniques," IEEE Trans. Microwave Theory Tech., vol. MTT-43, pp. 2073-2080, Sept. 1995.

[10] M. Hirano, K. Nishikawa, I. Toyoda, S. Aoyama, S. Sugitani, and K. Yamasaki, "Three-dimensional passive circuit technology for ultra-compact MMIC's," IEEE Trans. Microwave Theory Tech., vol. MTT-43, pp. 2845-2850, Dec. 1995.

[11] L. P. B. Katehi, G. M. Rebeiz, T. M. Weller, R. F. Drayton, H. J. Cheng, and J. F. Whitaker, "Micromachined circuits for millimeter- and sub-millimeter-wave applications," IEEE Antenna and Propagation Magazine, vol.35, no.5, pp.9-17, Oct. 1993.

[12] K.-K. M. Cheng and I. D. Robertson, "Quasi-TEM study of microshield lines with practical cavity sidewall profiles," IEEE Trans. Microwave Theory Tech., vol. MTT-43, pp. 2689-2694, Dec. 1995.

[13] W. Wang and Y. Guo, "Static ,analysis of millimeter wave transmission lines micromachined silicon substrate," in IEEE Antenna and propagation society International Symp. Dig., June 1994, pp.1960-1963.

[14] N. I. Dib and L. P. B. Katehi, "Impedance calculation for the microshield line," IEEE Microwave and Guided Wave Letters, vol.2, pp.406-408.

[15] Eswarappa, G. I. Costache, and W. J. R. Hoefer, "Finlines in rectangular and circular waveguide housings including substrate mounting and bending effects - finite element analysis," IEEE Trans. Microwave Theory Tech., vol. MTT-37, pp. 299-305, Feb. 1989.

[16] K. Wu and R. Vahldieck, "The method of lines applied to planar transmission lines in circular and elliptical waveguides," IEEE Trans. Microwave Theory Tech., vol. MTT-37, pp. 1958-1963, Dec. 1989.

[17] I. O. Vardiambasis, J. L. Tsalamengas, and J. G. Fikioris, "Hybrid wave propagation in circularly shield microslot lines," IEEE Trans. Microwave Theory Tech., vol. MTT-43, pp. 1960-1966, Aug. 1995.

[18] N. Yuan, C. Ruan, and W. Lin, "Analytical analysis of V, elliptic, and circular-shaped microshield transmission lines," IEEE Trans. Microwave Theory Tech., vol. MTT-42, pp. 855-859, May, 1994.

[19] T. Wang and K. Wu "An efficient approach to modeling of quasi-planar structures using the formulation of power conservation in spectral domain," IEEE Trans. Microwave Theory Tech., vol. MTT-43, pp.1136-1143, May 1995.

[20] T. Wang and K. Wu "Dynamic analysis of uniplanar guided-wave structures with trapezoidal conductor profile and microshielding enclosure," IEICE Trans. Electron., vol. E78C, pp.1100-1105, Aug. 1995.

[21] T. Wang and K. Wu "Effects of various suspended mounting schemes on mode characteristics of coupled slotlines considering conductor thickness for wideband MIC applications," IEEE Trans. Microwave Theory Tech., vol. MTT43, pp.1106-1114, May 1995.

Chapitre V

Design de coupleur uniplanaire en anneau avec inverseur de phase

Dans les deux précédents chapitres, les performances électriques des structures guide d'onde uniplanaires ont été discutées, et une attention particulière a été portée sur différentes configurations de blindage. Ce chapitre s'oriente vers les aspects utilitaires des structures guide d'onde uniplanaires en vue d'applications concrètes. Il présente le design de coupleur uniplanaire en anneau avec inverseur de phase. Les coupleurs ont été largement utilisés dans les systèmes de communications micro-ondes et les appareillages de mesures. En particulier, le coupleur hybride 3 dB est un dispositif indispensable dans la conception d'un très grand nombre de circuits micro-ondes, tels que les amplificateurs balancés, mélangeurs balancés, séparateurs de fréquences, déphaseurs, modulateurs et démodulateurs, circuits d'alimentation d'antenne en réseau, etc.... En général un coupleur est un composant à quatre ports. En considérant les déphasages entre les ports de sortie, les coupleurs communément utilisés sont classifiés en deux catégories: les coupleurs avec sorties déphasées de 90°, et ceux avec sorties déphasées de 0° ou de 180°. Les coupleurs à lignes parallèles et les coupleurs "branch line" sont des exemples bien connus de coupleurs hybride a 90°. L'anneau hybride est l'un des coupleurs hybrides à 0° ou à 180° les plus populaire. Pour certaines applications, principalement les mélangeurs, les modulateurs et les diviseurs de puissance, les coupleurs hybrides à 0° ou à 180° sont préférés aux schémas

correspondant de coupleurs hybrides à 90°, car l'isolation entre les deux ports d'entrée peut être indépendante de la valeur des impédances de charge balancées.

L'anneau hybride conventionnel possède une longueur d'onde et demi de circonférence, et est divisé en quatre sections. Trois sections ont une longueur identique et égale à un quart de longueur d'onde. L'anneau hybride est utilisé comme coupleur 3 dB directionnel. Le guide d'onde qui constitue l'anneau présente une admittance égale à celle des entrées/sorties divisées par 2. Les inconvénients résident essentiellement dans sa large taille, et sa faible bande passante limitée par la section de trois quart de longueur d'onde. Durant les dix dernières années, beaucoup d'efforts ont été consacrés pour améliorer les performances de ce type de coupleur. La plupart des techniques proposées utilisent une section d'un quart de longueur d'onde avec un inverseur de phase en remplacement de la plus grande section.

Les travaux plus récents sur les coupleurs hybrides en anneau ont principalement traité les circuits MIC en technologie micro-ruban, car les caractéristiques de ce type de ligne sont bien établies, et souvent disponibles dans de nombreuses tables de données. Cependant, les circuits micro-ruban sont aussi connus pour leurs défauts tels la dépendance de leurs propriétés électriques vis à vis de l'épaisseur du substrat, et les difficultés d'implantation d'éléments actifs à trois accès et de montage en parallèle. Comme mentionné auparavant, la technologie MIC uniplanaire utilisant seulement une face de diélectrique peut palier et résoudre de tels problèmes. Plusieurs études reposant sur l'utilisation du concept d'inverseur de phase, ont récemment été rapportées. Les designs ont été obtenus avec le souci de respecter les conditions d'adaptation à la fréquence centrale. Aucune description de design fonctionnant sur une large plage de

fréquences n'a été réalisée. Aucune procédure de conception de coupleurs hybrides en anneau en technologie uniplanaire avec inverseur de phase, n'a encore été proposée.

Ce chapitre permet la compréhension du fonctionnement physique du coupleur hybride en anneau avec inverseur de phase en conjonction avec sa modélisation et son étude numérique. Une nouvelle procédure de design est proposée. Les principales caractéristiques et les critères de design d'un coupleur hybride large bande en anneau avec inverseur de phase, sont rassemblés et présentés en détail. Les propriétés des différentes structures guides d'onde uniplanaires, utilisées dans la conception de ce type de coupleur, sont analysées et discutées. Le chapitre est illustré par un article actuellement soumis en vue d'être publié par la revue IEEE Transaction on Microwave Theory and Techniques.

Size-Reduction and Band-Broadening Design Technique of Uniplanar Hybrid Ring Coupler Using Phase Inverter for M(H)MIC's

Tongqing Wang*, Ke Wu, Senior Member, IEEE
*Nortel, Wireless Networks
P. O. Box 3511, Station C, Ottawa, Ontario, Canada K1Y 4H7
E-Mail: tqwang@nortel.ca

Poly-Grames Research Center
Departement de génie électrique et de génie informatique
École Polytechnique de Montréal,
C. P. 6079, Succ. Centre-Ville, Montreal, Québec, Canada H3C 3A7
E-Mail: wuke@grmes.polymtl.ca

Abstract

A hybrid coupler is one of the most fundamental building blocks in microwave and millimeter-wave system. Ring topology can be often found in the M(H)MIC design of narrow and broadband integrated coupler and mixers. In this work, we propose a new design theory and practice using a phase inverter for systematic size-reduction and band-broadening of a uniplanar hybrid ring coupler. Principal features and design criteria of broadband reverse-phase hybrid ring couplers are presented. Effective bandwidth of a new reverse-phase hybrid ring coupler can be increased by 28% for a design requirement of 20-dB return loss. In addition, we present a class of uniplanar

phase inverters and discuss their technical aspects. Experimental results show that the proposed phase inverter has more than 1.9 octave bandwidth with insertion loss better than 1 dB and phase shift error less than ± 20°. Measurements confirm also that the new uniplanar hybrid ring coupler provides attractive features for broadband applications. Its isolation is found to be better than 20 dB over a 1.8 octave bandwidth that is attributed to the phase inverter providing almost a frequency-independent phase shifting.

5.1 Introduction

Rapid growth in radio-frequency (RF) commercial sectors at microwave and millimeter-wave frequencies has trigged the search for new solutions in the design of cost-effective monolithic and hybrid microwave integrated circuits (M(H)MIC's). Such a demand has a significant impact on a number of design issues both at component and system levels, namely, size reduction, broadband operation and low-power consumption and low-noise requirement. A coupler can be found almost in every RF system. In particular, a 3 dB hybrid coupler is an indispensable building block for a large number of RF circuits such as balanced amplifier, balanced mixer, frequency discriminator, phase shifter, (de)modulator and feeding network in an antenna array. To a large extent, hybrid couplers in view of phase difference between the two output ports can be classified into two categories: 90° and 0°/180°. Parallel coupled-line and branch-line couplers are well-known examples of a 90° hybrid coupler and their electrical performance has been well documented in [1-4]. For certain applications, namely, mixer, modulator and isolating power splitter, a 0°/180° hybrid coupler is more preferred than its 90° counterpart since its isolation between two input ports may be independent of the value of two balanced-impedance loads. And also, a typical 0°/180° hybrid ring coupler has a wider bandwidth than the branch-line coupler [5].

A popular 0°/180° hybrid coupler is a rate-race microstrip ring. It has been used as a 3-dB directional coupler with the normalized $1/\sqrt{2}$ admittance of the input/output lines for the ring line. The essential drawbacks are its large size and limited bandwidth because of its three-quarter-wavelength section. Over the last decades, a large amount of research effort has been made to improve performance of this type of coupler. Several design techniques, for example, have been proposed to enhance the useful bandwidth

and also reduce the size. A one-quarter wavelength section with phase reversal was used in [6, 7] to replace its conventional three-quarter wavelength line. This phase-reversal section was realized by the use of a parallel-coupled line [6] with two diagonal grounding ends. Such a modified coupler achieved more than one octave bandwidth but has not found wide acceptance since it requires a very tightly coupled line section that is difficult to fabricate with microstrip topology using a conventional chemical etching technique. While in [7], a combination of microstrip and slot-line modes was used to realize the one-quarter wavelength network with phase reversal. Even though the bandwidth was extended to two octaves, both sides of the circuit substrate had to be etched that may need a precision photolithography process. Note that both circuits require ground pins for microstrip shorts that limit their use at low frequency. Subsequently, another broadband design method was proposed in [8] with the help of CAD. In this case, the bandwidth was broadened by dividing the three-quarter-wavelength equal-admittance section of the conventional hybrid ring by means of the hypothetical port concept and by adding quarter-wavelength transformers to the original ports. This approach achieved a 50% bandwidth. However, this circuit needs a very low impedance line, which is not convenient to fabricate with the microstrip topology. And also, it occupies a large circuit area because of the use of the quarter-wavelength transformers. In 1991, a method for designing a size-reduced 3-dB hybrid ring coupler was developed in [9] using fundamental $\lambda_g/8$ or $\lambda_g/6$ sections, in which λ_g refers to the guided wavelength at the center frequency. Unfortunately, this kind of size-reduced coupler presents a very narrow bandwidth.

Earlier works on the hybrid ring coupler were carried out for microstrip-based MIC's because characteristics of microstrip line are well understood and design databases are

also available. However, standard microstrip circuit is also known to suffer from some potential physical defects such as the dependency of electrical property on substrate thickness and difficult integration of three-terminal active devices and shunt elements. The uniplanar MIC technology that uses only one side of a substrate was proposed to overcome such problems [10]. It has been considered as a cost-effective alternative to the microstrip circuit for a large number of applications. Several uniplanar hybrid ring couplers have recently been reported with a concept of phase inverter. In [11], a narrow-band 0°/180° hybrid coupler was proposed on the basis of difference of characteristics of the balanced slot-line and unbalanced coplanar waveguide (CPW). More recently, broadband uniplanar 0°/180° hybrid ring couplers [12] that operate over an octave bandwidth were developed with the use of a combination of the CPW and slot-line. The phase inverters were obtained by applying CPW-slot-line balun and T-junction. A miniaturized uniplanar 0°/180° hybrid ring coupler having $0.67\lambda_g$ circumference was demonstrated in [13] and the circuit is composed of a coplanar strip ring and CPW feed lines. A crossover of two strips on the ring achieved a 180° phase shift. Nevertheless, these elements were designed to be matched at the center frequency. In practice, it is generally required that coupling, matching, isolation of coupler satisfy certain pre-designated specifications over a frequency range even though the circuit may not be perfectly matched at the center frequency. To our knowledge, there is a lack of systematic description of the broadband design procedure for the hybrid ring coupler using a phase inverter.

To begin with, this work presents a comprehensive design framework of hybrid ring coupler with phase inverter in connection with its network modeling and analysis. Principal features and design consideration of the reverse-phase hybrid ring coupler are

summarized in detail. And also, we derive and describe a set of useful generalized design equations. Then, a special section is devoted to the discussion of attributes of different uniplanar guided-wave structures for use in the coupler design. Some design data are given for micro-coplanar strip lines. A class of uniplanar phase inverter geometries are portrayed and described. To verify our developed design theory, we have fabricated and measured prototypes. Experimental results are presented to confirm our prediction for our proposed broadband design technique and attractive characteristics of the new hybrid ring coupler.

5.2 Design Theory of Hybrid Ring Coupler with Phase Inverter

5.2.1 Generalized Design Procedure

In the following, we will derive a set of original design equations for the hybrid ring coupler with phase inverter, which will be used in the design of our proposed size-reduced and band-broadening coupler. A generalized topology of hybrid ring coupler with an ideal phase inverter is sketched in Fig. 5.1. Electrical lengths and characteristic admittance of ring line are described herewith. The symbol y_0 of Fig. 5.1 denotes the characteristic admittance of attached feed lines (or input/output lines). Without loss of generality, a sub-network having a 180° phase shift represents the ideal phase inverter. This sub-network is characterized by such a two-port S-parameter matrix as

$$S = \begin{bmatrix} 0 & -1 \\ -1 & 0 \end{bmatrix} \tag{5.1}$$

It is easily shown that electrical behaviour of a line section involving the phase inverter remains the same regardless of the location of phase inverter. The coupler has a

symmetric axis denoted by a cross-line $A-A$. It is obvious that this axis divides the phase inverter into two identical 90° phase shifters.

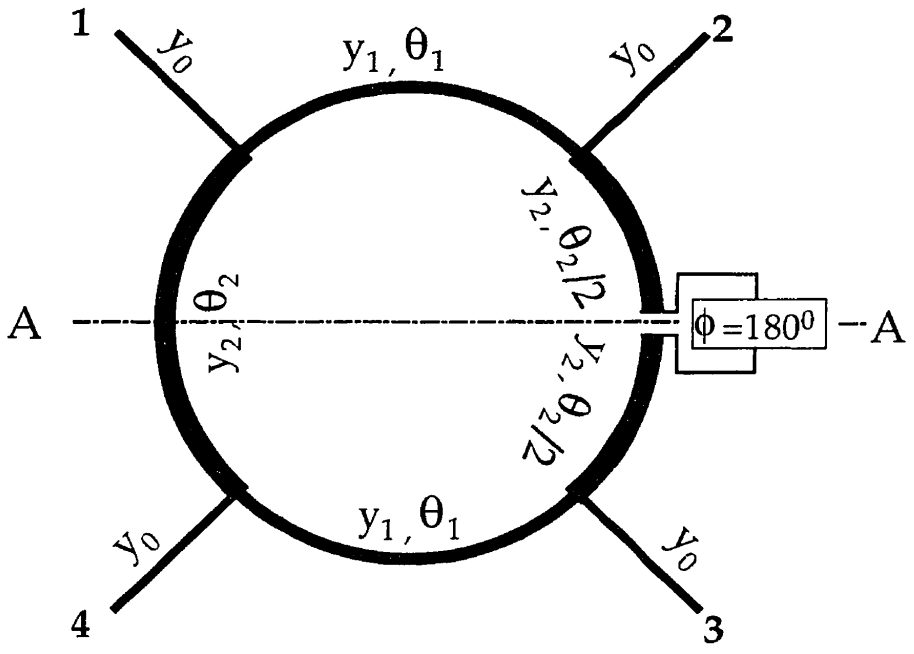

Fig. 5.1 Physical layout of a generalized hybrid-ring coupler with phase inverter.

Generally speaking, a coupler can be simply described by a four-port S-parameter matrix given by

$$S = \begin{bmatrix} S_{11} & S_{12} & S_{13} & S_{14} \\ S_{21} & S_{22} & S_{23} & S_{24} \\ S_{31} & S_{32} & S_{33} & S_{34} \\ S_{41} & S_{42} & S_{43} & S_{44} \end{bmatrix} \tag{5.2}$$

We can now re-write this characteristic matrix with the following simplified form, considering the symmetry and reciprocity of passive circuit,

$$S = \begin{bmatrix} S_{11} & S_{12} & S_{13} & S_{14} \\ S_{12} & S_{22} & S_{23} & S_{13} \\ S_{13} & S_{23} & S_{22} & S_{12} \\ S_{14} & S_{13} & S_{12} & S_{11} \end{bmatrix} \tag{5.3}$$

The S-parameters can be analytically derived from a convenient even- and odd-mode analysis [14], which essentially decomposes the four-port symmetrical structure into a pair of two-port structures.

Under the even- and odd-modes excitation, the resulting two-port networks are simply described by a set of equivalent lumped circuits as shown in Fig. 5.2, in which the shunt admittances $b_1(b_2)$ are given by

$$\begin{cases} b_1 = j \cdot y_2 \cdot \tan(\frac{\theta_2}{2}) \\ b_2 = -j \cdot \dfrac{y_2}{\tan(\frac{\theta_2}{2})} \end{cases} \tag{5.4}$$

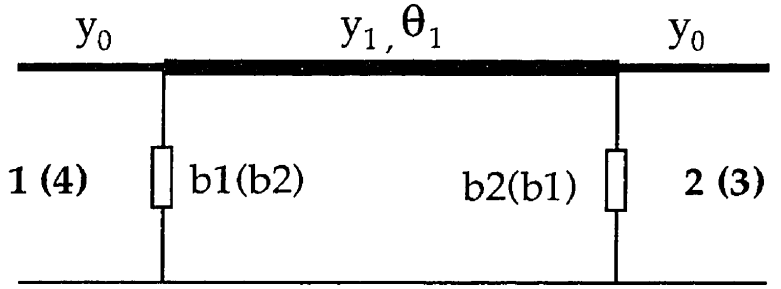

Fig. 5.2 Decomposed network and its equivalent circuit for even- and odd-mode excitation.

With a straightforward analytical manipulation, we can derive the following set of equations for the S-parameters.

$$
\begin{aligned}
s_{11} = s_{22} &= \frac{\cos\theta_1 \cdot z_0 \cdot (b_1 + b_2) + j \cdot z_0 \cdot y_1 \cdot \sin\theta_1 \cdot (1 + b_1 \cdot b_2 \cdot z_1^2 - y_0^2 \cdot z_1^2)}{2 \cdot \cos\theta_1 + (j \cdot z_1 \cdot \sin\theta_1 + \cos\theta_1 \cdot z_0) \cdot (b_1 + b_2) + j \cdot z_0 \cdot y_1 \cdot \sin\theta_1 \cdot (1 + b_1 \cdot b_2 \cdot z_1^2 + y_0^2 \cdot z_0^2)} \\
s_{12} &= \frac{2}{2 \cdot \cos\theta_1 + (j \cdot z_1 \cdot \sin\theta_1 + \cos\theta_1 \cdot z_0) \cdot (b_1 + b_2) + j \cdot z_0 \cdot y_1 \cdot \sin\theta_1 \cdot (1 + b_1 \cdot b_2 \cdot z_1^2 + y_0^2 \cdot z_0^2)} \\
s_{13} &= 0 \\
s_{14} = -s_{23} &= \frac{j \cdot z_1 \cdot \sin\theta_1 \cdot (b_2 - b_1)}{2 \cdot \cos\theta_1 + (j \cdot z_1 \cdot \sin\theta_1 + \cos\theta_1 \cdot z_0) \cdot (b_1 + b_2) + j \cdot z_0 \cdot y_1 \cdot \sin\theta_1 \cdot (1 + b_1 \cdot b_2 \cdot z_1^2 + y_0^2 \cdot z_0^2)}
\end{aligned}
\tag{5.5}
$$

in which $z_0 = 1/y_0$, and $z_1 = 1/y_1$.

The perfect matching condition of the input/output ports requires that s_{11} and s_{22} be zero. This leads to such a simple relation as

$$2 \cdot y_2 \cdot \cot\theta_1 \cdot \cot\theta_2 = y_1 \cdot (1 + y_2^2 \cdot z_1^2 - y_0^2 \cdot z_1^2) \tag{5.6}$$

From (5.5), the amplitude unbalance between two output ports 2 and 4 can be written as

$$\left|\frac{s_{12}}{s_{14}}\right| = \left|\frac{s_{12}}{s_{23}}\right| = \left|\frac{y_1 \cdot \sin\theta_2}{y_2 \cdot \sin\theta_1}\right| \tag{5.7}$$

It is well known that, for a lossless, reciprocal passive and linear four-port network, the S-parameters must obey the unity condition or power conservation condition

$$S \cdot S_t^* = I \tag{5.8}$$

in which S_t^* refers to the transpose and complex conjugate counterpart of S, I is the unit matrix.

Further from (5.8) and (5.7), we can obtain a pair of equations

$$|s_{12}|^2 = \frac{(1-|s_{11}|^2)\cdot|y_1\cdot\sin\theta_2|^2}{|y_1\cdot\sin\theta_2|^2+|y_2\cdot\sin\theta_1|^2}$$
$$|s_{14}|^2 = \frac{(1-|s_{11}|^2)\cdot|y_2\cdot\sin\theta_1|^2}{|y_1\cdot\sin\theta_2|^2+|y_2\cdot\sin\theta_1|^2} \qquad (5.9)$$

Obviously, the above theory is general, and may apply to the analysis and design of a ring coupler with ideal phase inverter and also arbitrary power ratio consideration.

With the help of the above equations, we can summarize principal features and electrical characteristics of a ring coupler with phase inverter as follows.

(a) The signal isolation between the two output ports is perfect and it is independent of frequency since $s_{13}=s_{24}=0$ as long as the general network condition is upheld.

(b) The phase difference between the two output ports is 0°/180° and it is also independent of frequency since $ang(s_{12}/s_{14})=0^0$ and $ang(s_{12}/s_{23})=180^0$.

(c) The power-split ratio between the two output ports is proportional to the square of the term $|y_1\cdot\sin\theta_2/y_2\cdot\sin\theta_1|$. If $\theta_1=\theta_2$, such a power split ratio is obviously

proportional to the square of the ratio of the two admittance variables of the ring as mentioned in [5] and it is independent of frequency.

5.2.2 Design Criteria of 3-dB Coupler

Generally speaking, a coupler design is more or less concerned with the determination of circuit parameters such that certain pre-designated performance specifications can be met over a frequency band of interest. These specifications refer usually to such factors as coupling, matching, and isolation. As indicated above, the isolation for a ring coupler with phase inverter can be made perfectly and it is also frequency-independent. Therefore, we need to only look into design aspects of coupling and matching conditions. In the design of a 3-dB coupler, the two output ports are required to be equal. We can then get from (5.7)

$$z_2 = z_1 \cdot \frac{\sin\theta_1}{\sin\theta_2} \tag{5.10}$$

where $z_2 = 1/y_2$. Note that the absolute sign in (5.10) is eliminated to consider that $\theta_1, \theta_2 < 180^\circ$. It is a typical case in coupler design.

With (5.10) and the perfect matching condition formulated in (5.6), a pair of design equations for a 3 dB ring coupler with phase inverter can be effectively set up by

$$\begin{aligned} z_1 &= z_0 \cdot \frac{\sqrt{2-(\cos\theta_1+\cos\theta_2)^2}}{\sin\theta_1} \\ z_2 &= z_0 \cdot \frac{\sqrt{2-(\cos\theta_1+\cos\theta_2)^2}}{\sin\theta_1} \end{aligned} \tag{5.11}$$

Judging from (5.11), we can claim that there are two degrees of freedom in the coupler design related to the choice of θ_1 and θ_2. Of course, they depend on the expected center frequency and other relevant requirements, for example, operating bandwidth or circuit size. Since the characteristic impedances z_1, z_2 of ring transmission lines have to be larger than zero, the following constraint relationship for θ_1 and θ_2 is established.

$$\theta_1 + \theta_2 > 65.53^0 \tag{5.12}$$

5.2.2.1 Broadband Design Technique

Let us look at (5.7), the two output ports are perfectly balanced and also they are frequency-independent if $\theta_1 = \theta_2 = \theta$ and $z_1 = z_2 = z$. For a broadband design, the circuit parameters of each ring section should be, therefore, set to be the same while the phase inverter is ignored. Since frequency response of coupling and input matching (or return loss) of the coupler is expected to be symmetrical with respect to the axis $\theta = 90^\circ$, it can be shown that the possible maximum bandwidth for certain specifications is achieved with $\theta = 90^\circ$ at the designated center frequency. In the conventional design, the input/output lines are perfectly matched at the center frequency, from which we obtain a classic value of $z = \sqrt{2} \cdot z_0$ for microstrip coupler. In general, the coupling and matching conditions for a broadband application are required only to meet certain tolerance limits over a specific bandwidth of interest even though the circuit may not be matched perfectly at the center frequency. With this argument in mind, we develop a new concept of broadband coupler design that is detailed as follows.

First of all, considering these conditions governed by $\theta_1 = \theta_2 = \theta$ and $z_1 = z_2 = z$, we can obtain from (5.9) and (5.11)

$$|S_{12}|^2 = |S_{14}|^2 = \tfrac{1}{2}\cdot\left(1-|S_{11}|^2\right)$$
$$z = z_0 \cdot \sqrt{2(1-\cot^2\theta)} \qquad (5.13)$$

This equation tells us that the design can be simplified into a design of input matching condition. Judging from (5.13), if the circuit is matched at θ_m, it is also simultaneously matched at $180^\circ - \theta_m$. In view of this fact, such two matching points are actually overlapped at the center frequency in the conventional or classical design. Since the frequency response is symmetrical with respect to the axis point $\theta = 90^\circ$, it is a matter of fact that the maximum effective bandwidth is obtainable only if the maximum in-band return loss is located at the center frequency ($\theta = 90^\circ$). Thus, the new proposed broadband design can be interpreted as a technique allowing the displacement of two matching points away from the classical design point always related to the center frequency. In this way, the calculation of circuit parameters is made once the return loss is defined at the center frequency for the in-band tolerance or specification requirement. It is obviously different from the classical approach.

With the above discussion, we can write down a set of new equations as

$$z = z_0 \cdot \sqrt{2(1-\frac{2}{10^{-\frac{L}{20}}+1})} \qquad (5.14)$$
$$\theta = 90^0 \qquad \text{(at the center frequency)}$$

in which L is the in-band maximum return loss in design consideration. Therefore, the choice of an appropriate ring impedance z depends on L. Obviously, this impedance tends to the conventional value as L goes towards infinity.

Fig. 5.3 plots theoretical curves of the normalized frequency response of return loss and coupling for the conventional and new 3-dB coupler designs. The design parameter in this example is set for a 20-dB in-band return loss limit. These comparative studies indicate that the normalized characteristic impedances of ring line are $\sqrt{2}$ (or 1.414) and 1.28 for the conventional and new design strategies, respectively. As shown in Fig. 5.3, the coupler with the modified design technique has two distinct match points over the frequency band of interest. Under the 20 dB return loss design requirement, the effective bandwidth of coupler is increased by 28% as compared to its conventional counterpart. Note that this 20-dB return loss is acceptable for most commercial applications. Clearly, this trade-off between the bandwidth and maximum in-band return loss gives the designer a freedom in dealing with performance requirements. In this example, the maximum deviation of the in-band coupling from the ideal case (or flatness) is –0.044 dB. Fig. 5.4 shows the relative bandwidth and maximum in-band deviation of coupling versus the input return loss, indicating that the new coupler design yields always a better bandwidth performance.

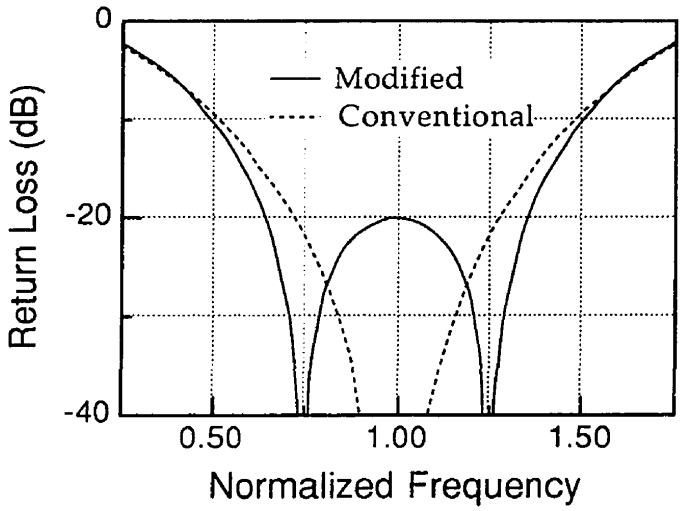

(a)

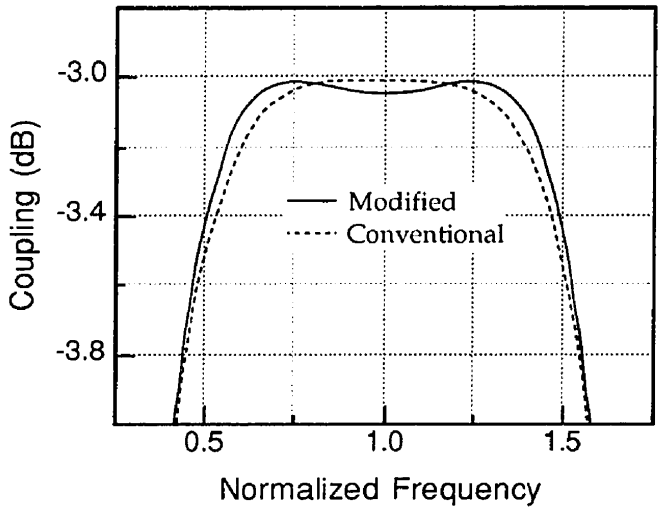

(b)

Fig. 5.3 Comparative normalized frequency responses of the return loss and coupling for hybrid ring couplers using the conventional and proposed design techniques. (a) Characteristics of the return loss. (b) Characteristics of the coupling.

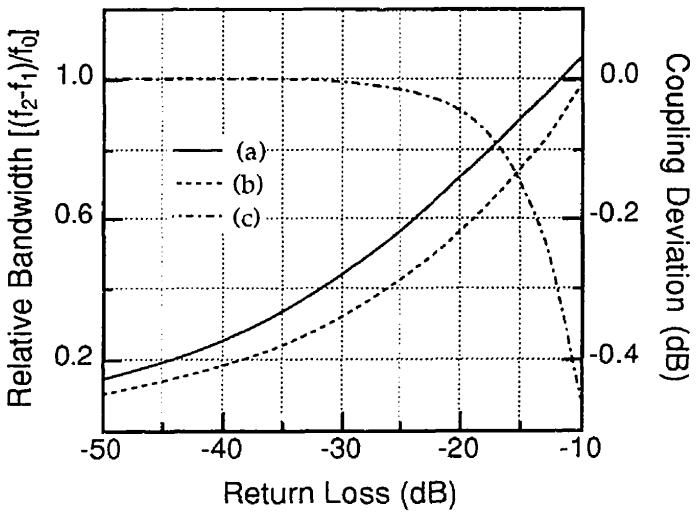

Fig. 5.4 Characteristic curves of relative bandwidth and coupling deviation versus the input return loss. Curve (a) refers to the relative bandwidth obtained from the new design scheme. Curve (b) is the relative bandwidth for the conventional design. Curve (c) represents the in-band maximum deviation of coupling.

5.2.2.2 Narrow-Band Design Technique

In some cases, the bandwidth may not be the primary concern in the coupler design. On the contrary, a narrow-band operation is desirable. Therefore, the input impedance should be matched at the center frequency as in case of the conventional design. The relevant circuit parameters can be usually calculated from (5.11). Since there are two degrees of freedom related to the choice of θ_1 and θ_2, these circuit parameters could be arbitrary. In practice, we prefer to have a compact coupler size. This motivation leads to the other design rule that can be applied to minimizing $\theta_1 + \theta_2$ under certain fabrication requirements. It can be seen from (5.12) that the circumference of a size-reduced coupler must be in any case larger than $3\lambda_g/8$. Fig. 5.5 shows theoretical prediction of the

normalized frequency response of return loss and coupling for a hybrid ring coupler having $0.5\lambda_g$ circumference with a set of circuit parameters: $\theta_1 = 30^0$, $\theta_2 = 60^0$, $z_1 = 0.7321 z_0$ and $z_2 = 0.4226 z_0$. We can see that the circuit is matched perfectly at the center frequency and the 20-dB return loss bandwidth is roughly 7%. The amplitude flatness over the designed bandwidth is about 0.09 dB. Note that the design equation using $\lambda_g/8$ or $\lambda_g/6$ sections in [9] is just a special case of (5.11) as the $0.5\lambda_g$ line section is replaced by a phase inverter. Although the above example is only related to the design of 3-dB coupler, our derived design equations are applicable to coupler design with arbitrary power ratio or division.

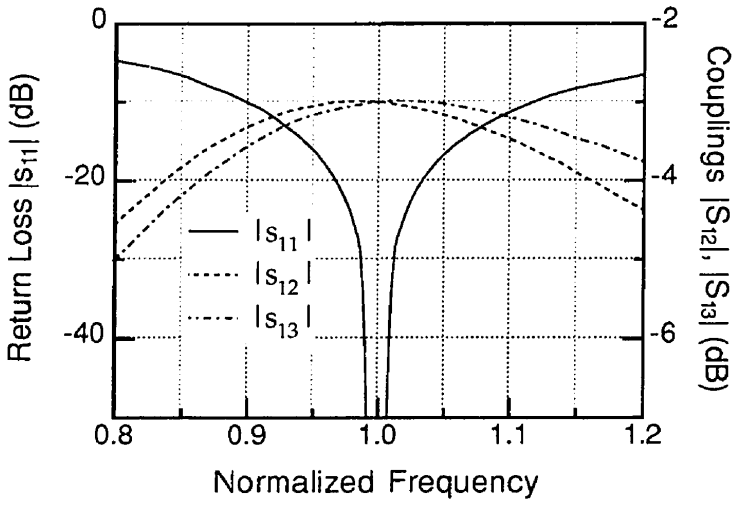

Fig. 5.5 Normalized frequency responses of the return loss and coupling for a narrow-band coupler design with such physical parameters as $\theta_1 = 30^0$, $\theta_2 = 60^0$, $z_1 = 0.7321 z_0$ and $z_2 = 0.4226 z_0$.

5.3 Uniplanar Guided-Wave Structure and Phase Inverter

As presented above, uniplanar MICs have become a competitive alternative to the conventional microstrip MICs. In the uniplanar scheme, key elements are designed with uniplanar guided-wave structures, which usually consist of CPW, coplanar strip (CPS), slot-line, and micro-coplanar strip (MCS) as illustrated in Fig. 5.6. Generally speaking, these lines have advantages of easy realization of short-circuited ends, and simple integration of series and shunt passive and active chip elements. As all conductors are located on the same side of substrate, it permits a high-level of integration and is well-suited to high-frequency design since the grounding connection through via-holes is eliminated and potential parasitic effects related to active device implementation may be minimized. In addition, potentially easy inter-transition or balun among different structures provides a great flexibility for circuit design. The essential attributes of these uniplanar structures are summarized in Table 1. Since the CPW is known to have two fundamental modes, air-bridge that suppresses slot-line mode is required in the circuit. Judging from the balanced and unbalanced characteristics of uniplanar guided-wave structures, a balun for large number of applications may be easily realized. Note that the geometry of Fig. 5.6(d) is named differently in [15, 16]. This structure consists of a ground plane, a strip and a substrate with electrical properties similar to those of microstrip line; the term MCS used in [17] is, in our opinion, appropriate. Our MCS geometry is slightly different from that of [17] in which the backside of the substrate is metallized.

Table 5.1 Basic attributes and properties of uniplanar guided-wave structures.

Guided-Wave Structure	Line	Mode	Number of Fundamental Modes	Loss of Radiation
CPW	unbalanced	Quasi-TEM	2	low
CPS	balanced	Quasi-TEM	1	medium
Slotline	balanced	TE	1	high
MCS	unbalanced	Quasi-TEM	1	medium

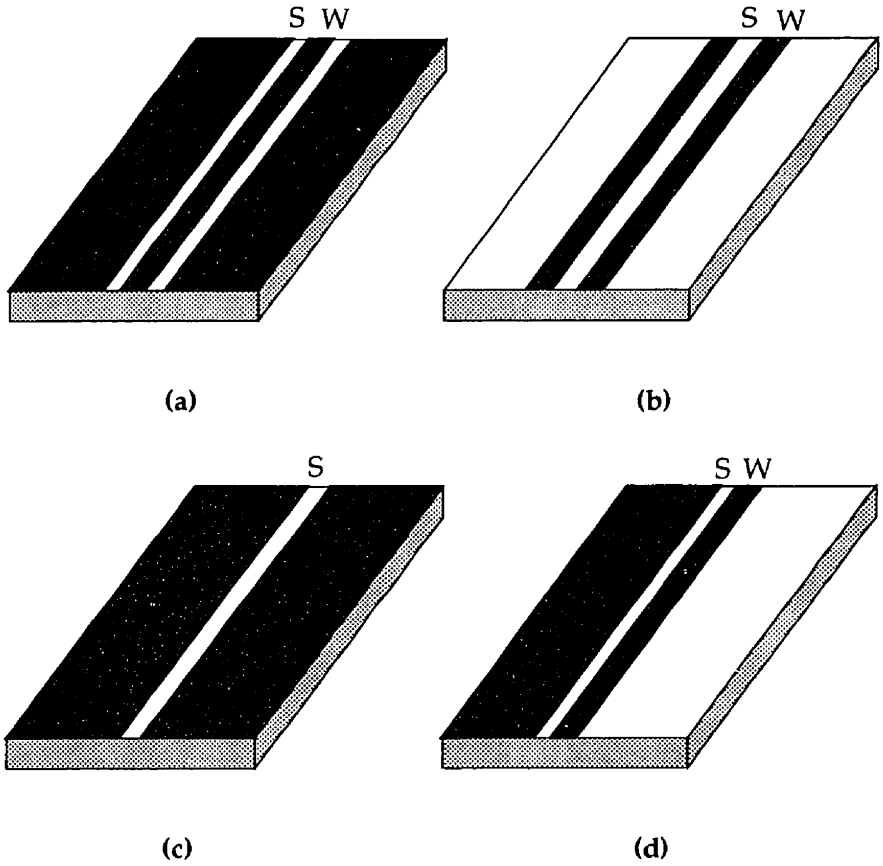

Fig. 5.6 Schematic view of a class of uniplanar guided-wave structures suitable for broadband and size-reduced hybrid ring coupler design. (a) Coplanar waveguide (CPW). (b) Coplanar strip (CPS). c) Slot-line, (d) Micro-coplanar strip (MCS).

For the MCS, only very limited accurate design databases derived from full-wave analysis are available in publications. To facilitate our subsequent design and experiments on the proposed design technique, we have used an enhanced spectral domain approach (ESDA) detailed in [18] to calculate parametric effects and electrical properties of MCS. Fig. 5.7(a) displays dispersion characteristics of MCS that are very useful for our design. It is shown that the effective dielectric constant increases with frequency while the line characteristic impedance increases at first with frequency and then becomes flat over the rest of frequency range. Our curves indicate also that the guided-wave characteristics are sensitive to the conductor thickness t. Fig. 5.7(b) gives MCS parametric effect of propagation constant and characteristic impedance against the strip width for different slot width. We observe that both effective dielectric constant and line impedance decrease with the strip width. It is also found that the variation of line impedance is more pronounced for small strip width. The characteristic impedance increases with the slot width, whereas the effective dielectric constant decreases. The effect of slot width on propagation characteristics is quite similar to that of the substrate height of the microstrip on propagation characteristics.

It has already been mentioned that a phase inverter is required in the design of a broadband and size-reduced ring coupler. In recent years, effects have been directed to the development of a broadband phase inverter. In general, a phase inverter may be obtained by means of reversing field orientations with reference to a particular ground plane. This mechanism can be easily realized with uniplanar techniques since all the conductors are located on the same side of substrate. Some broadband uniplanar phase inverters have been reported in [19, 20]. In accordance with the balanced and unbalanced features of uniplanar guided-wave structures, the phase inverter may be classified into three types: balanced, unbalanced and balun. Fig. 5.8 gives a schematic

sketch of circuit layouts of the balanced- and unbalanced-type phase inverters. They consist of single-type transmission line at the input and output ports and the phase reversal is done by a crossover of two lines. Fig. 5.8(a) and Fig. 5.8(b) present the balanced-type phase inverters, which are composed of the balanced-lines: CPS and slot-line. Fig. 5.8(c) and Fig. 5.8(d) are the unbalanced-type phase inverters that are made of the unbalanced lines: MCS and CPW. In Fig. 5.8, the radial stubs are used to obtain an open circuit at the cross point. Note that the field orientations over the radial stubs for the balanced-type are different from those for the unbalanced-type. In Fig. 5.8(b), the field orientations of the radial stubs are opposite, to name an example. It can be expected that radiation fields cancel out with each other, at least, at the normal direction. We can also see that Fig. 5.8(d) has a higher radiation loss than the others since its field orientations in the radial stubs are the same.

Fig. 5.9 portrays schematically the circuit layout and E-field profile of the balun-type phase inverters. They contain two balun transitions. The phase reversal is achieved by means of two baluns that are connected on opposite sides of each other (or back-to-back connection). It is shown that the field orientations with reference to the ground plane are reversed at the input and output ports. Fig. 5.9(a) and Fig. 5.9(b) consist of CPW, slot-line and radial stubs. The slot-line is connected to the opposite side of the CPW, and the radial stubs provide a broadband open circuit at the end of the remaining slot in the CPW. In Fig. 5.9(c) and Fig. 5.9(d), ground planes at the input and output ports are reversed by means of the balanced lines: slot-line and CPS. We can expect that these configurations are well-suited to broadband applications since there are no radial stubs and crossover bending line or bridge line. On the other hand, Fig. 5.9(c) and Fig. 5.9(d) become identical as long as the length of the balanced line is set to be zero.

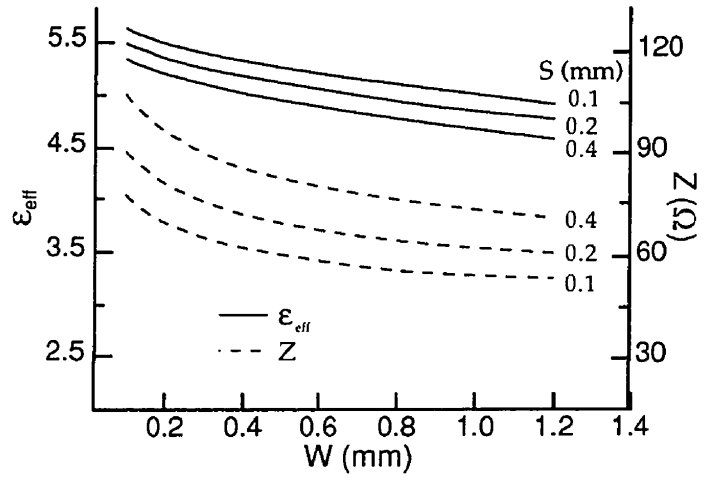

(a)

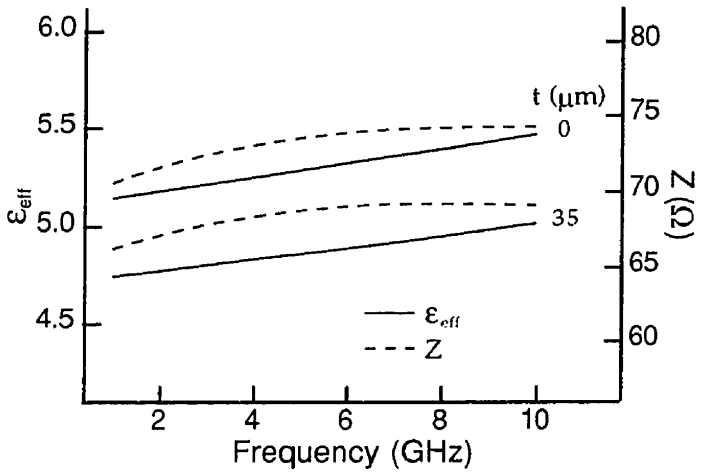

(b)

Fig. 5.7 Guided-wave characteristics of micro-coplanar strip (MCS) lines with substrate parameters of $h = 1.27$ mm (height) and $\varepsilon_r = 10.2$ (relative dielectric constant). (a) Effective dielectric constant ε_{eff} and characteristic impedance $Z(\Omega)$ versus frequency for different conductor thickness with $W = 0.4$ mm and $S = 0.2$ mm. (b) Effective dielectric constant ε_{eff} and characteristic impedance $Z(\Omega)$ versus the strip width for three different slot widths with $f = 2$ GHz.

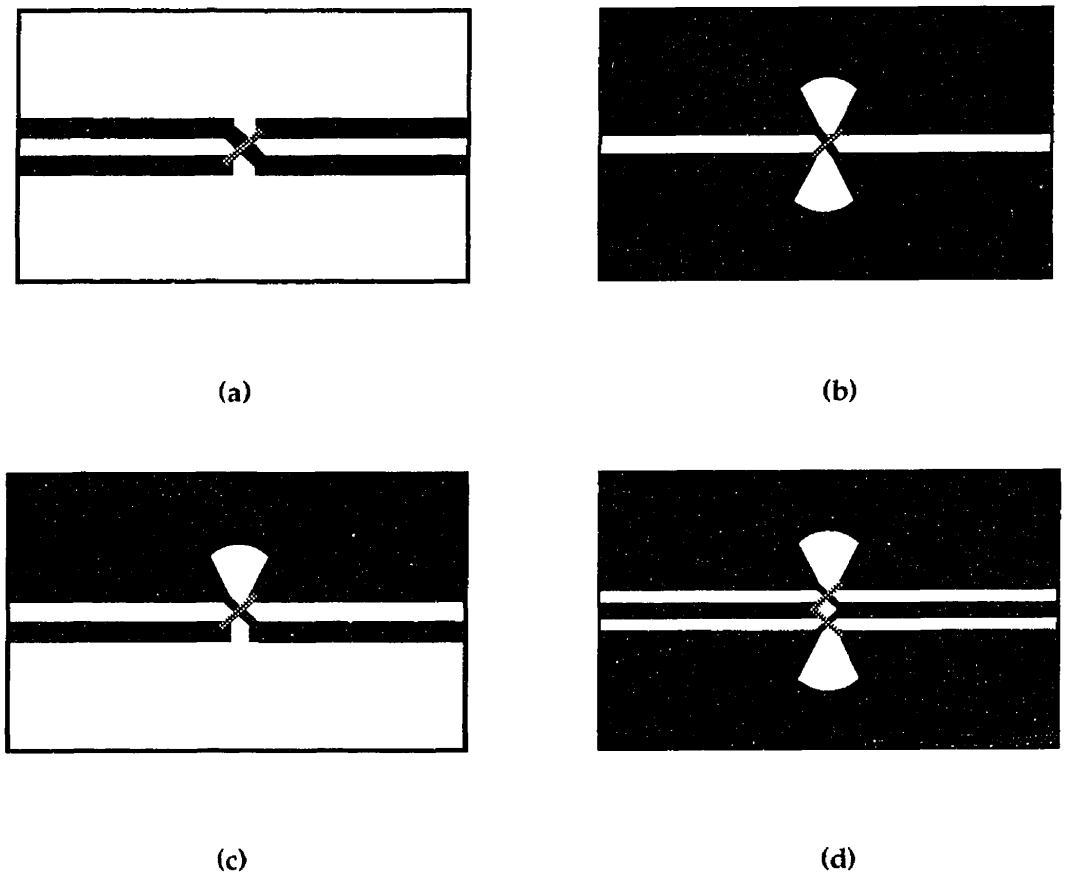

Fig. 5.8 Graphic sketch of uniplanar balanced- $\{(a).(b)\}$ and unbalanced-type $\{(c).(d)\}$ phase inverters.

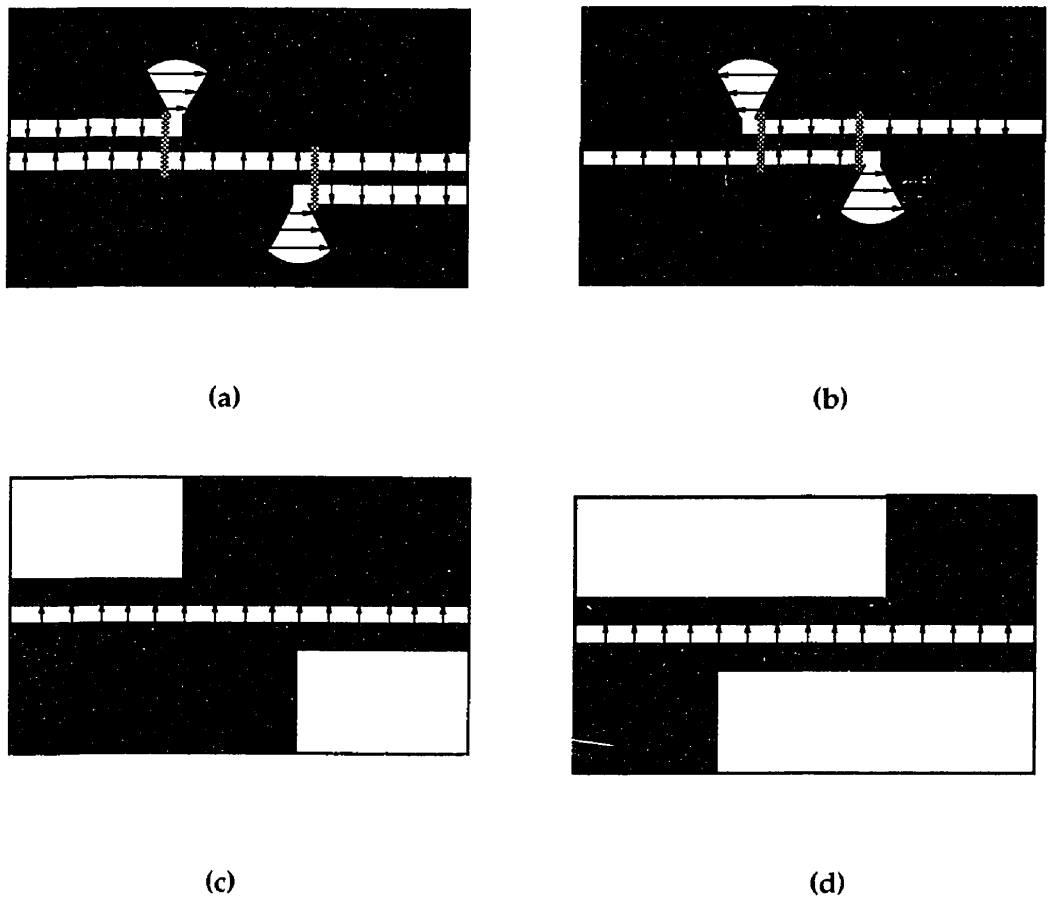

Fig. 5.9 Illustration of uniplanar balun-type phase inverters. (a) CPW-slotline-CPW. (b) Slot-line-CPW-slot-line. (c) MCS-slot-line-MCS. (d) MCS-CPS-MCS.

5.4 Experiments and results discussion

To confirm and validate our proposed design theory and criteria, broadband phase inverters and 3 dB couplers have been designed and measured, which used the above-discussed uniplanar schemes. The samples were fabricated on a RT/Duroid 6010 substrate with $\varepsilon_r = 10.2$ and a thickness of 1.27 mm (Rogers^{TM}). All circuit dimensions are designed with our ESDA algorithm developed in [18].

5.4.1 Phase Inverter

Fig. 5.10(a) shows the circuit layout of a broadband phase inverter. It is a balanced-type as shown in Fig. 5.8(a). In order to match the coupler geometry that is given in Fig. 5.11, two MCS lines and a copper-removed rectangular area are designed for the experimental sample. The circuit dimensions and rectangular area are characterized by 10×20 and 4×6 mm^2, respectively. The gap width (S) of MCS and CPS lines is set to be 0.25 mm. The strip widths are 0.6 and 1.1 mm, respectively. The gap width (G) of the crossover as shown in Fig. 5.10(a) is 0.4 mm. A set of coaxial test fixtures is used in the experimental set-up. A conventional Thru-Reflect-Line (TRL) calibration technique is used with an HP8510C network analyzer. The reference plane is set up at the middle of the circuit so as to eliminate the phase difference generated by the physical length of the circuit. Measured frequency response of the insertion loss and phase shift is plotted in Fig. 5.10(b). It is found that the insertion loss is smaller than 1 dB in the frequency range of 1.31 – 5 GHz. The effective bandwidth for less than ± 20° phase shift error is defined from 1.17 to 5 GHz. This experiment shows that the broadband performance of phase inverter is readily achievable with the uniplanar technique, and the circuit is ready for the broadband coupler design with the proposed scheme.

5.4.2 3-dB Hybrid Ring Coupler

Now, let us look into the detail of a 3 dB coupler design with its circuit layout illustrated in Fig. 5.11 that consists of a MCS ring line with a broadband CPS phase inverter. This coupler has four CPW to MCS T-junctions, three MCS arms and a phase inverter arm with a combination of MCS and CPS. The CPW feed lines (input and output ports) have a characteristic impedance of $z_0 = 50\Omega$, which corresponds to $W = 0.8$ mm and $S = 0.33$ mm. The MCS and CPS lines located on the ring circumference have a characteristic impedance of 64.2Ω with $W = 0.8$ mm and $S = 0.2$ mm for the MCS line, and $W = 1.3$ mm and S = 0.2 mm for the CPS line. The average circumference of the ring line is 62.8 mm, which points to the center frequency of 2.17 GHz. It should be noted that the effective dielectric constant of CPS on the ring is slightly different from that of MCS. For our experiments, this difference is ignored for our design convenience. Our coupler design is based on the network approach. The measurements were completed with an HP8510C network analyzer with a set of coaxial test fixtures, similar to the phase inverter experiments.

Fig. 5.12 gives a set of measured frequency responses for the return loss, coupling, isolation and phase difference. Fig. 5.12(a) shows the effective frequency bandwidth for a return loss better than –15 dB is from 1.5 to 2.7 GHz for $|s_{11}|$, $|s_{44}|$ and from 1.3 to 3 GHz for $|s_{22}|$, $|s_{33}|$, respectively. The two matching points are clearly observed in the frequency range as predicted by the proposed design theory. The measured frequency response agrees reasonably well with the theoretical curves as shown in Fig. 5.3(a). The bandwidth reduction for $|s_{11}|$and $|s_{44}|$ is essentially caused by the imperfect performance of the designed phase inverter as shown in Fig. 5.10(b). This is because the 180° constant phase shifting is assumed in the developed design theory over the frequency

bandwidth of interest, that is not the case in the above designed phase inverter. It may also be attributed to line curvature of the phase inverter in the design of coupler. Fig. 5.12(b) shows that the coupling for any ports is always within 3.5±0.5 dB over more than octave bandwidth from 1.43 to 2.95 GHz. Fig. 5.12(c) displays an important feature of the new coupler design. The isolation is better than 20 dB for more than 1.8 octave bandwidth. The differences between the two output ports are shown in Fig. 5.12(d). Results indicate that such phase difference errors for the in-phase and the out-of-phase is less than ±6.7° and ±5° over the frequency bandwidth from 1.5 to 3.5 GHz, respectively. These electrical performances are made with our non-negligible fabrication tolerance and other electrical and mechanical errors.

5.5 Conclusion

In this paper, a new design theory is successfully developed in an attempt to enhance electrical and mechanical performances of hybrid ring couplers for use in the design of M(H)MICs. This proposed size-reduction and band-broadening design technique of hybrid ring coupler makes use of phase inverter realised by hybrid uniplanar schemes. Interesting design features and performance enhancement factors are presented and summarized in detail for the reverse-phase hybrid ring coupler. A class of uniplanar phase inverters is described with three types of building blocks in the form of balanced-, unbalanced- and balun-types. The proposed concept provides freedom and trade-off in the design of broadband/narrow-band and size-reduced couplers compared with the conventional approach. New uniplanar phase inverter and 3-dB coupler have been designed in accordance with the proposed design scheme to confirm and validate our derived design equations. Experimental results show that the phase inverter has more than 1.9 octave bandwidth with an insertion loss better than 1 dB and a phase shift less

than ±20° in the designed frequency range. Our designed sample indicates that the proposed theory is useful for the design and realization of broadband and size-reduced couplers. This concept can be also applied in a straightforward manner to planar and nonplanar guided-wave structures other than the presented uniplanar geometry for coupler design.

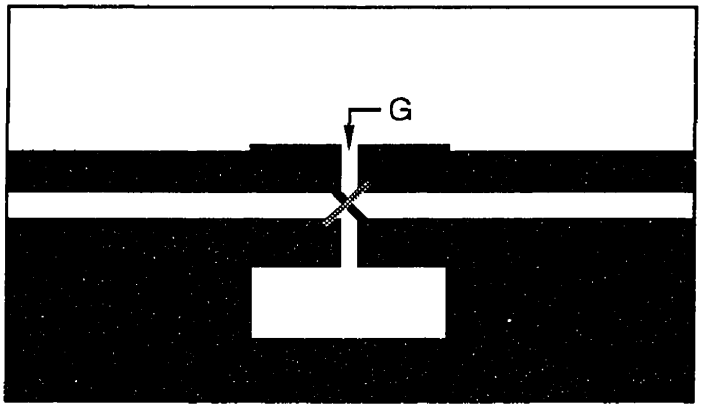

(a)

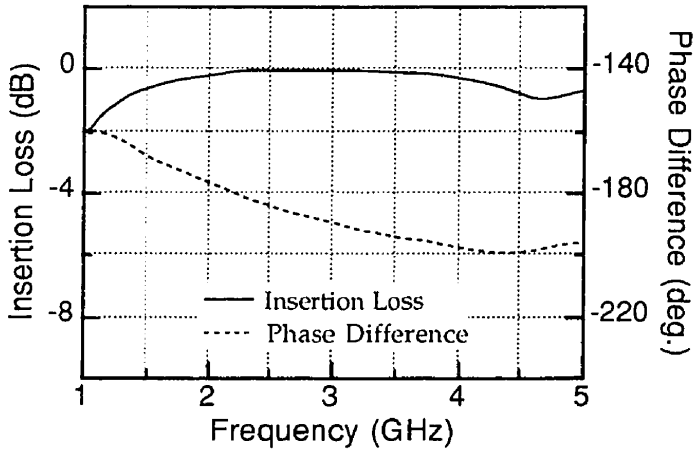

(b)

Fig. 5.10 Experimental balanced-type phase inverter consisting of MCS and CPS structures. (a) Uniplanar circuit layout. (b) Measured frequency response of the insertion loss and phase shift.

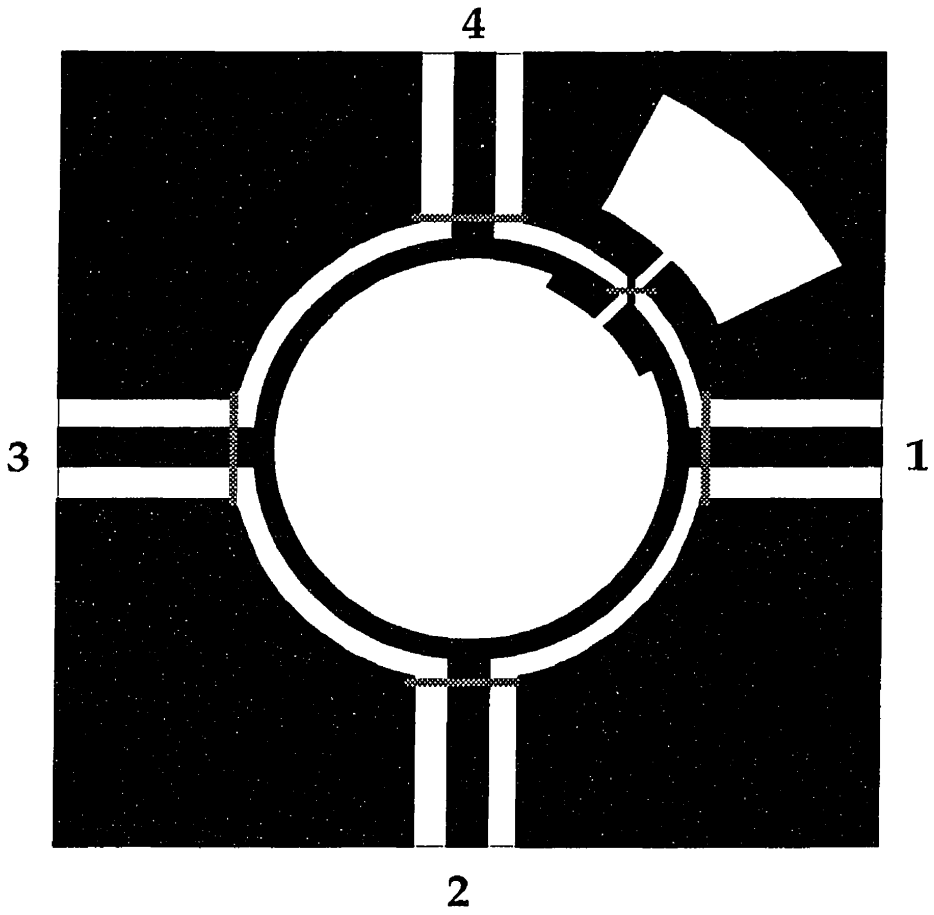

Fig. 5.11 Detailed circuit layout of a designed MCS-based hybrid ring coupler with CPS phase inverter for broadband and size-reduction experiments.

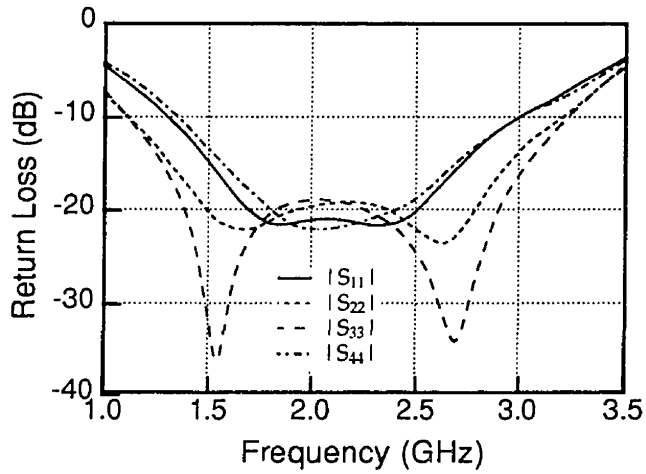

(a)

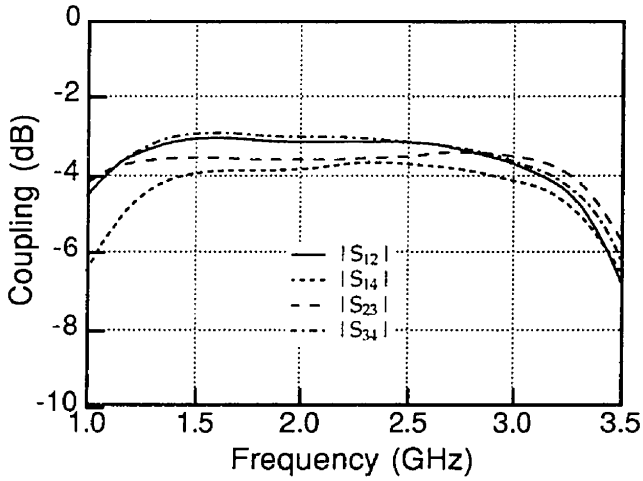

(b)

Fig. 5.12 Measured frequency-dependent characteristics for the designed MCS hybrid ring coupler with CPS phase inverter as shown in Fig. 5.11. (a) Return loss of 4 ports. (b) Coupling performance.

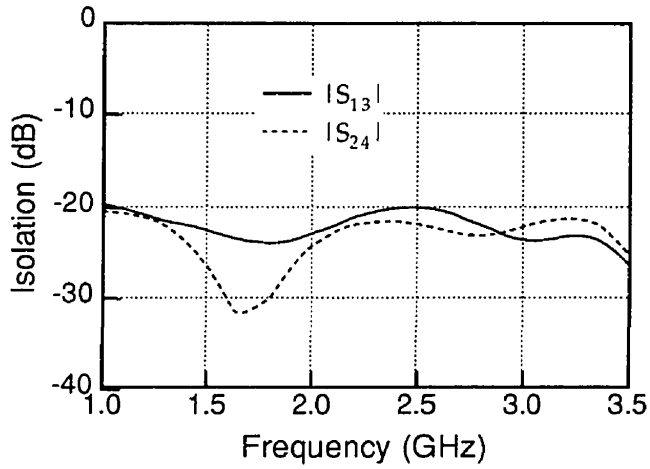

(c)

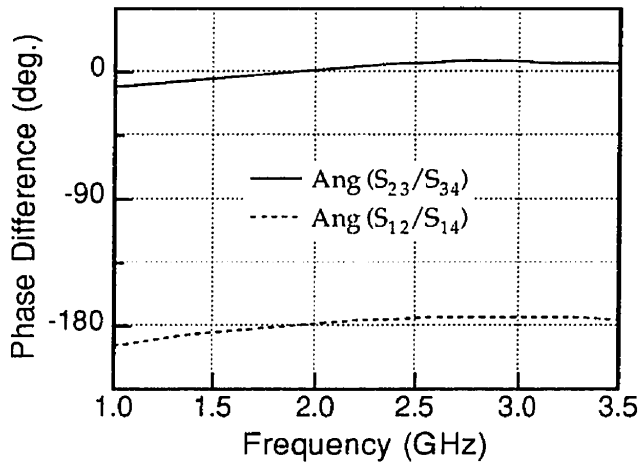

(d)

Fig. 5.12 Measured frequency-dependent characteristics for the designed MCS hybrid ring coupler with CPS phase inverter as shown in Fig. 5.11. (c) Isolation behavior. (d) Phase difference (error).

Acknowledgement

We would like to acknowledge financial support from the National Sciences and Engineering Research Council (NSERC) of Canada under a research grant. And also, we would like to appreciate very much technical assistance of Ou Zifei during the course of this research work.

References

[1] J. Lange, "Interdigitated strip-line quadrature hybrid," in *1969 G-MTT Int. Microwave Symp. Dig.*, pp. 10-13.

[2] B. Schiek, "Hybrid branchline coupler -- a useful new class of directional couplers," *IEEE Trans. Microwave Theory Tech.*, vol. MTT-22, pp. 864-869, Oct. 1974.

[3] R. K. Hoffman and J. Siegl, "Microstrip-slot coupler design, Part I and II," *IEEE Trans. Microwave Theory Tech.*, vol. MTT-30, pp. 1205-1216, Aug. 1982.

[4] A. F. Celliers and J. A. G. Malherbe, "Design curves for -3-dB branch-line couplers,' *IEEE Trans. Microwave Theory Tech.*, vol. MTT-33, pp. 1226-1228, Nov. 1985.

[5] C. Y. Pon, "Hybrid-ring directional coupler for arbitrary power division," *IRE Trans. Microwave Theory Tech.*, vol. 9, pp. 529-535, Nov. 1961.

[6] S. March, "A wide band stripline hybrid ring," *IEEE Trans. Microwave Theory Tech.*, vol. MTT-16, p. 361, June 1968.

[7] L. W. Chua, "New broad-band matched hybrids for microwave integrated circuits," in *1971 Proc. European Microwave Conf.*, pp. C4/5:1 - C4/5:4.

[8] D. I. Kim and Y. Naito, "Broad-band design of improved hybrid-ring 3-dB directional couplers," *IEEE Trans. Microwave Theory Tech.*, vol. MTT-30, pp. 2040-2046, Nov. 1982.

[9] D. I. Kim and G. S. Yang, "Design of new hybrid-ring directional coupler using $\lambda/8$ or $\lambda/6$ sections," *IEEE Trans. Microwave Theory Tech.*, vol. MTT-39, pp. 1779-1783, Oct. 1991.

[10] M. Muraguchi, T. Hirota, A. Minakawa, K. Ohwada, and T. Sugeta, "Uniplanar MMIC's and their applications," *IEEE Trans. Microwave Theory Tech.*, vol. MTT-36, pp. 1896-1901, Dec. 1988.

[11] T. Hirota, Y. Tarusawa, and H. Ogawa, "Uniplanar MMIC hybrids -- a proposed new MMIC structure," *IEEE Trans. Microwave Theory Tech.*, vol. MTT-35, pp. 576-581, June 1987.

[12] C. H. Ho, L. Fan, and K. Chang, "New uniplanar coplanar waveguide hybrid-ring couplers and Magic-T's," *IEEE Trans. Microwave Theory Tech.*, vol. MTT-42, pp. 2240-2248, Dec. 1994.

[13] M. Murgulescu, et. al., "New wideband, $0.67\lambda_g$ circumference 180^0 hybrid ring coupler," *Elect. Lett.*, vol. 30, pp.299-300, Feb. 1994.

[14] J. Reed and G. J. Wheeler, "A method of analysis of symmetrical fourport networks," *IRE Trans. Microwave Theory Tech.*, vol. 4, pp. 246-252, Oct. 1956.

[15] I. Kneppo and J Gotzman, "Basic parameters of nonsymmetrical coplanar lines," *IEEE Trans. Microwave Theory Tech.*, vol. MTT-25, p. 718, Aug. 1977.

[16] L. Fan and K. Chang, "Uniplanar MIC power dividers using coupled CPW and asymmetrical CPS," in *IEEE MTT-s Int. Microwave Symp. Dig.*, 1996, pp. 781-784.

[17] E. Yamashita, K. R. Li, E. Kaneko, and Y. Suzuki, "Characterization method and simple design formulas of MCS lines proposed for MMIC's," in *IEEE MTT-s Int. Microwave Symp. Dig.*, 1987, pp. 685-688.

[18] T. Wang and K. Wu, "An efficient approach to modeling of quasi-planar structures using the formulation of power conservation in spectral domain," *IEEE Trans. Microwave Theory Tech.*, vol. MTT-43, pp. 1136-1142, May 1995.

[19] T. Wang, Z. Ou, and K. Wu, "Experimental study of wideband uniplanar phase inverters for MICs," in *IEEE MTT-s Int. Microwave Symp. Dig.*, 1997, pp. 777-780.

[20] L. Fan, B. Heimer, and K. Chang, "Uniplanar hybrid couplers using asymmetrical coplanar strip lines," in *IEEE MTT-s Int. Microwave Symp. Dig.*, 1997, pp. 273-276.

Chapitre VI

Approche avec partition de domaines

En général, tout circuit intégré micro-ondes comprend deux éléments de base : des lignes de transmission et des discontinuités. La connaissance des caractéristiques de propagation des structures guide d'onde planaires, constitue une pierre de voûte sur laquelle repose le succès du design. La prédiction précise des performances d'un circuit est presque impossible sans une caractérisation appropriée des discontinuités. Ceci est particulièrement vrai aux hautes fréquences. Les discontinuités dans les circuits planaires surviennent aux jonctions entre les composants actifs et les lignes de transmission passive ou entre dispositifs passifs uniquement. Elles peuvent se présenter sous une grande forme de variétés possibles telles que des jonctions de lignes, des coudes, des interruptions de lignes, des sauts d'impédance, etc.... Ces configurations sont à l'origine d'une classe de problèmes électromagnétiques difficiles à résoudre. Une des raisons de ces difficultés provient du fait que l'analyse de ces discontinuités exige l'obtention d'informations sur des phénomènes locaux. Durant les dix dernières années, de nombreux efforts ont été concentrés sur le développement de techniques numériques en vue de modéliser précisément le circuit et la discontinuité en un seul bloc. Des méthodes efficaces telles que la méthode des lignes et la méthode spectrale permettent seulement l'analyse de structures simples. D'autres méthodes plus souples telles que la méthode des éléments finis et la matrice des lignes de transmission (TLM) élargissent le domaine possible d'étude à une classe de configurations de circuits plus complexes, mais leur efficacité et leur précision sont limitées.

Dans ce chapitre, une nouvelle approche reposant sur une partition de sous-domaines est proposée pour la caractérisation de circuits micro-ondes de forme arbitraire (résolution de problèmes aux valeurs propres et étude de discontinuités). Une matrice caractéristique reliant les valeurs des champs le long des frontières de petits sous-domaines est directement dérivée des équations de Maxwell en utilisant les techniques des différences centrées et de calcul par moyenne. Deux exemples numériques sont présentés pour valider la formulation. Le principal avantage de la technique proposée est qu'elle permet facilement une caractérisation d'une structure complexe avec une grande efficacité et une grande précision. Le chapitre est présenté par l'intermédiaire d'un article publié en avril 1996 dans la revue Microwave and Optical Technology Letters.

A Novel Domain-Partitioning Approach for Modeling Arbitrarily Shaped Microwave Circuits

Tongqing Wang, Jifu Huang, Ke Wu, Senior Member, IEEE
Poly-Grames, Dépt. de génie électrique et de génie informatique,
École Polytechnique, C. P. 6079, Succ. "Centre-Ville",
Montréal, Québec, Canada H3C 3A7

Abstract

A novel domain-partitioning approach (DPA) is presented for field-theoretical modeling and design of arbitrarily shaped microwave circuit problems. The new technique is derived from a finite-difference strategy with networking interconnection. Simple examples are demonstrated and compared with available results. The advantage of the proposed approach compared to other techniques in the discrete domain is highlighted by its efficiency and accuracy.

Key terms : numerical technique, guided-wave structure, finite difference.

6.1 Introduction

The state-of-the-art advance in microwave integrated circuits requires efficient and accurate modeling as well as field-theoretical design tools. To our knowledge, most of numerical techniques developed so far present efficient applications that are usually limited to a particular class of circuit geometries such as the spectral domain approach (SDA) [1] and the method of lines [2] for analysis of planar multilayered structures. The discrete domain techniques such as the finite-difference technique [3] and transmission line matrix (TLM) method [4, 5] are well known for their ability of handling complex geometries of guided-wave structures and circuits in both time- and frequency-domains. On the other hand, the finite-element method [6] and minimum autonomous block (MAB) approach [7, 8] have been also used in the analysis of a large class of microwave circuits. The features associated with these techniques have been well documented. When used in the modeling of complex planar circuits, these discrete techniques have a shortcoming of low convergence.

The domain-partitioning approach (DPA) is proposed in this letter to provide an alternative for the modeling of complex guided-wave structures and circuits. The new technique is based on a central finite-difference scheme coupled with a networking interconnection, thus preserving the advantages of the discrete domain techniques with the additional feature of rapid convergence.

6.2 Description of Domain-Partitioning Approach

The limited space of this letter only allows to brief the principle and feature of the proposed DPA. In field-theoretical analysis, an electromagnetic domain may be divided into a number of subdomains along the coordinate surface of an orthogonal coordinate

system as it has been done in [7]. Its analysis procedure may be decomposed into two steps. First, a modal solution is established by a characteristic matrix that relates boundary field quantities of the subdomain (local solution). The second step is to obtain a global characteristic equation by applying a networking interconnection on the basis of the field continuity condition at the interface of joined subdomains. Then, electrical parameters of the analysis domain are extracted with the algorithm developed in [5, 7]. Obviously, the key point in this analysis is how to derive the characteristic matrix of subdomain subject to the networking. This issue will be highlighted in the letter.

In the rectangular coordinate system, a typical subdomain is shown in Fig. 6.1 whose dimensions are denoted by Δ_x, Δ_y, and Δ_z, along the x, y, and z directions, respectively. Its six boundary planes are labeled by k (k = 1, 2, 3, 4, 5, and 6). Through applying the central finite-difference and averaging principles, Maxwell's curl equations are expressed in the following finite-difference form:

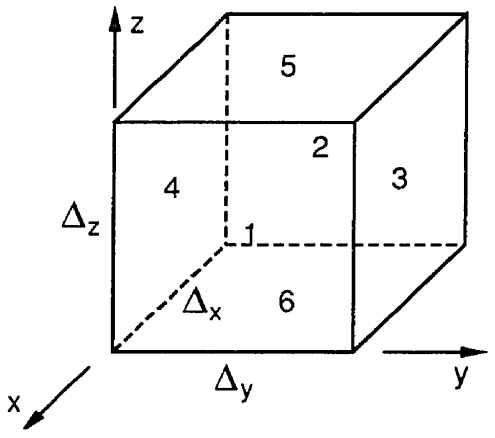

Fig. 6.1 Space view of a subdomain considered in the DPA

$$
\begin{aligned}
&j\omega\mu\tfrac{\Delta_1}{4}(H_{x3}+H_{x4})+\Delta_z(E_{z3}-E_{z4})-\Delta_y(E_{y5}-E_{y6})=0\\
&j\omega\mu\tfrac{\Delta_3}{4}(H_{y5}+H_{y6})+\Delta_x(E_{x5}-E_{x6})-\Delta_z(E_{z1}-E_{z2})=0\\
&j\omega\mu\tfrac{\Delta_5}{4}(H_{z1}+H_{z2})+\Delta_y(E_{y1}-E_{y2})-\Delta_x(E_{x3}-E_{x4})=0\\
&j\omega\varepsilon\tfrac{\Delta_1}{4}(E_{x3}+E_{x4})-\Delta_z(H_{z3}-H_{z4})+\Delta_y(H_{y5}-H_{y6})=0\\
&j\omega\varepsilon\tfrac{\Delta_3}{4}(E_{y5}+E_{y6})-\Delta_x(H_{x5}-H_{x6})+\Delta_z(H_{z1}-H_{z2})=0\\
&j\omega\varepsilon\tfrac{\Delta_5}{4}(E_{z1}+E_{z2})-\Delta_y(H_{y1}-H_{y2})+\Delta_x(H_{x3}-H_{x4})=0\\
&j\omega\mu\tfrac{\Delta_1}{4}(H_{x5}+H_{x6})+\Delta_z(E_{z3}-E_{z4})-\Delta_y(E_{y5}-E_{y6})=0\\
&j\omega\mu\tfrac{\Delta_3}{4}(H_{y1}+H_{y2})+\Delta_x(E_{x5}-E_{x6})-\Delta_z(E_{z1}-E_{z2})=0\\
&j\omega\mu\tfrac{\Delta_5}{4}(H_{z3}+H_{z4})+\Delta_y(E_{y1}-E_{y2})-\Delta_x(E_{x3}-E_{x4})=0\\
&j\omega\varepsilon\tfrac{\Delta_1}{4}(E_{x5}+E_{x6})-\Delta_z(H_{z3}-H_{z4})+\Delta_y(H_{y5}-H_{y6})=0\\
&j\omega\varepsilon\tfrac{\Delta_3}{4}(E_{y1}+E_{y2})-\Delta_x(H_{x5}-H_{x6})+\Delta_z(H_{z1}-H_{z2})=0\\
&j\omega\varepsilon\tfrac{\Delta_5}{4}(E_{z3}+E_{z4})-\Delta_y(H_{y1}-H_{y2})+\Delta_x(H_{x3}-H_{x4})=0
\end{aligned}
\qquad (6.1)
$$

where $E_{x(y,z)k}$ and $H_{x(y,z)k}$ are tangential electric and magnetic fields at the boundary plane (k), respectively. Δ_k is the area of the boundary plane (k)

As the subdomain tends to be very small compared to the guided-wavelength the boundary tangential fields may be approximated by the field quantities at the central point of each boundary plane. In this way, the electromagnetic properties of the subdomain are dictated by a characteristic matrix relating the tangential fields at the central point of boundary plane. The field-matching between two joined boundary planes now becomes a point-matching. The point-matching can be realized in the same manner as a port connection described in the well-established network theory. To avoid a complicated mathematical explanation, a set of tangential electromagnetic field representations at each boundary plane (k) are introduced and shown in Fig. 6.2. A set

of new variables, based on the wave parameter concept in microwave circuit analysis, are defined as follows:

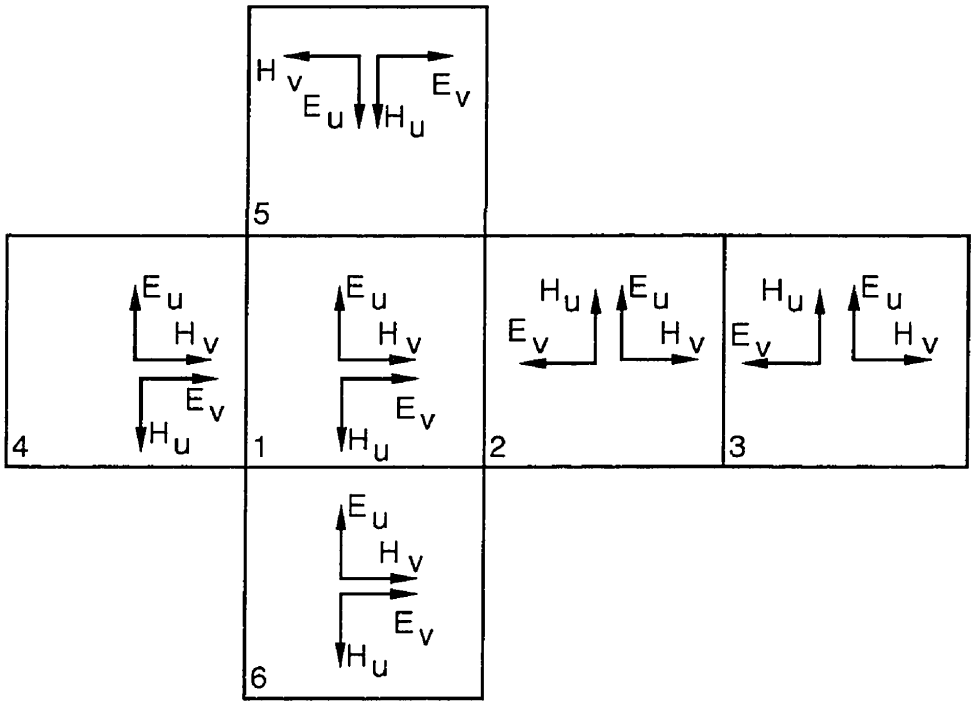

Fig. 6.2 Arrangement of surface field quantities of the subdomain

$$\begin{bmatrix} a_{1(2)} \\ b_{1(2)} \end{bmatrix}_k = \frac{1}{2\sqrt{Z_0}} \begin{bmatrix} 1 & Z_0 \\ 1 & -Z_0 \end{bmatrix} \begin{bmatrix} E_{u(v)} \\ H_{v(u)} \end{bmatrix}_k \tag{6.2}$$

in which $Z_0 = \sqrt{\frac{\mu}{\varepsilon}}$ is the wave impedance of the medium. $E_{u(v)k}$ and $H_{u(v)k}$ are the tangential electric and magnetic fields at the central point of the boundary plane (k), respectively. The a_{ik} and b_{ik} (i=1 and 2) are termed as incident and reflected waves,

respectively. On the basis of the above transformation and (6.1), the characteristic equation in each subdomain can be obtained as

$$
\begin{aligned}
b_{11} &= \frac{s_1(s_3-s_2)}{p_1p_3}a_{11} + \frac{s_1^2-(s_2+1)(s_3+1)}{p_1p_3}a_{12} + \frac{s_2}{p_1}(a_{13}+a_{14}) + \frac{s_3}{p_3}(a_{15}-a_{16}) \\
b_{12} &= \frac{s_1^2-(s_2+1)(s_3+1)}{p_1p_3}a_{11} + \frac{s_1(s_3-s_2)}{p_1p_3}a_{12} + \frac{s_2}{p_1}(a_{13}+a_{14}) - \frac{s_3}{p_3}(a_{15}-a_{16}) \\
b_{13} &= \frac{s_1}{p_1}(a_{11}+a_{12}) + \frac{s_2(s_3-s_1)}{p_1p_2}a_{13} + \frac{s_2^2-(s_1+1)(s_3+1)}{p_1p_2}a_{14} + \frac{s_3}{p_2}(a_{25}-a_{26}) \\
b_{14} &= \frac{s_1}{p_1}(a_{11}+a_{12}) + \frac{s_2^2-(s_1+1)(s_3+1)}{p_1p_2}a_{13} + \frac{s_2(s_3-s_1)}{p_1p_2}a_{14} - \frac{s_3}{p_2}(a_{25}-a_{26}) \\
b_{15} &= \frac{s_1}{p_3}(a_{11}-a_{12}) + \frac{s_3(s_1-s_2)}{p_2p_3}a_{15} + \frac{s_3^2-(s_1+1)(s_2+1)}{p_2p_3}a_{16} - \frac{s_2}{p_2}(a_{23}-a_{24}) \\
b_{16} &= -\frac{s_1}{p_3}(a_{11}-a_{12}) + \frac{s_3^2-(s_1+1)(s_2+1)}{p_2p_3}a_{15} + \frac{s_3(s_1-s_2)}{p_2p_3}a_{16} + \frac{s_2}{p_2}(a_{23}-a_{24}) \\
b_{21} &= \frac{s_1(s_2-s_3)}{p_1p_3}a_{21} + \frac{s_1^2-(s_2+1)(s_3+1)}{p_1p_3}a_{22} + \frac{s_2}{p_1}(a_{23}-a_{24}) + \frac{s_3}{p_3}(a_{25}+a_{26}) \\
b_{22} &= \frac{s_1^2-(s_2+1)(s_3+1)}{p_1p_3}a_{21} + \frac{s_1(s_2-s_3)}{p_1p_3}a_{22} - \frac{s_2}{p_1}(a_{23}-a_{24}) + \frac{s_3}{p_3}(a_{25}+a_{26}) \\
b_{23} &= \frac{s_3}{p_2}(a_{15}+a_{16}) + \frac{s_1}{p_1}(a_{21}-a_{22}) + \frac{s_2(s_1-s_3)}{p_1p_2}a_{32} + \frac{s_2^2-(s_1+1)(s_3+1)}{p_1p_2}a_{24} \\
b_{24} &= \frac{s_3}{p_2}(a_{15}+a_{16}) - \frac{s_1}{p_1}(a_{21}-a_{22}) + \frac{s_2^2-(s_1+1)(s_3+1)}{p_1p_2}a_{32} + \frac{s_2(s_1-s_3)}{p_1p_2}a_{24} \\
b_{25} &= \frac{s_2}{p_2}(a_{13}-a_{14}) + \frac{s_1}{p_3}(a_{21}+a_{22}) + \frac{s_3(s_2-s_1)}{p_2p_3}a_{25} + \frac{s_3^2-(s_1+1)(s_2+1)}{p_2p_3}a_{26} \\
b_{26} &= -\frac{s_2}{p_2}(a_{13}-a_{14}) + \frac{s_1}{p_3}(a_{21}+a_{22}) + \frac{s_3^2-(s_1+1)(s_2+1)}{p_2p_3}a_{25} + \frac{s_3(s_2-s_1)}{p_2p_3}a_{26}
\end{aligned}
\tag{6.3}
$$

with

$$
s_1 = \frac{1}{jk\cdot\Delta_x}; \qquad s_2 = \frac{1}{jk\cdot\Delta_y}; \qquad s_3 = \frac{1}{jk\cdot\Delta_z}
$$

$$
p_1 = s_1 + s_2 + 0.5; \qquad p_2 = s_2 + s_3 + 0.5; \qquad p_3 = s_1 + s_3 + 0.5
$$

With reference to the algorithm developed in [5, 7], electrical characteristics of guided-wave structures can be computed. It is noted that the fundamental difference between the proposed DPA and the MAB in [7] is the derivation of the characteristic matrix of subdomain. In [7], the characteristic matrix is obtained by the virtual channel and homogeneous excitation while in our method this matrix is established by the central finite-difference and averaging principles.

6.3 Results and discussion

Since the central finite-difference and averaging scheme are used throughout, second-order numerical accuracy can be expected. In order to validate the proposed DPA concept, a computer program has been implemented to verify two typical waveguide and planar circuit problems for which a comparison can be made between this new technique and other approaches.

Fig. 6.3 displays a bilateral D-band filter response which was obtained by different techniques and experiment. It is obvious that our results agree very well with the measurement [9]. The proposed DPA is better than the MAB method as far as the numerical accuracy of modeling a waveguide problem is concerned. In Fig. 6.4, the effective dielectric constant is shown as a function of frequency. The results of this technique are compared with those obtained from the SDA and TLM with time-domain node which are implemented by ourselves. It is noted that the same discretization mesh is used in both the DPA and TLM analysis. Clearly, the present results are in better agreement with those of the SDA than the TLM method. It is well known that the SDA, which is able to describe analytically the field singularity, usually presents an accuracy better than that of discrete techniques as far as a planar circuit is concerned. Our

calculation has also shown that the new technique is more efficient than the TLM algorithm with time-domain node in terms of convergence.

6.4 Conclusion

A new technique called the domain-partitioning approach is proposed for accurate and efficient modeling of guided-wave structures and microwave integrated circuits possibly with arbitrary shape. The framework of the proposed technique is built up with the combination of the central finite difference and networking interconnection. Simple examples are used to verify its numerical accuracy compared to other techniques, indicating its superior accuracy and efficiency in the planar circuit analysis.

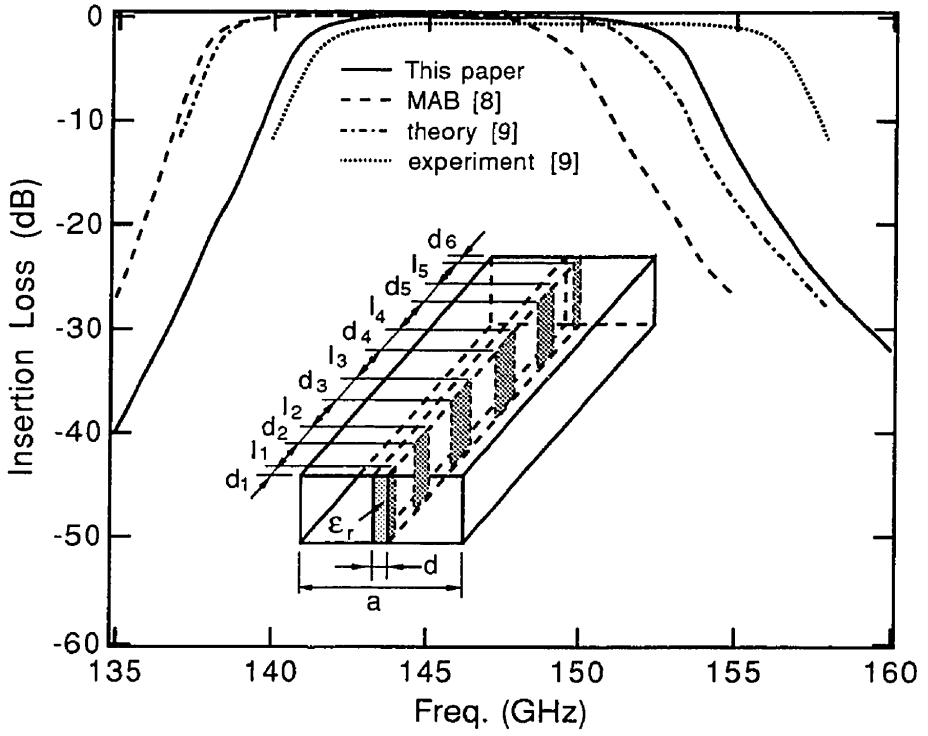

Fig. 6.3 Theoretical and measured responses of a bilateral D-band filter with the structural parameters : $a = 1.651$ mm, $d = 0.0762$ mm, $\varepsilon_r = 2.1$, $d_1 = d_6 = 0.03175$ mm, $d_2 = d_5 = 0.3365$ mm, $d_3 = d_4 = 0.4318$ mm, $l_1 = l_5 = 0.887$ mm, $l_2 = l_4 = 0.8989$ mm, $l_3 = 0.8992$ mm.

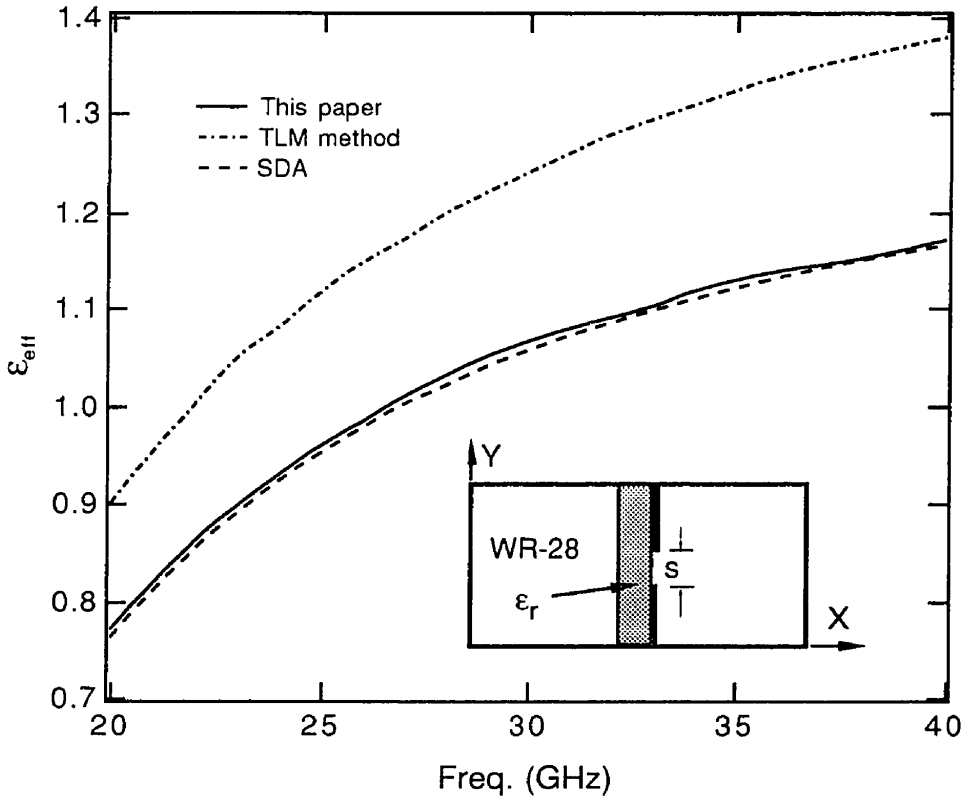

Fig. 6.4 Dispersion characteristics of a WR-28 unilateral finline obtained by the proposed technique, the TLM method and the SDA (using RT/Duroid 5880 substrate with a thickness of 0.254 mm and $s = 0.461$ mm).

References

[1] T. Wang and K. Wu, "Enhanced spectral domain analysis of coupled slotlines with septum and pedestal considering finite thickness of conductors for wideband MIC's," in IEEE MTT-S Int. Microwave Symp. Dig., 1994, pp.1037-1040.

[2] K. Wu, R. Vahldieck, J. L. Fikart, and H. Minkus, "The influence of finite conductor thickness and conductivity on fundamental and higher-order modes in miniature hybrid MIC's (MHMIC's) and MMIC's," IEEE Trans. Microwave Theory Tech., vol. 41, no. 3, pp. 421-430, Mar. 1993.

[3] Dok H. Choi, Wolfgang J. R. Hoefer, "The finite-difference time-domain method and its application to eigenvalue problems," IEEE Trans. Microwave Theory Tech., vol. MTT-34, no. 12, pp. 1464-1470, Dec. 1986.

[4] P. B. Johns, "A symmetrical condensed node for the TLM method," IEEE Trans. Microwave Theory Tech., vol. MTT-35, no. 4, pp. 370-377, Apr. 1987.

[5] H. Jin, and R. Vahldieck, "The frequency-domain transmission line matrix method --- a new concept," IEEE Trans. Microwave Theory Tech., vol. MTT-40, no. 12, pp. 2207-2218, Dec. 1992.

[6] J. Wang, and R. Mittra, "A finite element cavity resonance method for waveguide and microstrip line discontinuity problems," IEEE Trans. Microwave Theory Tech., vol. MTT-42, no. 3, pp. 433-440, Mar. 1994.

[7] V. V. Nikol'skii and T. I. Lavrova, "The method of minimum autonomous blocks and its application to waveguide diffraction problems," Radiotekhnika i Elektronika, vol. 23, no. 2, p.241, 1978 [Radio Engng. and Electron. Phys., 23, no. 2 (1978)].

[8] J. Machac, "Analysis of discontinuities in waveguiding structures by MAB method," IEE Proceedings-H, vol. 139, no. 4, pp. 351-357, Aug. 1992.

[9] L. Q. Bui, D. Ball, and T. Itoh, "Broad-band millimeter-wave E-plane bandpass filters," IEEE Trans. Microwave Theory Tech., vol. 32, no. 12, pp. 1655-1658, Dec. 1984.

Chapitre VII

Synthèse et conclusion

L'étude de circuits MIC en technologie planaire et en technologie non-planaire a mené au développement de deux techniques de modélisation numérique. La réalisation et l'utilisation des programmes qui en ont été déduits a permis de mettre en lumière les propriétés électriques de diverses configurations de circuits planaires et non planaires. Les principales caractéristiques de ces circuits sont leurs hautes performances par comparaison avec leur faible coût potentiel.

Il est montré que le principal désavantage des circuits MIC blindés réside dans les difficultés d'ajustement des caractéristiques électriques une fois les circuits fabriqués. Une méthode de caractérisation numerique extrêmement précise a dû être mise au point pour modéliser des structures guides d'onde composites. Ceci constitue une étape fondamentale dans le processus de réalisation des circuits MIC. Le travail fut donc organisé selon les étapes suivantes.

Une version améliorée de la méthode spectrale a été proposée pour la caractérisation de structures guide d'onde multicouches et multi-conducteurs. La formulation est déduite de la méthode spectrale conventionnelle et du théorème de conservation de la puissance. Les caractéristiques dominantes de l'approche proposée concernent la simplification du développement analytique des fonctions de Green, et l'extension des avantages inhérents à la méthode spectrale traditionnelle, à l'étude de structure guide

d'onde planaires complexes et réelles en tenant compte de l'épaisseur finie de la métallisation et de blindage de forme changeante ou non. Grâce au théorème de conservation de la puissance, le nombre de termes spectraux dans chaque sous-région peut être choisi indépendamment, impliquant ainsi la possibilité d'un calcul numérique plus rapide et plus efficace non seulement en temps CPU mais aussi en taille de mémoire requise. La principale limitation de cette méthode (ESDA) est que chaque sous-région se doit d'être homogène et isolée dans la direction latérale.

Une attention considérable a été prêtée à l'étude des propriétés des structures guide d'onde uniplanaires, avec différents types d'assemblage de blindage. Trois configurations suspendues pour des lignes à fentes couplées ont été présentées. Les caractéristiques des différents schémas de montage ont été détaillées et discutées notamment leur influence sur la fréquence de coupure des premiers modes d'ordre supérieurs. Les profiles des champs des modes fondamentaux dans les lignes à fentes couplées avec des socles de différentes tailles ont été présentés. Deux topologies de blindage, nommément une topologie de blindage adapté et une topologie de blindage réalisable en une étape, ont été étudiées et décrit. Ils ont été développés en tenant compte des exigences liées aux lignes de transmission et aux capacités des techniques de fabrication. Une classe de structure guide d'onde uniplanaire avec micro-blindage circulaire, elliptique, en losange ou trapézoïdal, a été caractérisées. L'effet des cavités métalliques de blindage sur la largeur de bande monomode des lignes micro-blindées reposant sur des membranes de diélectrique a été illustré et quantifié.

Le coupleur hybride en anneau étant un des composants les plus fondamentaux des systèmes micro-ondes et en ondes millimétriques, une étude du fonctionnement

physique d'un coupleur hybride en anneau en technologie uniplanaire, avec inverseur de phase a été réalisé. Un nouveau type de design a été présenté. Les critères de design en vue d'une réduction en taille et d'un élargissement de la largeur de bande sont discutés. Une classe d'inverseurs de phase, de type balancé, non balancé ou balancé et non balancé à la fois (type balun) a été décrite. Une étude expérimentale valide le nouveau concept de design. Les mesures du circuit réalisé indiquent que le coupleur proposé est parfaitement adapté pour des applications larges bandes.

Le développement des performances des circuits MIC requière des outils plus souples permettant la modélisation de circuits complexes y compris des discontinuités. Une nouvelle approche basée sur une partition de sous-domaines, a été proposée pour caractériser des circuits micro-ondes de forme arbitraire (résolution de problèmes aux valeurs propres et étude de discontinuités). L'algorithme est établi en suivant le schéma des différences finies combiné au traitement classique de réseau d'interconnexions. Une matrice caractéristique reliant les valeurs des champs le long des frontières de petits sous-domaines est directement dérivée des équations de Maxwell. Le principal avantage de la technique proposée est qu'elle permet facilement une caractérisation d'une structure complexe avec une grande efficacité et une grande précision. Il est possible d'envisager une large utilisation de cette technique par des application CAO de circuits MIC planaires et non planaires.

Avec la croissance des circuits MIC pour les applications liées aux techniques d'ingénerie, des études de circuits MIC plus pertinentes sont nécessaires pour développer les circuits et des sous-systèmes à hautes performances, à plus faibles coûts, et de tailles plus compactes. Un effort parallèle pour l'amélioration de l'efficacité et de la

précision des outils de CAO est requis. Les travaux futurs en continuité avec cette thèse devraient tenir compte des différents aspects suivants.

La méthode ESDA a été utilisée pour la caractérisation des substrats diélectriques isotropes sans perte. Une extension directe de cette technique peut être développée pour tenir compte des matériaux anisotropes et avec pertes. Ceci permettrait une modélisation encore plus précise lors des étapes de conception du design de circuits MIC. Ceci devient très important aux hautes fréquences ou pour les applications liés à des configurations supportant des modes non quasi-TEM et non TEM.

Un travail important reste à faire pour explorer la totalité du potentiel de l'approche qui consiste en une partition en sous-domaines. Bien que l'approche par partition de domaine dans cette thèse soit établie à partir d'un réseau à deux ports, il peut être étendu au modèle d'un réseau multi-ports. La matrice caractéristique des sous-régions peut être développée sous la forme de matrices chaines dans le but de simplifier l'algorithme de calcul des valeurs propres ou des discontinuités, et d'accroître l'efficacité en termes de mémoire et de temps CPU. L'extension à réaliser devrait aussi bien sûr pouvoir tenir compte des pertes, et des matériaux anisotropes, dans différents systèmes de coordonnées.

Les recherches futures concernant le design de coupleur hybride en anneau doivent être dirigées vers l'amélioration des performances et vers le développement de nouveaux circuits. Une application évidente de ces coupleurs proposés est leur utilisation dans le design de mélangeurs balancés ou de modulateurs.

Bibliographie

ALESSANDRI, F., BAINI, G., MONGIARDO, M. et SORRENTINO, R. (1993). 3-D mode matching technique for the efficient analysis of coplanar MMIC discontinuities wit finite metallization thickness. IEEE Trans. Microwave Theory and Tech., 41, 1625-1629.

ALI, F. et HORTON, J. B. (1995). Special Issue of Emerging Commercial and Consumer Circuits, Systems, and Their Applications. IEEE Transactions on Microwave Theory and Techniques, 43, no. 7, part II.

AN, H., WANG, T., BOSISIO, R. G. et WU, K. (1994). Cavity-restrained multistacked dielectric omnidirectional antenna for microwave and millimeter-wave wireless communications. Electron. Lett., 30, 2086-2087.

BEYER, A. (1981). Analysis of the characteristics of an earthed fin line. IEEE Trans. Microwave Theory Tech., 29, 676-680.

BIRD, T. S., et al (1994). Millimeter-wave antenna and propagation studies for indoor wireless LANs. IEEE AP-S Int. Symp. Dig., 336-339.

BORNEMANN, J. et ARNDT, F. (1986). Calculating the characteristic impedance of finlines by transverse resonance method. IEEE Trans. Microwave Theory Tech., 34, 85-92.

BORNEMANN, J. (1991). A scattering-type transverse resonance technique for the calculation of (M)MIC transmission line characteristics. IEEE Trans. Microwave Theory Tech., 39, 2083-2088.

BUI, L. Q., BALL, D. et ITOH, T. (1984). Broad-band millimeter-wave E-plane bandpass filters. IEEE Trans. Microwave Theory Tech., 32, 1655-1658.

CELLIERS, A. F. et MALHERBE, J. A. G. (1985). Design curves for -3-dB branch-line couplers. IEEE Trans. Microwave Theory Tech., 33, 1226-1228.

CHAN, C. H., NG, K. T. et KOUKI, A. B. (1989). A mixed spectral-domain approach for dispersion analysis of suspended planar transmission lines with pedestals. IEEE Trans. Microwave Theory Tech., 37, 1716-1723.

CHANG, K. (1985). Millimeter-wave planar integrated circuits and subsystems. Infrared and Millimeter Waves, 14, 79-187.

CHEN, S. W. et ZAKI, K. A. (1991). Dielectric ring resonators loaded in waveguide and on substrate. IEEE Trans. Microwave Theory and Tech., 39, 2069-2076.

CHENG, K.-K. M. et ROBERTSON, I. D. (1995). Quasi-TEM study of microshield lines with practical cavity sidewall profiles. IEEE Trans. Microwave Theory Tech., 43, 2689-2694.

CHOI, D. H. et HOEFER, W. J. R. (1986). The finite-difference time-domain method and its application to eigenvalue problems. IEEE Trans. Microwave Theory Tech., 34, 1464-1470.

CHUA, L. W. (1971). New broad-band matched hybrids for microwave integrated circuits. Proc. European Microwave Conf., C4/5:1 - C4/5:4.

COHN, S. B. (1969). Slot line on a dielectric substrate. IEEE Transactions on Microwave Theory and Techniques, 17, 768-778.

COLLIN, R. E (1991). Field theory of guided waves. Second edition, New York.

DIB, N. I. et KATEHI, L. P. B. (1992). Impedance calculation for the microshield line. IEEE Microwave and Guided Wave Letters, 2, 406-408.

DIB, N. I., et al. (1991). Study of a novel planar transmission line. IEEE MTT-S Digest, 2, 623-626.

DIB, N. I., SIMONS, R. N. et KATEHI, L. P. B. (1995). New uniplanar transitions for circuit and antenna applications. IEEE Trans. Microwave Theory Tech., 43, 2868-2873.

DRAYTON, R. F. et KATEHI, L. P. B. (1995). Development of self-packaged high frequency circuits using micromachining techniques. IEEE Trans. Microwave Theory Tech., 43, 2073-2080.

DREHER, A. (1992). The method of lines and the integral equation method for the analysis of planar antennas (in German). Fortschritt Berichte, 21, VDI-Verlag Gmbh, Dusseldorf.

DRHER, A et PREGLA, R. (1993). Full-wave analysis of radiating planar resonators with the method of lines. IEEE Trans. Microwave Theory and Tech., 41, 1363-1368.

ESPES, P., COMBES, P. F., GOUTOULE, J. M. et THERON, B. (1989). Asymmetrical finline for space applications using millimeter waves. IEEE Trans. Microwave Theory Tech., 37, 289-298.

ESWARAPPA, COSTACHE, G. I. et HOEFER, W. J. R. (1989). Finlines in rectangular and circular waveguide housings including substrate mounting and bending effects - finite element analysis. IEEE Trans. Microwave Theory Tech., 37, 299-305.

FAN, L. et CHANG, K. (1996). Uniplanar mic power dividers using coupled CPW and asymmetrical CPS. IEEE MTT-s Int. Microwave Symp. Dig., 781-784.

FAN, L., HEIMER, B. et CHANG, K. (1997). Uniplanar hybrid couplers using asymmetrical coplanar strip lines. IEEE MTT-s Int. Microwave Symp. Dig., 273-276.

GRIEG, D. D. et ENGELMANN, H. F. (1952). Proc. IRE 40, 1644-1650.

HIRANO, M., NISHIKAWA, K., TOYODA, I., AOYAMA, S., SUGITANI, S. et YAMASAKI, K., (1995). Three-dimensional passive circuit technology for ultra-compact MMIC's. IEEE Trans. Microwave Theory Tech., 43, 2845-2850.

HIROTA, T., TARUSAWA, Y., et OGAWA, H. (1987). Uniplanar MMIC hybrids - a proposed new MMIC structures. IEEE Trans. Microwave Theory Tech., 35, 576-581.

HO, C. H., FAN, L. et CHANG, K. (1993). Broad-band uniplanar hybrid-ring and branch-line couplers. IEEE Trans. Microwave Theory Tech., 41, 2116-2124.

HO, C. H., FAN, L. et CHANG, K. (1994). New uniplanar coplanar waveguide hybrid-ring couplers and Magic-T's. IEEE Trans. Microwave Theory Tech., 42, 2240-2248.

HOFFMAN, R. K. et SIEGL, J. (1982). Microstrip-slot coupler design, Part I and II. IEEE Trans. Microwave Theory Tech., 30, 1205-1216.

HOFFMAN, R. (1987). Handbook of Microwave Integrated Circuits. Artech House, Norwood, MA.

HUANG, J. W. et TZUANG, C.-K. C. (1994). Mode-coupling-avoidance of shielded conductor-backed coplanar waveguide(CBCPW) using dielectric lines compensation. IEEE MTT-S Int. Microwave Symp. Dig., 149-152.

ITOH, T. (1980). Spectral domain immitance approach for dispersion characteristics of generalized printed transmission lines. IEEE Trans. Microwave Theory Tech., 28, 733-736.

ITOH, T. (1989). Overview of quasi-planar transmission lines. IEEE Trans. Microwave Theory and Tech., 37, 275-280.

ITOH, T., ed. (1989). Numerical Techniques for Microwave and Millimeter-Wave Passive Structures. John Wiley & Sons, NY.

JACKSON, R. W. (1989). Mode conversion at discontinuities in finite-width conductor-backed coplanar waveguide. IEEE Trans. Microwave Theory and Tech., 37, 1582-1589.

JANSEN, R. H. (1979). Unified user-oriented computation of shielded, covered and open planar microwave and millimeter-wave transmission-line characteristics. Microwave Opt. Acoust., 3, 14-22.

JANSEN, R. H. (1985). The spectral-domain approach for microwave integrated circuits. IEEE Trans. Microwave Theory Tech., 33, 1043-1056.

JIN, H. et VAHLDIECK, R. (1992). The frequency-domain transmission line matrix method --- a new concept. IEEE Trans. Microwave Theory Tech., 40, 2207-2218.

JOHNS, P. B. (1987). A symmetrical condensed node for the TLM method. IEEE Trans. Microwave Theory Tech., 35, 370-377.

KATEHI, L. P. B. , REBEIZ, G. M., WELLER, T. M., DRAYTON, R. F., CHENG, H. J. et WHITAKER, J. F. (1993). Micromachined circuits for millimeter- and sub-millimeter-wave applications. IEEE Antenna and Propagation Magazine, 35, 9-17.

KIM, D. I. et NAITO, Y. (1982). Broad-band design of improved hybrid-ring 3-dB directional couplers. IEEE Trans. Microwave Theory Tech., 30, 2040-2046.

KIM, D. I. et YANG, G. S. (1991). Design of new hybrid-ring directional coupler using $\lambda/8$ or $\lambda/6$ sections. IEEE Trans. Microwave Theory Tech., 39, 1779-1783.

KITAZAWA, T. (1991). Analysis of shielded striplines and finlines with finite metallization thickness containing magnetized ferrites. IEEE Trans. Microwave Theory Tech., 39, 70-74.

KITAZAWA, T et al. (1991). Planar transmission lines with finitely thick conductors and loss substrates. IEEE MTT-S digest, 769-772.

KITAZAWA, T., POLIFKO, D. et OGAWA, H. (1992). Analysis of CPW for $LiNbO_3$ optical modulator by extended spectral-domain approach. IEEE Microwave and Guided Wave Letters, 2, 313-315.

KNEPPO, I. et GOTZMAN, J. (1977). Basic parameters of nonsymmetrical coplanar lines. IEEE Trans. Microwave Theory Tech., 25, 718.

KOBAYASHI, Y et TANAKA, S. (1980). Resonant modes of a dielectric rod resonator short-circuited at both ends by parallel conducting plates. IEEE Trans. Micro-wave Theory and Tech., 28, 1077-1085.

KOBAYASHI, Y. et SENJU, T. (1993). Resonant modes in shield uniaxial-anisotropic dielectric rod resonators. IEEE Trans. Microwave Theory and Tech., 41, 2198-2205.

KROWNE, C. M. (1984). Fourier transformed matrix method of finding propagation characteristics of complex anisotropic layered media. IEEE Trans. Microwave Theory Tech., 32, 1617-1625.

LANGE, J. (1969). Interdigitated strip-line quadrature hybrid. G-MTT Int. Microwave Symp. Dig., 10-13.

LEBARIC, J. E. et KAJFEZ, D. (1989). Analysis of dielectric resonator cavities using the finite integration technique. IEEE Trans. Microwave Theory and Tech., 37, 1740-1747.

LEE, J. F., WILKINS, G. M. et MITTRA, R. (1993). Finite-element analysis of axisymmetric cavity resonator using a hybrid edge element technique. IEEE Trans. Microwave Theory and Tech., 41, 1981-1987.

LIANG, X. P. et ZAKI, K. A. (1993). Modeling of cylindrical dielectric resonators in rectangular waveguides and cavities. IEEE Trans. Microwave Theory and Tech., 41, 2174-2181.

LIN, Y. D. et CHI, P.-M. (1994). Mode-coupling phenomena of packaged coplanar waveguide with mounting grooves. IEEE MTT-S Int. Microwave Symp. Dig., 1145-1148.

LO, W. T., et al. (1993). Resonant Phenomena in conductor-backed coplanar waveguides (CBCPW's). IEEE Trans. Microwave Theory and Tech., 41, 2099-2107.

MACHAC, J. (1992). Analysis of discontinuities in waveguiding structures by MAB method. IEE Proceedings-H, 139, 351-357.

MAJ, S. et POSPIESZALKI, M. (1984). A composite multilayered cylindrical dielectric resonator. IEEE MTT-s Int. Microwave Symp. Dig., 190-192.

MANSOUR, R. R. et MACPHIE, R. H. (1987). A unified hybrid-mode analysis for planar transmission lines with multilayer isotropic/anisotropic substrates. IEEE Trans. Microwave Theory Tech., 35, 1382-1391.

MARCH, S. (1968). A wide band stripline hybrid ring. IEEE Trans. Microwave Theory Tech., 16, 361.

MEINEL, H. (1995). Recent advances on millimeter wave PCN system development in Europe. 1995 IEEE Microwave Systems Conference Proceedings, 3-6.

MENZEL, W. (1985). Integrated fin-line components for communication, radar, and radiometerapplications. Infrared and Millimeter Waves, 13, 77-121.

MESA, F. L., MARQUÉS, R. et HORNO, M. (1991). A general algorithm for computing the bidimensional spectral Green's dyad in multilayered complex bianisotropic media: the equivalent boundary method. IEEE Trans. Theory Tech., 39, 1640-1649.

MURAGUCHI, M., HIROTA, T., MINAKAWA, A., OHWADA, K. et SUGETA, T. (1988). Uniplanar MMIC's and their applications. IEEE Trans. Microwave Theory and Tech., 36, 1896-1901.

MURGULESCU, M., et. al. (1994). New wideband, $0.67\lambda_g$ circumference 180^0 hybrid ring coupler. Elect. Lett., 30, 299-300.

NAGHED, M. et WOLFF, I. (1990). Equivalent capacitances of coplanar wave guide discontinuities and interdigitated capacitors using a 3-deimensional finite difference method. IEEE Trans. Microwave Theory and Tech., 38, 1805-1815.

NG, K. T. et CHAN, C. H. (1989). Unified solution of various dielectric-loaded ridge waveguides with a mixed spectral-domain method. IEEE Trans. Microwave Theory Tech., 37, 2080-2085.

NIKOL'SKII, V. V. et LAVROVA, T. I. (1978). The method of minimum autonomous blocks and its application to waveguide diffraction problems. Radiotekhnika i Elektronika, 23, 241 [Radio Engng. and Electron. Phys., 23].

PON, C. Y. (1961). Hybrid-ring directional coupler for arbitrary power division. IRE Trans. Microwave Theory Tech., 9, 529-535.

PUCEL, R. A., ed. (1985). Monolithic Microwave Integrated Circuits. IEEE Press, NY.

REED, J. et WHEELER, G. J. (1956). A method of analysis of symmetrical fourport networks. IRE Trans. Microwave Theory Tech., 4, 246-252.

RIAZIAT, M., MAJIDI-AHY, R. et FENG, I. J. (1990). Propagation modes and dispersion characteristics of coplanar waveguides. IEEE Trans. Microwave Theory and Tech., 38, 245-251.

SCHIEK, B. (1974). Hybrid branchline coupler -- a useful new class of directional couplers. IEEE Trans. Microwave Theory Tech., 22, 864-869.

SHARMA, A. K. et ITOH, T. (1993). Special Issue on Modeling and Design of Coplanar Monolithic Microwave and Millimeter-Wave Integrated Circuits . IEEE Transactions on Microwave Theory and Techniques, 41, no. 9.

SHIGESAWA, H., TSUJI, M. et OLINER, A. A. (1988). Conductor-backed slot line and coplanar waveguide: dangers and full-wave analysis. IEEE MTT-s Int. Microwave Symp. Dig., 199-202.

SHIGESAWA, H., TSUJI, M. et OLINER, A. A. (1990). A new mode-coupling effect on coplanar waveguide s of finite width. IEEE MTT-s Int. Microwave Symp. Dig., 1063-1066.

SCHMIDT, L. P. et ITOH, T. (1980). Spectral domain analysis of dominant and higher order modes in fin-lines. IEEE Trans. Microwave Theory Tech., 28, 981-985.

SCHULZ, U. et PREGLA, R. (1980). A new technique for the analysis of the dispersion characteristics of planar waveguides. AEU, Band 34, 169-173.

TSUJI, M. et SHIGESAWA, H. (1994). Packaging of printed-circuit lines: a dangerous cause for narrow pulse distortion. IEEE Trans. Microwave Theory Tech., 42, 1784-1790.

TUKO, M. A. et WOLFF, I. (1992). Novel 36 GHz GaAs frequency doublers using (M)MIC coplanar technology. IEEE MTT-S Int. Microwave Symp. Dig., 1167-1170.

VARDIAMBASIS, I. O., TSALAMENGAS, J. L. et FIKIORIS, J. G. (1995). Hybrid wave propagation in circularly shield microslot lines. IEEE Trans. Microwave Theory Tech., 43, 1960-1966.

WANG, J. et MITTRA, R. (1994). A finite element cavity resonance method for waveguide and microstrip line discontinuity problems. IEEE Trans. Microwave Theory Tech., 42, 433-440.

WANG, T. et SUN, Z. (1992). Analysis of novel wideband ridge-loaded finline including finit metallisation thickness and substrate mounting grooves. Electron. Lett., 28, 2356-2357.

WANG, T. et WU, K. (1994). Enhanced spectral domain analysis of coupled slotlines with septum and pedestal considering finite thickness of conductors for wideband MIC's. IEEE MTT-S Int. Microwave Symp. Dig., 1037-1040.

WANG, T. et WU, K. (1995). Effects of various suspended mounting schemes on mode characteristics of coupled slotlines considering conductor thickness for wideband MIC application. IEEE Trans. Microwave Theory Tech., 43, 1106-1114.

WANG, T. et WU, K. (1995). An efficient approach to modeling of quasi-planar structures using the formulation of power conservation in spectral domain. IEEE Trans. Microwave Theory Tech., 43, 1136-1142.

WANG, T., AN, H., WU, K., LAURIN, J. J. et BOSISIO, R. G. (1995). A novel leaky-mode cylindrical dielectric resonator used as feeds of omnidirectional antenna for wireless communications. IEEE MTT-s Int. Microwave Symp., 657-660.

WANG, T. et WU, K. (1995). Dynamic analysis of uniplanar guided-wave structures with trapezoidal conductor profile and microshielding enclosure. IEICE Trans. Electron., E78C, 1100-1105.

WANG, T., OU, Z. et WU, K. (1997). Experimental study of wideband uniplanar phase inverters for MICs. IEEE MTT-s Int. Microwave Symp. Dig., 777-780.

WANG, W. et GUO, Y. (1994). Static ,analysis of millimeter wave transmission lines micromachined silicon substrate. IEEE Antenna and propagation society International Symp. Dig., 1960-1963.

WEN, C. P. (1969). Coplanar Waveguide: A surface strip transmission line suitable for non-reciprocal gyromagnetic device application. IEEE Transactions on Microwave Theory and Techniques, 17, 1087-1090.

WU, K. et VAHLDIECK, R. (1989). The method of lines applied to planar transmission lines in circular and elliptical waveguides. IEEE Trans. Microwave Theory Tech., 37, 1958-1963.

WU, K., VAHLDIECK, R., FIKART, J. L. et MINKUS, H. (1993). The influence of finite conductor thickness and conductivity on fundamental and higher-order modes in miniature hybrid MIC's (MHMIC's) and MMIC's. IEEE Trans. Microwave Theory Tech., 41, 421-430.

WU, K. (1994). A combined efficient approach for analysis of nonradiative dielectric (NRD) waveguide components. IEEE Trans. Microwave Theory and Tech., 42, 672-2177.

WU, K., XU, Y. et BOSISIO, R. G. (1994). Theoretical and experimental analysis of channelized coplanar waveguides (CCPW) for wideband applications of integrated microwave and millimeter-wave circuits. IEEE Trans. Microwave Theory Tech., 42, 1651-1659.

YAMASHITA, E., LI, K. R., KANEKO, E. et SUZUKI, Y. (1987). Characterization method and simple design formulas of MCS lines proposed for MMIC's. IEEE MTT-s Int. Microwave Symp. Dig., 685-688.

YUAN, N., RUAN, C. et LIN, W. (1994). Analytical analysis of V, elliptic, and circular-shaped microshield transmission lines. IEEE Trans. Microwave Theory Tech., 42, 855-859.

Annexe I

A Analyse spectrale d'un résonnateur diélectrique cylindrique rayonant

Cette annexe montre comment la méthode spectrale perfectionnée décrite au chapitre II, a été complétées pour rendre possible la modélisation de résonateur diélectrique cylindrique rayonnant. Le résonateur diélectrique est compris entre deux plaques métalliques parallèles. L'analyse est orientée vers l'étude des modes TM à perte d'ordres, faibles dans le résonateur. L'annexe est constituée par un article publié en décembre 1996 dans la revue IEEE Transaction on Microwave Theory and Techniques.

Spectral-Domain Analysis of Radiating Cylindrical Dielectric Resonator for Wireless Communications

T. Wang, Student Member, IEEE, H. An, Member, IEEE, K. Wu, Senior Member, IEEE, J. J. Laurin, Member, IEEE, R. G. Bosisio, Fellow, IEEE

POLY-GRAMES Research Center
Dept. de génie électrique et de génie informatique, École Polytechnique
C. P. 6079, Succ. Centre-Ville, Montréal, Canada H3C 3A7

Abstract

A novel class of leaky-mode cylindrical dielectric resonators including mounting holder and radial-step has been recently proposed as a feed structure for omnidirectional antennas that are suitable for wireless communication systems. In this work, a spectral-domain modeling is developed and used for analysis of these composite cylindrical dielectric resonators considering single and double radiating slots. The dielectric resonators are bounded between two parallel conducting plates so that leaky-wave propagation takes place under some electrical and geometrical conditions. Results and discussion are focused on the properties of low-order leaky TM-modes. Influences of various structural parameters on resonant frequency and quality factor of leaky dielectric resonators are presented in detail. A set of experiments are made to verify the proposed theoretical approach.

A.1 Introduction

Wireless communication techniques at microwave and millimeter-wave frequencies have received much attention from the high-frequency research community. Various wireless local area networks (WLAN's), which can make data links and share resources without resorting to physical connections, are being proposed for a number of applications such as intra-office communications and indoor wireless telephone services. The main advantage of the WLAN's is that the cost of rewiring an office is effectively eliminated for each time it is reorganized or repartitioned. In these communication systems, low-cost, low-profile, and high-performance omnidirectional antennas are strongly desired [1].

It is well known that a dielectric rod resonator positioned between two parallel conducting plates has two possible resonant states, namely, trapped and leaky states. In the leaky state, a portion of electromagnetic energy leaks continuously away from the resonator in the radial direction. As pointed out in [2], TM_{nm0} modes in this resonator are always in the leaky state in particular when $n=0$ for which modal fields remain uniform in the azimuthal or ϕ direction. Based on such a feature, a novel omnidirectional antenna, which consists of a cylindrical dielectric rod with relative dielectric constant ε_r and two metal disks with mounting holders, has been proposed to satisfy the requirement of wireless communications [3]. Compared with the conventional dielectric rod resonator inserted between parallel metallic plates, this new geometry has two distinct advantages. One is that a firm coaxial mounting between dielectric resonator with the supporting structure and coaxial feed can be easily achieved so that the desired resonant modes with an ideal omnidirectional radiation pattern are excited. The other is that operating frequency and radiation impedance are

controlled by adjusting the size of the mounting holder, that is, the width of radiating slot. The latter is of great importance for practical design. Obviously, the proposed antenna presents a narrow bandwidth that is the common denominator of resonant antennas. Therefore, electrical parameters of such a leaky-mode dielectric resonator, namely the resonant frequency and quality factor, are essential for its performance analysis and successful design. This antenna may be approximately modeled by a radiating cylindrical resonator that is bounded between two parallel metallic disks [4]. Nevertheless, only a few simple symmetrical structures with single radiating slot were discussed in [4]. As is well known, the radiation characteristics of antennas are mainly governed by the radiation aperture dimensions and field distribution. In a practical application, a complex geometry involving double radiating slots may be used to enhance the antenna gain or alter its electric properties [3]. In order to suppress the even-mode of the double radiating slot configuration, the coupling ring is usually considered.

Dielectric resonator is one of the fundamental building blocks in microwave and millimeter-wave circuits. Its potential low-cost and widespread applications have been stimulating the search for an efficient analysis method that is able to accurately model the electromagnetic property of resonance and radiation. A number of numerical techniques have been proposed, the finite element [5], the finite integration technique [6], the mode matching methods [7-10], and the method of lines [11, 12], to name a few examples. In these approaches, radial and axial mode matching procedures are widely used. However, field edge singularities existing in the proposed structure make it difficult or deficient for these techniques to solve relevant field problems numerically with high efficiency and good convergence.

In the analysis of planar guided-wave structures, it has been widely recognized that spectral domain approach (SDA) is the most efficient technique and also very simple in analytical formulation. In the spectral-domain analysis, the field edge singularity can be well satisfied by an appropriate choice of basis function. Its early applications and theoretical framework were reviewed in [13]. Recently, much effort has been made to extend the SDA to model a class of complicated quasi-planar structures. In [14, 15], for example, an enhanced SDA was developed and successfully used in the analysis of a class of complex quasi-planar guided-wave structures.

In this paper, the enhanced SDA is further extended to calculate resonant frequency and quality factor of the proposed composite cylindrical dielectric resonator considering single and double radiating slots. The method essentially is a combination of the spectral-domain analysis technique used for solving partial differential equations with the power conservation theorem. Compared to other approaches, this method is more efficient in terms of analytical formulation and numerical accuracy. Numerical results are presented for the low-order leaky TM-mode property of the proposed resonator. Influences of various structural parameters on resonant frequency and quality factor are discussed in details. Experimental results are in good agreement with theoretical predictions thereby validating the proposed analysis technique.

A.2 Theoretical Analysis

Three-dimensional and cross-sectional views of the proposed resonator are shown in Fig. A.1. In the cylindrical coordinate system(r, ϕ, z), a resonance may take place in this structure under the form of three kinds of modes with respect to z-axis: TM-mode, TE-mode, and hybrid-mode. In the following, only leaky TM-modes with invariant

fields in ϕ-direction are considered. In the leaky state, a free-running oscillation in the resonator can be described by a complex resonant frequency. The fields should have such a time-dependence as $e^{j\varpi t}$ in which $\varpi = \omega + j\alpha$ is complex angular frequency; ω and α are resonant frequency and damping factor, respectively.

In Fig. A.1, the whole structure is divided into three homogenous subregions labeled by I, II, and III. The region I is defined in $0 \le \rho \le r_1$, the region II in $r_1 < \rho \le r_2$, and the region III in $r_2 < \rho < +\infty$. In accordance with Fourier's transform, electromagnetic fields in each subregion can be expressed as follows

$$\begin{bmatrix} \vec{E} \\ \vec{H} \end{bmatrix}_i = \sum_{n=-\infty}^{+\infty} \begin{bmatrix} \tilde{\vec{E}}(\rho) \\ \tilde{\vec{H}}(\rho) \end{bmatrix}_i^n \cdot e^{j(\varpi \cdot t - \beta_{zi}^n \cdot z)} \qquad (A.1)$$

where

$$\begin{pmatrix} \tilde{\vec{E}}(\rho) \\ \tilde{\vec{H}}(\rho) \end{pmatrix}_i^n = \frac{1}{a_i} \int_{a_i} \begin{pmatrix} \vec{E} \\ \vec{H} \end{pmatrix}_i \cdot e^{-j(\varpi \cdot t - \beta_{zi}^n \cdot z)} \cdot dz \qquad (A.2)$$

and

$$\beta_{zi}^n = (2n - k)\frac{\pi}{a_i}, \qquad k = \begin{cases} 1 & Ez -- \text{odd Function} \\ 2 & Ez --\text{Even Function} \end{cases}$$

i stands for the subregions (I, II, and III) and n for the spectral term; a_i is the height of subregion such as h and w that are described in Fig. A.1b, or h_1, w and h_2 in Fig. A.1c.

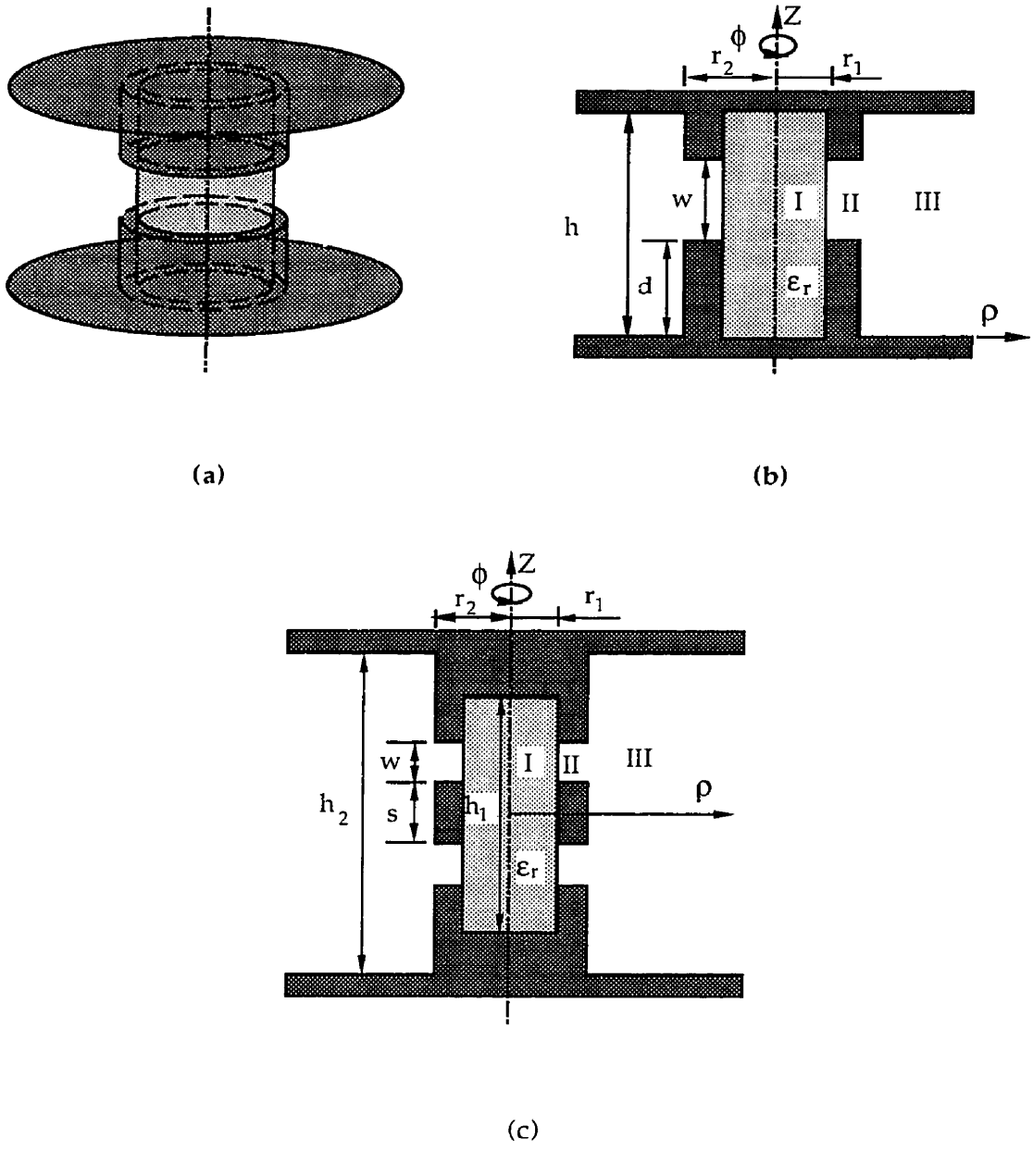

Fig. A.1 Complete views of the proposed radiating cylindrical dielectric resonator. (a) Three-dimensional geometr. (b) Single radiating slot. (c) Double radiating slots.

From the Maxwell's curl equations, the field components of a TM-mode with no ϕ-direction variation in the spectral domain can be described by the following equation

$$\begin{aligned}
&\frac{d\tilde{E}_{zi}}{d\rho} = j\frac{\beta_{\rho i}^2}{\varpi\varepsilon_i}\tilde{H}_{\phi i} \\
&\frac{1}{\rho}\cdot\frac{d(\rho\tilde{H}_{\phi i})}{d\rho} = j\varpi\varepsilon_i\tilde{E}_{zi} \\
&\tilde{E}_{\rho i} = \frac{\beta_{zi}}{\varpi\varepsilon_i}\tilde{H}_{\phi i}
\end{aligned} \qquad (A.3)$$

where $\beta_{\rho i}^2 = \varpi^2\mu\varepsilon_i - \beta_{zi}^2$, and the spectral term superscript (n) is suppressed. In terms of the solution of ($A.3$), the following equations relating the tangential electric field to its magnetic counterpart at boundary apertures of each subregion are obtained, such that

$$\begin{aligned}
&\tilde{H}_{\phi 1}^{+} = \frac{j\varpi\varepsilon_1}{\beta_{\rho 1}}\cdot\frac{\mathcal{J}_1(\beta_{\rho 1}r_1)}{\mathcal{J}_0(\beta_{\rho 1}r_1)}\cdot\tilde{E}_{z1}^{+} \\
&\begin{bmatrix}\tilde{H}_{\phi 2}^{-} \\ \tilde{H}_{\phi 2}^{+}\end{bmatrix} = C\cdot\begin{bmatrix}\left(\mathcal{H}_1^{[2]}(\beta_{\rho 2}r_1)\mathcal{H}_0^{[1]}(\beta_{\rho 2}r_2) - \mathcal{H}_1^{[1]}(\beta_{\rho 2}r_1)\mathcal{H}_0^{[2]}(\beta_{\rho 2}r_2)\right)\cdot E_{z2}^{-} - j\cdot\dfrac{4\cdot E_{z2}^{+}}{\pi\beta_{\rho 2}r_1} \\ j\cdot\dfrac{4\cdot E_{z2}^{-}}{\pi\beta_{\rho 2}r_2} + \left(\mathcal{H}_0^{[2]}(\beta_{\rho 2}r_1)\mathcal{H}_1^{[1]}(\beta_{\rho 2}r_2) - \mathcal{H}_0^{[1]}(\beta_{\rho 2}r_1)\mathcal{H}_1^{[2]}(\beta_{\rho 2}r_2)\right)\cdot E_{z2}^{+}\end{bmatrix} \\
&\tilde{H}_{\phi 3}^{-} = \frac{j\varpi\varepsilon_3}{\beta_{\rho 3}}\cdot\frac{\mathcal{H}_1^{[2]}(\beta_{\rho 3}r_2)}{\mathcal{H}_0^{[2]}(\beta_{\rho 3}r_2)}\cdot\tilde{E}_{z3}^{-}
\end{aligned} \qquad (A.4)$$

where

$$C = \frac{j\varpi\varepsilon_2}{\beta_{\rho 2}}\cdot\frac{1}{\mathcal{H}_0^{[2]}(\beta_{\rho 2}r_1)\mathcal{H}_0^{[1]}(\beta_{\rho 2}r_2) - \mathcal{H}_0^{[1]}(\beta_{\rho 2}r_1)\mathcal{H}_0^{[2]}(\beta_{\rho 2}r_2)}$$

the superscripts (-) and (+) denote the inner and outer boundary apertures of the subregion in question, respectively. $\mathcal{J}_{0,1}$ are Bessel functions of the first kind; $\mathcal{H}_{0,1}^{[1]}$ and $\mathcal{H}_{0,1}^{[2]}$ are Hankel functions of the first and second kinds, respectively. Note that the arguments of Bessel and Hankel functions are complex for leaky-modes.

In the space domain, the transverse electric and magnetic fields with reference to the radial-direction should satisfy boundary conditions at the interface of two joined subregions. On the basis of the complementary property between $\bar{E}_t$ and $\bar{J}_t$ at the interface, the power conservation in the radial direction should hold, that is,

$$\begin{cases} \int_{h_1} (E_{z1}^{+} \cdot H_{\phi 1}^{+*}) \cdot dz = \int_{w} (E_{z2}^{-} \cdot H_{\phi 2}^{-*}) \cdot dz \\ \int_{w} (E_{z2}^{+} \cdot H_{\phi 2}^{+*}) \cdot dz = \int_{h_2} (E_{z3}^{-} \cdot H_{\phi 3}^{-*}) \cdot dz \end{cases} \tag{A.5}$$

It is noted that for the double radiating slots, the integration in (*A*.5) over the subregion II is a sum of integrals with respect to upper and lower slots. Now invoking Parseval's theorem, (*A*.5) in the spectral domain can be written as

$$\begin{cases} \frac{1}{h_1} \sum_{n=-\infty}^{+\infty} (\tilde{E}_{z1}^{+} \tilde{H}_{\phi 1}^{+*})^n - \frac{1}{w} \sum_{n=-\infty}^{+\infty} (\tilde{E}_{z2}^{-} \tilde{H}_{\phi 2}^{-*})^n = 0 \\ \frac{1}{w} \sum_{n=-\infty}^{+\infty} (\tilde{E}_{z2}^{+} \tilde{H}_{\phi 2}^{+*})^n - \frac{1}{h_2} \sum_{n=-\infty}^{+\infty} (\tilde{E}_{z3}^{-} \tilde{H}_{\phi 3}^{-*})^n = 0 \end{cases} \tag{A.6}$$

By substituting (*A*.4) into (*A*.6), a set of linear homogeneous equations is derived. the unknown complex frequency ϖ can be obtained simply through application of Galerkin's technique. Quality factor Q_f is calculated from the definition given in [16],

$$Q_f = \frac{\omega}{2\alpha} \tag{A.7}$$

On the other hand, an appropriate choice of basis function is the cornerstone for numerical efficiency. In the present analysis, the following basis functions are used to describe the tangential electric fields at the boundary apertures in each subregion,

$$f_\zeta(z) = \frac{\cos\left(\zeta\pi\left(\frac{z}{w/2}+1\right)\right)}{\left[1-\left(\frac{z}{w/2}\right)^2\right]^{1/2}} \tag{A.8}$$

where

$$\zeta = \begin{cases} m-\frac{k}{2} & \textit{for} \text{ single slot} \\ \frac{m-1}{2} & \textit{for} \text{ double slot} \end{cases}$$

in which m is positive integer, and they are expanded in the spectral domain such that

$$\tilde{f}_m^n(\beta_{zi}^n) = \begin{cases} (-1)^{m-1} j^{2-k} \frac{\pi w}{4}\left[J_0\left(\beta_n^n \frac{w}{2} + (m-\frac{k}{2})\pi\right) + (-1)^k J_0\left(\beta_n^n \frac{w}{2} - (m-\frac{k}{2})\pi\right)\right] & \text{for single slot} \\ (j)^{m-1} \frac{\pi w}{4}\left[J_0\left(\beta_n^n \frac{w}{2} + \frac{m-1}{2}\pi\right) + (-1)^{m-1} J_0\left(\beta_n^n \frac{w}{2} - \frac{m-1}{2}\pi\right)\right] & \text{for double slots} \end{cases} \tag{A.9}$$

A.3 Numerical Results and Experimental Verification

On the basis of the above-described theoretical framework, an algorithm for calculation of the resonant frequency and Q-factor is implemented for the proposed cylindrical

dielectric resonators with single and double radiating slots. To verify our modeling technique, the resonator described in [2] presenting a special case of our structure is calculated. Numerical results obtained from this technique are the same as [2]. In addition, our experimental results, which will be shown later, further confirm the validity of the proposed technique.

In the analysis of dielectric resonators, the mode classification is important for circuit design and applications. The resonant modes in a cylindrical dielectric resonator with single and double radiating slots are considerably complicated and more difficult to specify in terms of the variation in coordinate directions (r, ϕ, z). In the following, the modes will be designated as TM^{r}_{0m}, where the first subscript (0) indicates the invariant nature of modal field in ϕ-direction while the second subscript (m) presents the order of resonant frequency of interest, and the superscript (r) illustrates the type of structure and relevant modal field profile. For a single radiating slot, $r=s$, and for a double radiating slot, $r=e$ or o indicating the symmetrical plane $z=0$ is an electric wall or magnetic wall, respectively.

Fig. A.2 shows characteristics of the resonant frequency and quality factor for the first two TM-modes versus the dielectric-rod height. It is observed that the resonant frequency increases while the quality factor decreases with an increasing dielectric rod height when the size of metal disks remains unchanged. The quality factor of TM^{s}_{02} is more sensitive to the change of height, particularly, in the case of a smaller height. As shown in [2], a leaky state can be converted into a trapped state provided that the order of z-dependent variation of fields be increased.

To validate the numerical modeling, a set of measurements for resonant frequency of TM_{02}^{s}-mode were made with three heights of dielectric rod. The experimental setup is similar to that used in [2]. The frequency response of a transmission-type resonator was measured using a network analyzer. Fig. A.2 shows the theoretical simulation and experimental results which are in good agreement. The slight deviation may be attributed to the effect of finite radius of the metal disks used in the measurement. Furthermore, there is a difference between the measurement setup using a forced-running oscillation and the damped free-running oscillation model that is used in the numerical analysis. For a resonant-type radiating problem, the assumption of a free-running oscillation is not consistent with reality. As discussed in [17], such a model results in a spatially growing wave along the radial direction. Nevertheless, a large number of research works have shown that this theoretical model is a good approximation of the practical situation.

Fig. A.3 illustrates the significant influence of the radiating slot width on resonant frequency and quality factor in a single radiating slot resonator. The resonant frequency increases with the radiating slot width. This is because the loaded capacitance due to the radiating slot decreases with an enlarging radiating slot width. On the other hand, the effect of radiating slot width on quality factor of the first two leaky-modes is completely different. The quality factor of TM_{01}^{s} is almost unchanged while that of TM_{02}^{s} decreases with an increasing radiating slot width. Such a change in quality factor implies that a range of radiation impedances of interest may be obtained by an appropriate choice of radiating slot width. This is important for the antenna design.

Effects of dielectric constant of the resonator on the resonant property of low-order radiating modes in a single radiating slot resonator are described in Fig. A.4. It is seen that the resonant frequency decreases with increasing dielectric constant while the quality factor tends to be larger. This effect is more pronounced with a lower dielectric constant. It can be explained by the fact that the electromagnetic energy becomes more and more concentrated around the dielectric region as the dielectric constant of resonator increases. To demonstrate the influence of radiating slot position on resonant property in a single radiating slot resonator, Fig. A.5 plots curves of resonant frequency and quality factor against the position (d) of radiating slot. It is observed that the quality factor of TM_{02}^{z} increases as the position (d) decreases. This indicates that radiation becomes stronger for a symmetric radiating slot than for its asymmetric counterpart.

In the antenna application, a double radiating slot configuration could be used in order to efficiently adjust its radiation properties. In the following, resonance characteristics of low-order modes are discussed for double radiating slot resonators. Fig. A.6 shows the resonant frequency and quality factor of the low-order even-modes for electric wall at $z=0$ and odd-modes for magnetic wall at $z=0$ as a function of the radiating slot width. The results clearly suggest that the influence of radiating slot on the even- and odd-modes be different. In case of the even-mode, the double radiating slots act in a similar way as its single counterpart on the resonant property of low-order modes. In case of the odd-mode, however, the effect of radiating slot width on quality factor is significant. The resonant frequency of TM_{01}^{z} remains always unchanged. This may be explained by the field distribution of the mode. Influences of the spacing between two radiating slots on resonant characteristics of low-order even- and odd-modes are

presented in Fig.A.7. It is seen that the resonant frequency and quality factor of TM_{02}^{z} reach maximum and minimum values as s = 8 mm, respectively. This behavior is similar to that observed in Fig. A.5 for a single radiating slot resonator. In addition, the effect of the spacing (s) on the resonant property of the odd-mode is quite complicated. The quality factor of TM_{02}^{z} is smaller than that of TM_{01}^{z} as the spacing is chosen between 10 mm and 14 mm. The resonant frequency of TM_{02}^{z} is sensitive to the spacing. Fig. A.8 demonstrates influence of the height (h_2) on resonant frequency and quality factor of the low-order even-modes. The resonant frequency of TM_{01}^{z} tends to decrease with the height (h_2) while that of TM_{02}^{z} reaches a maximum value when $s = 24$ mm. Finally, it is noted that the proposed method can be also used to determinate the field distribution at the radiating slots. This is important in the radiation pattern analysis.

A.4 Conclusion

This paper presents a comprehensive analysis of a class of composite cylindrical resonators with single and double radiating slots, which are proposed as feeds of omnidirectional antennas suitable for wireless communication systems. The enhanced SDA is extended to the calculation of complex resonant frequency of the proposed radiating resonators. Interesting electrical performance and characteristics in terms of resonant frequency and quality factor considering the low-order radiating modes are presented and discussed for radiating resonators with single and double slots. Effects of different structural parameters on resonant frequency and quality factor are given in detail for the design purpose. Theoretical results compare well with our experimental results, thereby validating the proposed modeling. The analysis technique developed in this work can also be used to model a large class of resonators with an enclosure cavity.

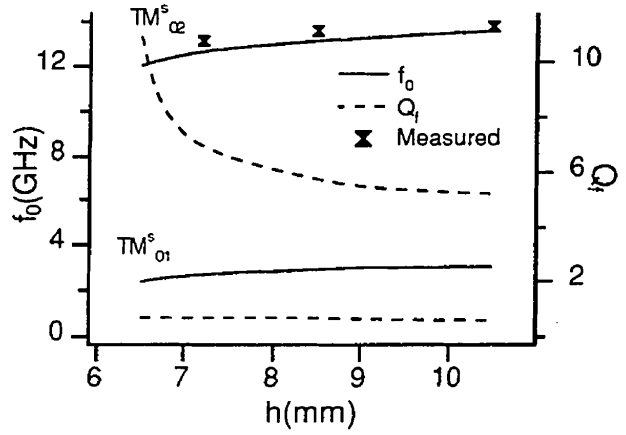

Fig. A.2 Resonant frequency and quality factor versus the height of dielectric rod in the single radiating slot resonator with $r_1 = 7.2$ mm, $r_2 = 7.7$ mm, $d = 3$ mm, $w = h - 6$ mm, and $\varepsilon_r = 2.56$.

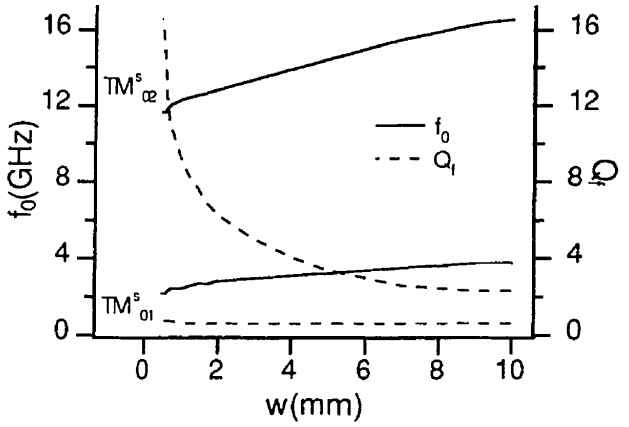

Fig. A.3 Effects of radiating slot width on resonant frequency and quality factor for the first two radiating resonant modes in the single radiating slot resonator with $r_1 = 8$ mm, $r_2 = 8.5$ mm, $h = 10$ mm, $2d = h - w$, and $\varepsilon_r = 2.04$.

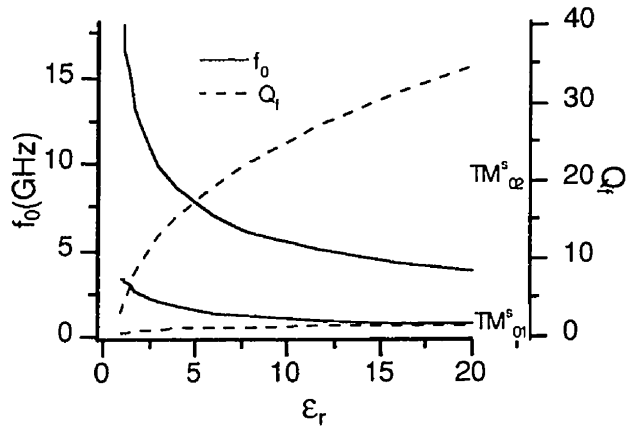

Fig. A.4 Effects of dielectric constant of the dielectric rod on resonant frequency and quality factor for the first two radiating resonant modes in the single radiating slot resonator with $r_1 = 8$ mm, $r_2 = 8.5$ mm, $h = 10$ mm, $d = 4.5$ mm, and $w = 1$ mm.

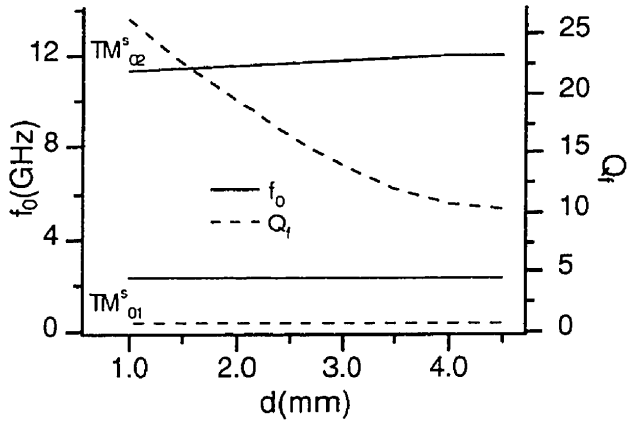

Fig. A.5 Effects of radiating slot height (d) on resonant frequency and quality factor for the first two radiating resonant modes in the single radiating slot resonator with $r_1 = 8$ mm, $r_2 = 8.5$ mm, $h = 10$ mm, $w = 1$ mm, and $\varepsilon_r = 2.04$.

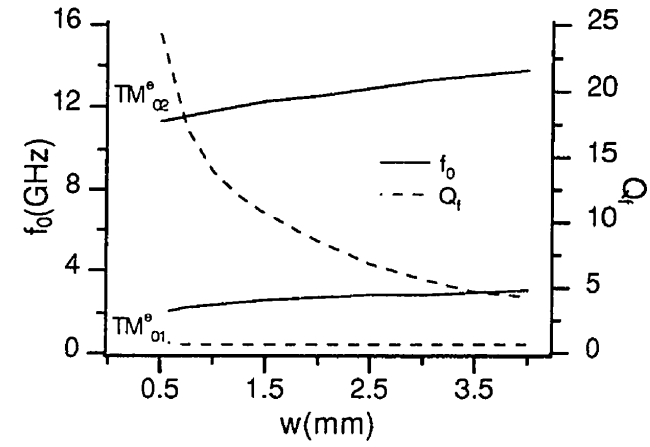

(a)

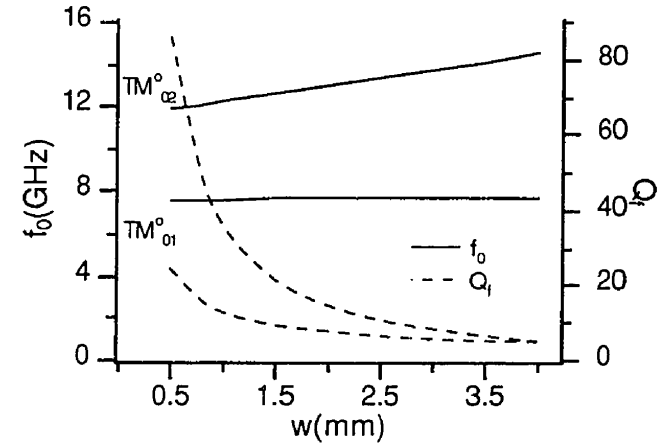

(b)

Fig. A.6 Resonant characteristics as a function of radiating slot width in the double radiating slot resonator with $r_1 = 8$ mm, $r_2 = 8.5$ mm, $h_1 = h_2 = 20$ mm, $s = 6$ mm, and $\varepsilon_r = 2.04$. (a) Even-mode and (b) odd-mode.

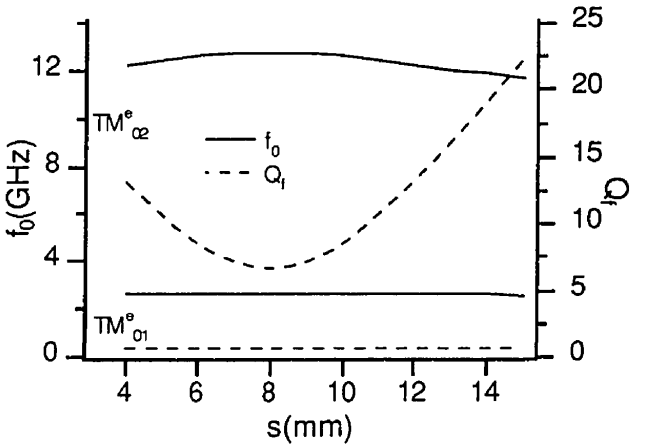

(a)

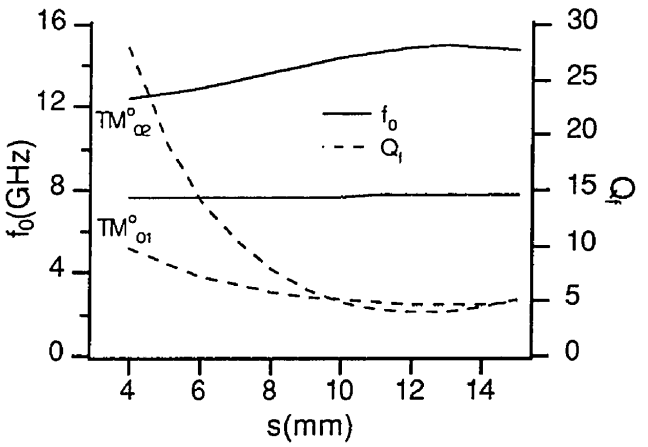

(b)

Fig. A.7 Electrical characteristics in terms of resonant frequency and quality factor against the spacing (s) between two radiating slots in the double radiating slot resonator with $r_1 = 8$ mm, $r_2 = 8.5$ mm, $h_1 = h_2 = 20$ mm, $w = 2$ mm, and $\varepsilon_r = 2.04$. (a) Even-mode and (b) odd-mode.

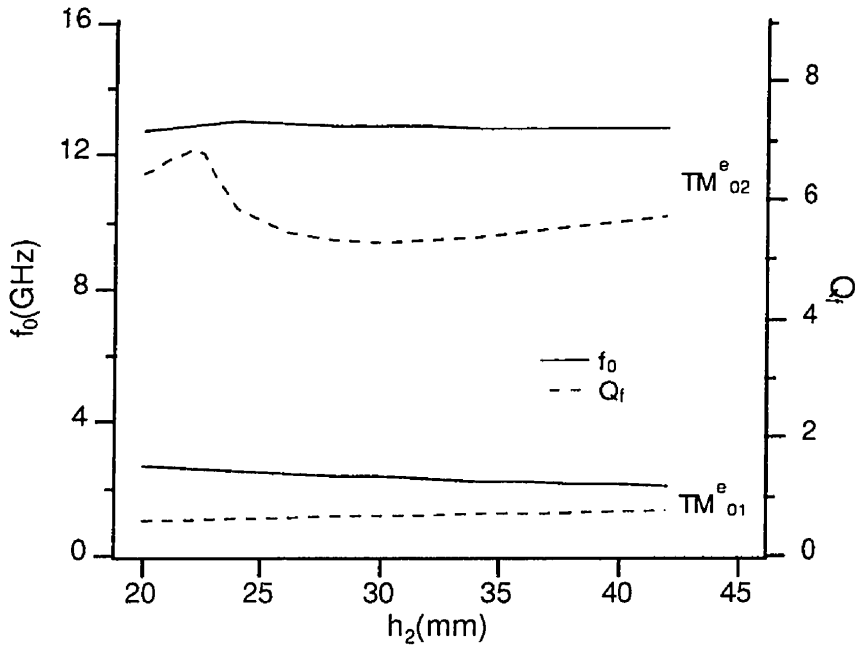

Fig. A.8 Resonant frequency and quality factor of the even-mode with the variation of the height h_2 in the double radiating slot resonator with $r_1 = 8$ mm, $r_2 = 8.5$ mm, $h_1 = 20$ mm, $w = 2$ mm, $s = 8$ mm, and $\varepsilon_r = 2.04$.

References

[1] T. S. Bird, et al, "Millimeter-wave antenna and propagation studies for indoor wireless LANs", in 1994 *IEEE AP-S Int. Symp. Dig.*, pp.336-339.

[2] Y. Kobayashi and S. Tanaka, "Resonant modes of a dielectric rod resonator short-circuited at both ends by parallel conducting plates", *IEEE Trans. Microwave Theory and Tech.*, vol. MTT-28, pp.1077-1085, Oct. 1980.

[3] H. An, T. Wang, R.G. Bosisio, and K. Wu, "Cavity-restrained multistacked dielectric omnidirectional antenna for microwave and millimeter-wave wireless communications", *Electron. Lett.*, vol. 30, No. 25, pp.2086-2087, 1994.

[4] T. Wang, H. An, K. Wu, J. J. Laurin, and R. G. Bosisio, "A novel leaky-mode cylindrical dielectric resonator used as feeds of omnidirectional antenna for wireless communications", in 1995 *IEEE MTT-s Int. Microwave Symp*, pp.657-660.

[5] J. F. Lee, G. M. Wilkins, and R. Mittra, "Finite-element analysis of axisymmetric cavity resonator using a hybrid edge element technique", *IEEE Trans. Microwave Theory and Tech.*, vol. MTT-41, pp.1981-1987, Nov. 1993.

[6] J. E. Lebaric and D. Kajfez, "Analysis of dielectric resonator cavities using the finite integration technique", *IEEE Trans. Microwave Theory and Tech.*, vol. MTT-37, pp.1740-1747, Nov. 1989.

[7] Y. Kobayashi and T. Senju, "Resonant modes in shield uniaxial-anisotropic dielectric rod resonators", *IEEE Trans. Microwave Theory and Tech.*, vol. MTT-41, pp.2198-2205, Dec. 1993.

[8] X. P. Liang and K. A. Zaki, "Modeling of cylindrical dielectric resonators in rectangular waveguides and cavities", *IEEE Trans. Microwave Theory and Tech.*, vol. MTT-41, pp.2174-2181, Dec. 1993.

[9] S. W. Chen and K. A. Zaki, "Dielectric ring resonators loaded in waveguide and on substrate", *IEEE Trans. Microwave Theory and Tech.*, vol. MTT-39, pp.2069-2076, Dec. 1991.

[10] S. Maj and M. Pospieszalki, "A composite multilayered cylindrical dielectric resonator", in 1984 *IEEE MTT-s Int. Microwave Symp. Dig.*, pp.190-192.

[11] A. Drher and R. Pregla, "Full-wave analysis of radiating planar resonators with the method of lines", *IEEE Trans. Microwave Theory and Tech.*, vol. MTT-41, pp.1363-1368, Aug. 1993.

[12] K. Wu, "A combined efficient approach for analysis of nonradiative dielectric (NRD) waveguide components", *IEEE Trans. Microwave Theory and Tech.*, vol. MTT-42, pp.672-2177, Apr. 1994.

[13] R. H. Jansen, "The spectral-domain approach for microwave integrated circuits," *IEEE Trans. Microwave Theory Tech.*, vol. MTT-33, pp. 1043-1056, Oct. 1985.

[14] Tongqing Wang and Ke Wu "An Efficient approach to modeling of quasi-planar structures using the formulation of power conservation in spectral domain," *IEEE Trans. Microwave Theory Tech.*, vol. MTT-43, pp.1136-1143, May 1995.

[15] T. Wang and K. Wu, "Effects of various suspended mounting schemes on mode characteristics of coupled slotlines considering conductor thickness for wideband MIC application," *IEEE Trans. Microwave Theory Tech.*, vol. MTT-43, pp.1106-1114, May 1995.

[16] R. E. Collin, *Field theory of guided waves*, Second edition, New York, 1991.

[17] A. Dreher, "The method of lines and the integral equation method for the analysis of planar antennas" (in German), Fortschritt Berichte, ser. 21, no.116, VDI-Verlag Gmbh, Dusseldorf, 1992.

IMAGE EVALUATION TEST TARGET (QA-3)

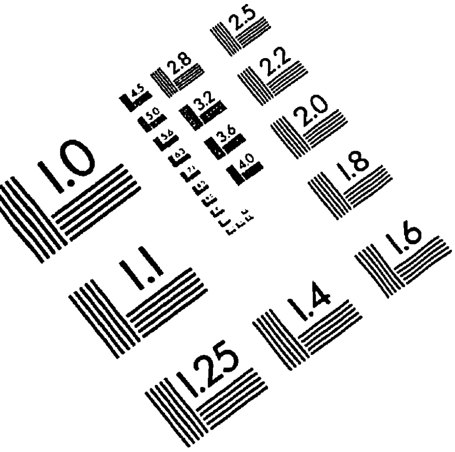
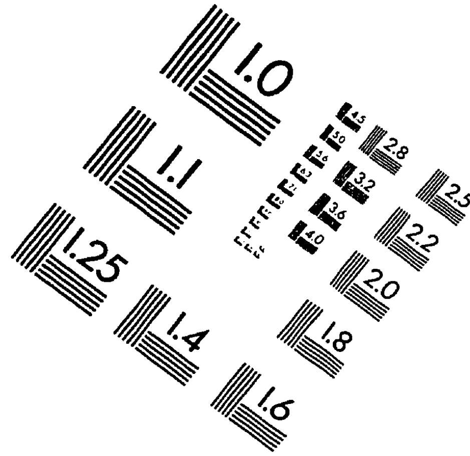

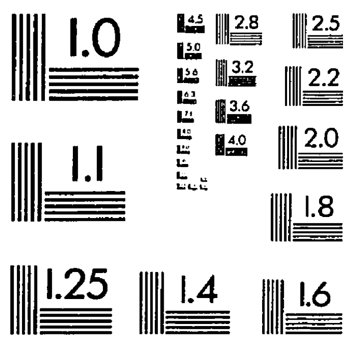

150mm

6″

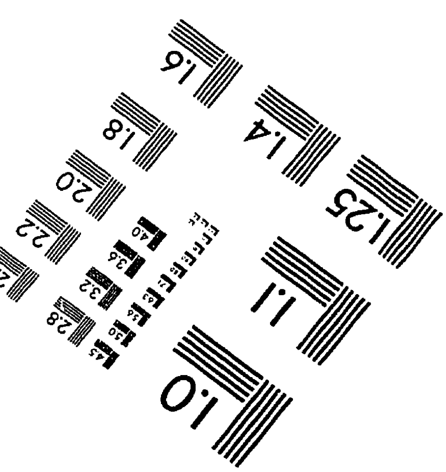
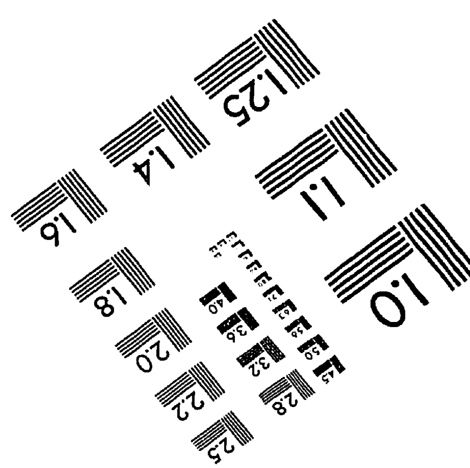

APPLIED IMAGE, Inc
1653 East Main Street
Rochester, NY 14609 USA
Phone: 716/482-0300
Fax: 716/288-5989